Molecular Dynamic Simulations of Diffusion and Phase Behaviors of Colloidal Particles in Two-Component Liquid Systems

by

Wei Gao

A Dissertation Presented in Partial Fulfillment
of the Requirements for the Degree
Doctor of Philosophy

Approved May 2017 by the
Graduate Supervisory Committee:

Lenore Dai, Chair
Yang Jiao
Heather Emady
Yongming Liu
Matthew Green

ARIZONA STATE UNIVERSITY

August 2017

ABSTRACT

A comprehensive and systematic investigation on the diffusion and phase behaviors of nanoparticles and macromolecules in two component liquid-liquid systems via Molecule Dynamic (MD) simulations is presented in this dissertation.

The interface of biphasic liquid systems has attracted great attention because it offers a simple, flexible, and highly reproducible template for the assembly of a variety of nanoscale objects. However, certain important fundamental issues at the interface have not been fully explored, especially when the size of the object is comparable with the liquid molecules. In the first MD simulation system, the diffusion and self-assembly of nanoparticles with different size, shape and surface composition were studied in an oil/water system. It has been found that a highly symmetrical nanoparticle with uniform surface (e.g. buckyball) can lead to a better-defined solvation shell which makes the "effective radius" of the nanoparticle larger than its own radius, and thus, lead to slower transport (diffusion) of the nanoparticles across the oil-water interface. Poly(N-isopropylacrylamide) (PNIPAM) is a thermoresponsive polymer with a Lower Critical Solution Temperature (LCST) of 32°C in pure water. It is one of the most widely studied stimulus-responsive polymers which can be fabricated into various forms of smart materials. However, current understanding about the diffusive and phase behaviors of PNIPAM in ionic liquids/water system is very limited. Therefore, two biphasic water-ionic liquids (ILs) systems were created to investigate the interfacial behavior of PNIPAM in such unique liquid-liquid interface. It was found the phase preference of PNIPAM below/above its LCST is dependent on the nature of ionic liquids. This potentially allows us to manipulate the interfacial behavior of macromolecules by tuning

the properties of ionic liquids and minimizing the need for expensive polymer functionalization. In addition, to seek a more comprehensive understanding of the effects of ionic liquids on the phase behavior of PNIPAM, PNIPAM was studied in two miscible ionic liquids/water systems. The thermodynamic origin causes the reduction of LCST of PNIPAM in imidazolium based ionic liquids/water system was found. Energy analysis, hydrogen boding calculation and detailed structural quantification were presented in this study to support the conclusions.

ACKNOWLEDGMENTS

First and foremost, I want to express my deepest gratitude to my advisor, Dr. Lenore L. Dai. I appreciate all her encouragement, guidance, and flexibility to make my doctoral experience so productive and enjoyable. I also owe many thanks to my co-advisor, Dr. Yang Jiao, who guided me in learning Molecular Dynamic Simulations which eventually lead to my dissertation work. The knowledge, skills, and advice he has passed on me will be always invaluable to me. My deepest appreciation also extends to my other committee members, Dr. Heather Emady, Dr. Matthew Green and Dr. Yongming Liu, for their invaluable support, time and knowledge which make my research much more extensive.

I am very grateful that I have had the privilege of working with my fellow group members and collaborators. I am especially thankful to Dr. Stella Nickerson, for her time and patience in discussing my research and teaching me how to use Gromacs to perform MD simulations. I also want to thank Dr. Elizabeth Nofen, Dr. Haobo (Evan) Chen, Dr. Prithwish Chatterjee and Dr. Vipin Argawal. I am so lucky to have such a group of brilliant and marvelous colleagues accompany me on my journey of pursing my Ph.D.

I also owe my greatest gratitude to my dear families, especially my husband, Bin Mu. It is beyond my words to thank him for being such a fantastic husband in so many ways: providing great advices about my research, carrying so much burdens of the housework and being such a great daddy to my daughter— It would be impossible for me to pursue my Ph.D degree without his love, understanding and support. Of course, I must thank my little girl Claire, who has been bringing so much happiness and power to me

since she was born. She is the major factor making me determined to get my Ph.D. I also want to thank my upcoming baby, Alice, who started her journey in my tummy just about the same time when I started writing my dissertation, which has been adding so much joy and excitement to this process.

Last, but most importantly, I must say “Thank You!” to my parents for loving me unconditionally and endlessly. My mom, who was the first female scientist of the prestigious Chinese Academy of Science in her hometown village, has been always a lifetime inspiration for me. My father was the most knowledgeable person I’ve ever met. I can never forget our long conversations about science, history, and far-away countries. He was the one who made me dream about pursing my higher education in America since I was a kid. I want to dedicate my dissertation to him, who, I believe, is watching me from heaven and must be so happy that I finally finish my Ph.D.

TABLE OF CONTENTS

Page

CHAPTER Page

Page

LIST OF TABLES

Table Page

Table Page

LIST OF FIGURES

Figure Page

Figure Page

Figure Page

Figure Page

Figure Page

Figure Page

Figure Page

Figure Page

1. INTRODUCTION

Diffusion and phase behavior of colloidal particles in liquid-liquid systems have received a considerable amount of attention. Surface catalysis, solid-state emulsion, microfluidic devices, membrane separation, and cell membranes are real-world circumstances in which particles are usually spatially confined at interface.[1–6] Behavior of colloids in spatially confined environment is more complicated than that in unbounded three-dimensional bulk liquid. The diffusion and self-assembly process of colloidal particles at interface are affected not only by the physical and chemical properties of the particles themselves, but also by the two immiscible phases which form the interface. While many studies exist regarding the colloidal system composed of oil and water, there have been limited studies of nanoparticles and polymer molecules in liquid-liquid systems composed of water and ionic liquids, which have shown great potential as a new strategy to modify the function of ionic liquids.[7] In particular, there is a strong need of using molecular dynamics simulation to elucidate the interaction mechanism between colloidal particles and solvent species. In our study, we employed Molecular Dynamic simulations as our tool to conduct a systematic and comprehensive investigation of nanoparticles and macromolecule at/across liquid-liquid interfaces. In addition, macromolecule in miscible ionic liquids-water systems were also studied in this thesis to seek a better understanding of the interactions between ionic liquids and macromolecules.

Chapter 2 is divided into three sections dedicated to provide the readers some fundamental understanding and background knowledge of the "key roles' in this dissertation. In the first section, we introduced the theories and applications about the diffusion and self-assembly of colloidal particles at liquid-liquid interface. Next, in

section 2.2, the unique properties of ionic liquids, especially their miscibility and solubility characteristics were discussed in greater details. In section 2.3, we provided background information about a "smart material", Poly(N-isopropylacrylamide) (PNIPAM), which is a thermoresponsive macromolecule with a Lower Critical Solution Temperature (LCST) of 32˚C. The most widely accepted mechanism to explain PNIPAM's sudden extended-to-coiled phase transition at LCST was introduced. Our motivations of studying the phase behaviors of PNIPAM in two-component liquid-liquid systems, in particular, ionic liquids/water systems were explained in this section.

Chapter 3 describes the methodology utilized in this thesis work—Molecular Dynamic (MD) simulations. This computational method calculates the time dependent behavior of a molecular system. It can provide microscopic-level information, such as atomic positions and velocities and "translate" this microscopic information into macroscopic observables including temperature, pressure, energy, heat capacities, and so on. MD simulation is a powerful tool to investigate the structure, interactions, dynamics and thermodynamics of nanoparticles and macromolecules and its complexes at atomic level. All MD simulations in this thesis were performed using the GROMACS package, an open-source and free software widely used for dynamic simulations. We also introduced the theories and principle behind the software. For example, we introduced our integration method and periodic boundary conditions (PBC). In addition, we explained the methodologies to maintain constant temperatures and pressures in our simulation systems. In particular, special attentions were given to discuss our force fields selections and verifications.

Systematical investigation on the effects of nanoparticles' size, shape and surface composition on their diffusive behaviors at/across the water/oil interface were conducted in Chapter 4. This chapter was mainly motivated for two reasons: first, the kinetics of particle adsorption onto the liquid interface is not completely understood, especially when the particle size is comparable to the liquid molecular size. Second, there are only limited studies about effects of anisotropic particle's shapes on the self-assembly and diffusion behaviors of nanoparticles in liquid-liquid systems. Thus, in this chapter, four different nanoparticles were created for our study: modified hydrocarbon nanoparticles with a mean diameter of 1.2 nm (1.2HCPs), modified hydrocarbon nanoparticles with a mean diameter of 0.6 nm (0.6HCPs), singled-walled-carbon nanotubes (SWCNTs), and buckyballs. We found that the diffusion coefficients of 0.6HCP and 1.2HCP were larger than the corresponding values predicted using the Stokes-Einstein (SE) equation and attributed this deviation to the small particle size and the anisotropy of the interface system. In addition, we found the derivative of the Potential of Mean Force (PMF) served as an effective driving force for the particles along the direction perpendicular to the interface which lead to the values of diffusion coefficients of 0.6HCP and 1.2HCP were close to each other. We also found that nanoparticles with isotropic shape and uniform surface, such as buckyballs, tend to have smaller diffusion coefficients than those of nanoparticles with comparable dimensions but anisotropic shapes and non-uniform surface composition, e.g, SWCNT and 0.6HCP. One possible hypothesis for this behavior is that the "perfect" isotropic shape and uniform surface of buckyballs result in a better defined "solvation shell" (i.e., a shell of solution molecules), which leads to a larger "effective radius" of the particle, and thus, a reduced diffusion coefficient.

The objective of Chapter 5 is to study the interfacial behaviors of PNIPAM in the biphasic water-ionic liquids (ILs) systems. Currently, our understanding of macromolecule's interfacial behaviors at the water-ILs interface is far from clear, in which the interaction mechanisms between thermal-responsive macromolecules and solvent molecules are least investigated. Thus, in this chapter, extended PNIPAM (equilibrated below its Lower Critical Solution Temperate, "LCST") and coiled PNIPAM (equilibrated above its LCST) were studied in two different water-ionic liquids systems: water-[BMIM][PF_6] system, and water-[BMIM][TF_2N]. It was found PNPAM exhibited obvious phase preference in the water-[BMIM][PF_6] system: the extended PNIPAM preferred the water phase, while the coiled PNIPAM tended to equilibrate at the IL side of the interface. However, in the water-[BMIM][TF_2N] the phase preference of PNIPAM was independent to its equilibrated configurations: both extended and coiled PNIPAM equilibrated at the IL phase close to the interface. Interaction energies between PNIPAM and different species in the solvents were calculated to find the thermodynamic origin of PNIPAM's interfacial behavior in two different water-IL systems. In addition, detailed structural quantification via the radial distribution functions were calculated to precisely determine the interacting functional groups between PNIPAM and solvent molecules. We found that in the water-[BMIM][PF_6] system, BMIM cation were mainly responsible for attracting extended PNIPAM to the IL phase. While in the water-[BMIM][TF_2N] system TF_2N anion played the most significant role in pulling both extended and coiled PNIPAM into the IL side of the interface.

The objective of Chapter 6 is to extend our studies of PNIPAM in a different type of two-component liquid-liquid system—miscible ionic liquids/water systems. Recent

studies showed the imidazolium based ionic liquids can alter the phase behavior of PNIPAM in aqueous solutions. However, the interaction mechanism between macromolecules and ions in ILs/water systems is barely studied. In this chapter, a pure water system and two miscible ionic liquids/water systems, [BMIM][I]/water and [BMIM][Cl]/water systems were created for our study. PNIPAM was simulated in these systems below and above its LCST, at 295K and 350K respectively. Extended-to-coiled phase transition was observed in all three simulation systems. Energy analysis was performed to understand the thermodynamic origin of the phase behaviors in different systems. We found the enthalpy change in the pure water system was significantly higher than the ionic liquid/water systems, which may explain why PNIPAM tended to have a LCST type transition at lower temperatures in the imidazolium based IL/water systems. In addition, it was found that the number of inter-molecular hydrogen bonds between PNIPAM and water were notably lower in the miscible ionic liquids/water systems than the pure water systems, suggesting fewer hydrogen bonds were required to break in the ionic liquid/water systems, which may also explain why PNIPAM could precipitated in the ionic liquid/water system at lower temperatures. Detailed structural quantification via Radial Distribution Functions (RDF) was applied to reveal the interacting functional groups on different molecules. We found PNIPAM had strong interactions with both cations and anions of the ionic liquids. However, the PNIPAM-cation (BMIM) and PNIPAM-anions (I^-, Cl^-) interactions had different origins. The PNIPAM-BMIM cation interactions were mainly from the nonpolar groups, the isopropyl side chain of PNIPAM and the butyl group of BMIM cation, while the PNIPAM-anions (I^-, Cl^-) interactions mostly took place between the charged part of PNIPAM (amide hydrogen, carbonyl

carbon) and the anions (I^-, Cl^-). In addition, we found the interactions between PNIPAM and I^- were significantly stronger than Cl^-. Based on a series of energy analysis and RDF calculations, it was found I^- had weaker associations with other "competing species" such as BMIM cation and water molecules in the simulation box than Cl^-. This may cause I^- having relatively stronger interaction with PNIPAM than Cl^-. Finally, all the works in this dissertation were concluded and summarized in the last chapter, Chapter 7.

2. BACKGROUND AND MOTIVATION

2.1. Colloidal Particles at Liquid-Liquid Interfaces

The interface between two immiscible liquids, such as oil and water, is often termed as a liquid-liquid interface. It is well known that particles can reside at liquid-liquid interfaces due to a reduction in interfacial energy.[8] Such composite structures have attracted lots of attention in recent years because they offer a simple, flexible, and highly reproducible template for the assembly of a large variety of nanoscale objects. Driven by lowering the interfacial tension between two liquid phases, small objects (< 10 microns) including solid particles and macromolecules such as polymers, proteins, bacteria, and viruses are readily adsorbed onto the liquid-liquid interface to form a stable colloidal system.[3,9,10]

This self-assembled system can find many applications and is central to several emerging technologies. For example, the self-assembly of nanoparticles at fluid interfaces including both liquid–liquid and liquid–vapor interfaces have enabled the preparation of high quality two-dimensional materials,[11] which can be used for the fabrication of freestanding metal films,[12] ultra-thin cross-linked membranes,[13–16] and capsules.[17–19] On the other hand, colloidal properties can be modified by the adsorption of solid particles to generate stabilized micrometer-scale structures such as nanoparticle-armored fluid droplets or phase-arrested gels.[20,21] Small particles adsorbed at fluid interfaces have played an important role in industrial processes related to foams and emulsions. It has been known for many years that particles, instead of surfactants at interfaces can be exploited to tune the stability of an emulsion, called Pickering emulsion, in which small particles form a barrier between the interface of the droplet (dispersed phase) and the

continuous phase to inhibit the coalescence of droplets, and generate kinetically stable emulsions.[22–25] This section will introduce some basic concepts and fundamental equations related to colloidal particles at liquid-liquid interfaces and then provide a brief discussion of their potential applications.

From the viewpoint of thermodynamics, the adsorption of solid particles onto fluid interfaces is a spontaneous process toward a lower total free-energy configuration.[26] For a spherical particle adsorbed at the oil-water interface as shown in Figure 2.1, the free energy of particle detachment is minimum at equilibrium and is given by the equation:

$$\Delta \boldsymbol{G} = \boldsymbol{\pi r^2 \gamma_{ow}(1 \pm cos\theta)^2} \qquad \text{(Equation 2-1)}$$

Assuming the system containing an oil phase, a water phase, and a spherical particle, in Equation 2-1 "*r*" represents the particle radius, γ_{OW} is the oil-water interfacial tension, and θ is the three-phase contact angle measured through the water phase. The sign inside the bracket is positive for absorption into or desorption from oil and negative for absorption into or desorption from water. This calculation for particle desorption energy quantifies how strongly particles are held at the interface. Three phase contact angle (θ) of the particle indicates the position where total interfacial energy reaches a minimum.[26] It is the angle between the tangents to the solid surface and the liquid-liquid interface measured through one of the liquids in each point of the three-phase contact line where the solid and two liquids meet.[27] An example of a spherical particle at oil-water interface is shown in Figure 2.1.

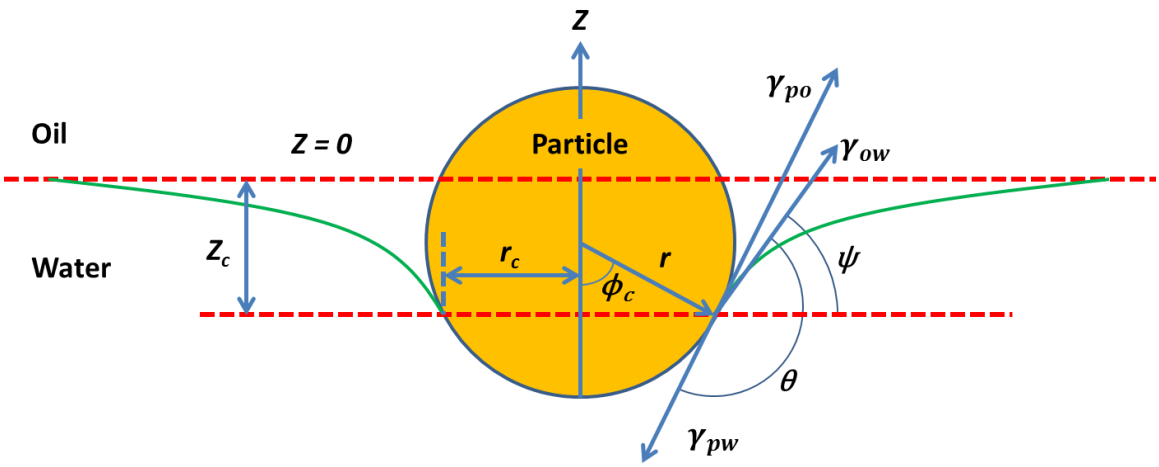

Figure 2-1 Scheme of a spherical particle with radius *r* and contact angle θ residing at the oil-water interface.

For a spherical colloidal particle with a smooth surface at the oil and water interface, the contact angle can be defined in terms of the interfacial tensions by Young's equation[27] (Equation 2-2)

$$\boldsymbol{cos\theta} = \frac{\boldsymbol{\gamma_{PO}-\gamma_{PW}}}{\boldsymbol{\gamma_{OW}}} \qquad \text{(Equation 2-2)}$$

where γ_{OW}, γ_{PO}, and γ_{PW} representing the interfacial tensions of the water/oil surface oil/particle surface, and water/particle surface, respectively. According to Equation 2-1, the desorption energy depends on the square of the particle radius, as plotted in Figure 2.2 (a)**,** taking $\theta = 90^o$ and $\gamma = 50$ mN/m.[26,28] For particles with intermediate hydrophobicity ($\theta = 90^o$) and the size ranging from several nanometers to several microns, the desorption energy is in large excess with respect to the thermal energy, 1 kT, so that particle attachment is essentially irreversible.[26,28] Only for extremely small particles ($r \leq 1$ nm), does this energy become comparable to the thermal energy and attachment may be reversible. Wettability is another important parameter in the

equation.[26] The particle is most strongly held at a contact angle of $\theta = 90^o$,when it is equally wet by both liquids, and the adsorption strength drops off quickly on either side of $\theta = 90^o$.[26] This effect is illustrated in Figure 2.2 (b),[26,29,30] which shows the dependence of the energy required to remove a 10 nm spherical particle from the oil-water interface with an interfacial tension γ_{ow}=36 mN/m on the contact angle.[26,29,30] As we introduced above, the excess free energy has a larger impact on smaller particles, and more discussion related to the three-phase contact angle can be found from the literature.[31]

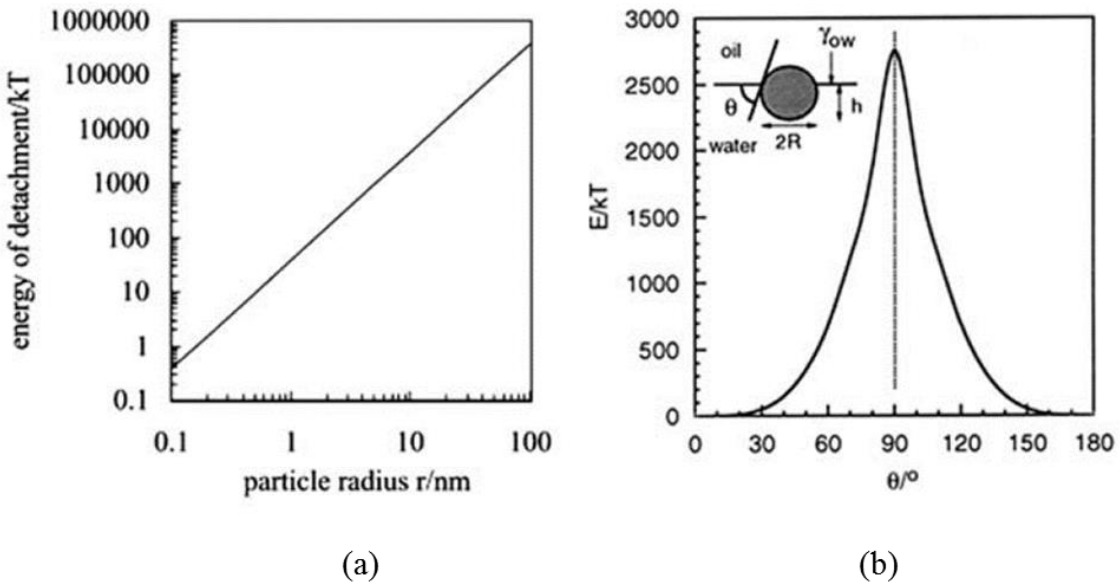

(a) (b)

Figure 2-2 Variation of adsorption/desorption energy (E) of a particle at the planar oil/water interface at 298 K with respect to (a) particle radius and (b) contact angle. Adapted from reference 22 and 23, respectively.

For many technological processes, it is important to know the conditions at which a solid particle can be adsorbed and stay attached in equilibrium at the fluid interface. The equilibrium position of a particle at a fluid interface can be estimated by analyzing

the minimum free energy of the system or by analyzing the force balance on the particle. To simplify the discussion here, we only consider a solid spherical particle with radius *r* in equilibrium at the oil-water interface when the particle density ρ_p is larger than that of water, ρ_w, and oil ρ_o ($\rho_p > \rho_w > \rho_o$, Figure 2.1). In this case, the oil-water interfacial tension is the primary factor determining the particle stability at the interface. The force balance analysis is given by:

$$F_\gamma + F_P = mg$$

where F_γ is the vertical capillary force:

$$F_\gamma = -2\pi r\gamma_{ow} sin\emptyset_c sin(\emptyset_c + \theta)$$

and F_P is the integration of the hydrostatic pressure distribution around the entire particle surface:

$$F_p = -\rho_w V_{pw} g + \rho_o V_{po} g - (\rho_w - \rho_o) g Z_c A_c$$

where V_{pw} is the particle volume immersed in water:

$$V_{pw} = \frac{\pi r^3 (2 - 3cos\emptyset_c + cos^3\emptyset_c)}{3}$$

and V_{po} is the particle volume immersed in oil:

$$V_{po} = \frac{4\pi r^3}{3} - V_{pw}$$

The surface tension and contact angle calculated from these equations will be used to validate the molecular dynamic simulation system created to study the particle diffusion behavior detailed in Chapter 4.

As discussed above, the quantification of how strongly colloidal particles are adsorbed and predicting where the particles reside in vertical position at an interface, are

essential in many diverse applications. For example, a strong adsorption providing higher colloidal stability over time is highly desirable for Pickering emulsions, while a lower adsorption of nanoparticles in biomedical applications is more desirable since the increased nanoparticle lifetime in the blood stream will improve drug release, or increase the imaging window when they are used as contrast agents. Meanwhile, estimating and controlling the vertical position (immersion depth) of nanoparticles will have a big impact on optimizing plasmonic and optical properties of the self-assembled system. For example, the plasmonic properties of nanoparticles are affected by their vertical position with respect to the interface due to the difference in the dielectric constant of the two fluids. Yang et al. showed how the localized surface plasmon resonance (LSPR) absorption band of gold nanoparticles changed significantly depending on the immersion depth of the nanoparticle at the water-oil interface.[32] The vertical position also changed the plasmonic modes and formation of hot-spots on the assemblies of nanoparticles. Several attempts have appeared in the past few years to control this immersion depth to address optical applications. Wang et al. used reagents including dodecanethiol and tetramethylammonium at an oil or water phase respectively to modify the immersion depth of gold nanoparticles at the interface.[33] Booth et al. employed an electrochemical modulation for this control.[34] Lin et al. used a gel trapping method after the assembly of nanoparticles at the air – water interface to build a substrate with partially immersed nanorods.[35] Although great effort has been made, most of these approaches are, however, far from being optimized as they lack the critical quantification of the contact angle of the partially immersed nanoparticles and the fundamental understanding of transport of nanoparticles at/across a fluid interface is far from clear.[36,37] In addition, the overall

diffusion behavior of synthetic particles at fluid interfaces is closely related to the interactions of biological macromolecules, proteins, and virus capsids with liquid interfaces and cell membranes, and a detailed study of diffusion in non-biological system will build a solid ground for similar studies in the biological systems.

Since Pickering emulsion is one of the important applications for investigating colloidal particles at liquid-liquid interfaces, it would be useful to provide a comparison between classical surfactant-stabilized emulsions and solids-stabilized emulsions first. As illustrated in Figure 2.3,[38] a classical emulsion is stabilized by surfactant, while solid particles are absorbed onto the liquid-liquid interface and serve as stabilizers to prevent the liquid-liquid coalescence in Pickering emulsion. It is named after the British chemist S. U. Pickering, whose paper is considered the first report of this phenomenon in 1907,[39] but actually, this effect was reported 4 years earlier by W. Ramsden in 1903.[40] Figure 2.4 shows a series of 3D images of Pickering emulsion. Although it was quite clear since the paper by Pickering in 1907 that such emulsion had definite advantages in comparison to the classical surfactant-based emulsions, the later were preferred and showed considerable development in various types of applications. Pickering emulsions were largely ignored for a long period and only gained a renewed interest quite recently.[26,41]

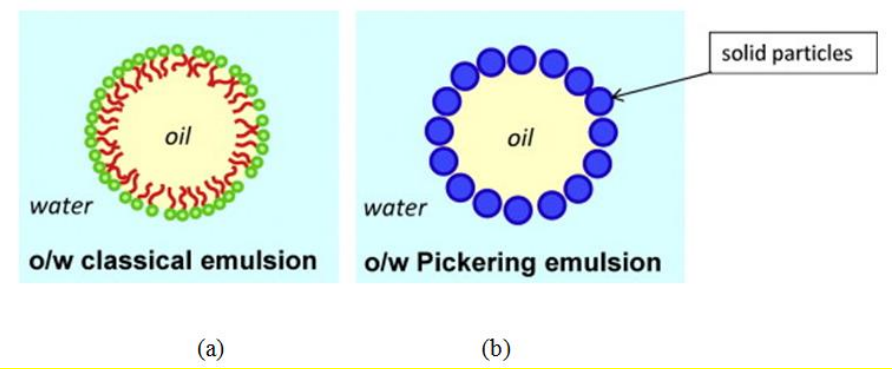

Figure 2-3 Sketch of (a) a classical (surfactant-based) emulsion, (b) a Pickering emulsion. The solid particles adsorbed at the oil–water interface stabilize the droplets in place of the surfactant molecules. Adapted from reference 31.

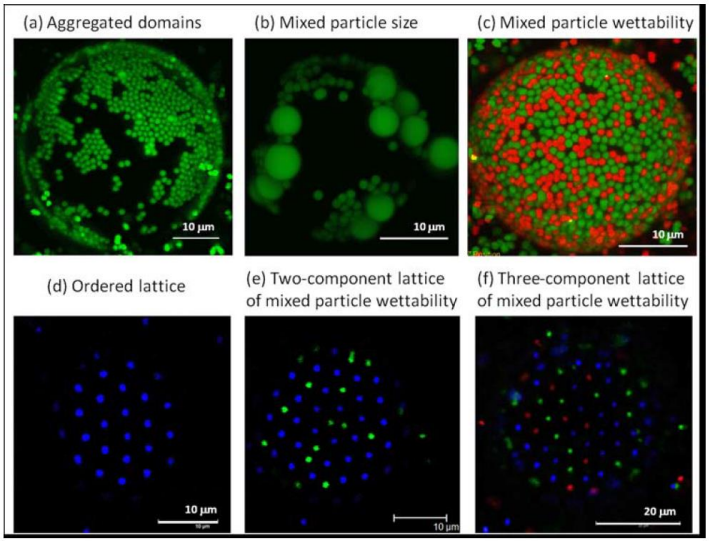

Figure 2-4 Confocal laser-scanning microscope images showing the rich morphology of microparticles at PDMS-in-water Pickering emulsion interfaces. a–c) The solid particles are 1.1 µm in diameter except in (b), which is a mixture of 1.1- and 4-µm particles. The solid particles are S-PS except in (c), which is a mixture of S-PS (in *green*) and C-PS particles (in *red)*. d–f) The particle size is 1.0 µm. The solid particles are S-PS (in *blue*), aldehyde sulfate-treated polystyrene (AS-PS, in *green*), and C-PS (in *red*). Adapted from reference 19 and 33.

The particle-laden character of Pickering emulsion brings about specific properties to emulsions. First, the emulsion stability is usually significantly improved in Pickering emulsion, Ostwald ripening can be slowed down or even arrested due to the high desorption energy of particles at liquid-liquid interfaces.[26] Second, the "surfactant-

free" feature makes Pickering emulsion particularly attractive in food, cosmetic and pharmaceutical applications where surfactants usually show adverse effects such as irritancy, cytotoxity, and hemolytic behavior.[41] For example, emulsions stabilized by titanium oxide are potential alternatives to replace conventional surfactants and lead to new skin care and sunscreen formulations.[42] Starch particles are an excellent candidate to stabilize emulsions of sensitive and bioactive ingredients in food and pharmaceutical products.[43] Another interesting feature of Pickering emulsion is that the size of the emulsion droplets is more predictable than the surfactant-based emulsion.[22] Droplet size is an important parameter in emulsions science, because it affects various aspects of emulsions such as stability, rheological properties, aesthetic appeal, etc. In Pickering emulsion, the size of droplet is always bigger than the solid stabilizing particles.[22,44] Solid particles of nano-scaled size (or sub-micron, about 100nm) allow the stabilization of droplets as small as few micrometers diameter; and micron-sized solid particles are capable of stabilizing larger droplets, the diameter of which can possibly reach few millimeters.[41]

Using self-assembly of nanostructure at liquid-liquid interfaces as a template to synthesis novel materials is another major application of this phenomenon today. The liquid-liquid interface provides a molecularly sharp, defect free focal plane for the assembly of solid materials.[45] For example, A.D. Dinsmore et al. has fabricated a novel material, "colloidosome," using colloid particle self-assembly on an oil-water interface.[17] "Colloidosomes," by analogy of liposomes, are a kind of hollow and elastic capsule. Their size is easily adjusted ranging from micrometers to millimeters; and their permeability and elasticity are also highly controllable. By encapsulation of active

ingredients such as drugs, proteins, vitamins, flavors gas bubbles, or even living cells, colloidosome can have a wide variety of applications. For example, they can be used for immunoisolation of living cells. Colloidosomes would provide a rigid scaffold that supports the living cell while simultaneously protecting it from the immune system and allowing free diffusion of gases and nutrients.[17,46]

In addition, liquid-liquid interfaces can also provide a convenient and highly efficient condition to form Janus particles, such that hydrophobic and hydrophilic domains are formed in situ.[45,47] For example, The Granick group[48] introduced a simple and inexpensive method of preparing Janus nanoparticle based on the formation of an oil-in-water emulsion with silica particles: at the liquid−liquid interface of emulsified molten wax and water, untreated particles adsorbed and were frozen in place when the wax solidified. The exposed surfaces of the immobilized particles were modified chemically. Finally, wax was dissolved, and the inner surfaces were modified chemically. Gram-scale quantities or more of Janus particles can be synthesized by taking this approach. Pardhy et al. created laponite-PS Janus colloids by using a double Pickering emulsion technique.[49,47] First, a Pickering emulsion was created with laponite platelets stabilizing styrene nano-droplets. After polymerization, the armored colloids were used to form colloidosomes of wax in water. After trapping the particles by solidifying the wax, the sides of the colloids exposed to water were modified by an ion-exchange procedure, leading to Janus particles with different charge and surface potential values on the two hemispheres.

Due to the numerous applications and interesting characteristics, lots of effort has been made towards the synthesis of self-assembled microparticles/nanoparticles at liquid-

liquid interface in the past 30 years. However, some fundamental aspects of this phenomenon have not been fully explored. One of the remaining challenges is to understand multiphase interactions, self-assembly processes, and self-assembled structures of nanoparticles, especially when the size of the particles is comparable with the molecular dimension of the surrounding liquids.[50] There are few reports on the effect of anisotropic particle shapes in Pickering emulsions.[1,26] In addition, the kinetics of particle adsorption onto liquid interfaces is also not completely understood.[26]

Molecular Dynamics (MD) simulations have been a powerful tool for understanding the properties of assemblies of molecules in terms of their structure and the microscopic interactions between them. It provides us a unique opportunity to reveal the atomic details behind the macroscopic phenomena. For example, Moreira and Skaf reported a significant reduction of hydrogen bonds near the water/carbon tetrachloride interface and the dipole moments of water show preference of aligning along the interface.[51] The work by Zhang et al. suggest that there are inner and outer layers near the water-octane interface and that the water dipoles point in opposite directions at the different layers.[52]

Recently, Dai's research group has simulated the self-assembly and diffusion of nanoparticles in ionic liquid-water, and ionic liquid-oil systems.[53,54] For the IL/water system, the nanoparticles rapidly approached the IL–water interface and equilibrated more into the IL phase although they were initially in the water phase. In contrast, when the nanoparticles were dispersed in the hexane phase, they slowly approached the IL–hexane interface but remained primarily in the hexane phase. The different equilibrium positions of nanoparticles were explained by the calculation of potential of mean force

(PMF), in which the "energy well" of the PMF profile corresponds the equilibrium locations of nanoparticles in the IL-water and IL-oil system respectively. In addition, Interesting ordering and charge distributions at the IL-water, and IL-oil interfaces were also revealed in these studies.

In a later chapter, we will use Molecular Dynamics simulations as our tool to carry out a systematic numerical investigation of the effects of structural and chemical parameters of nanoparticles on diffusion kinetics at/across liquid-liquid interfaces. It is expected that a fundamental understanding of nanoparticle diffusion in liquid systems could be obtained from this study, and a microscopic mechanism theory could be proposed to explain macroscopic observations.

2.2.Ionic Liquids—Solvents of the Future

Ionic liquids (ILs) are salts in the liquid states, and they are also referred as "fused salts" or "molten salts".[55] Under most circumstances, including this report, ILs are particularly referred to as "room temperature ionic liquids"—the molten salts which melting point is below 100 ^{o}C.[56] Unlike common liquids, such as water and hexane, mostly consisting of electrically neutral molecules, ionic liquids are composed entirely of ions. On the other hand, unlike most ionic compounds, such as NaCl, which exists as crystalline structure at room temperature, the components of ionic liquids are irregularly shaped and do not readily form a crystalline lattice structure.[57] Thus, they remain in liquid status at room temperature and even to temperatures as low as -96°C.[28,58] Figure 2.5 gives a basic comparison of ILs to crystalline salts and conventional oils.[28]

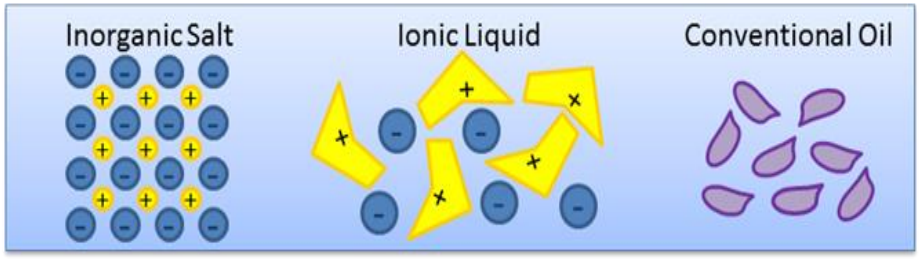

Figure 2-5 General comparison of inorganic salts, ionic liquids, and conventional oils. Adapted from reference 21.

Ionic liquids have many unique and fascinating properties. They can act much like good organic/inorganic solvents, dissolving both polar and nonpolar species. In many cases, they have been found to perform much better than traditional solvents.[59] One great advantage of ionic liquids is that they have far wider liquid ranges than molecular solvents. Liquid range, also known as liquidus range, is the temperature range between melting point or glass transition temperature and boiling point or thermal decomposition temperature.[60] Most ionic liquids slowly form glasses at low temperature, and these glass transition temperatures for ionic liquid tend to be very low (<-50 °C).[61] As for the upper limit of their liquid range, ionic liquids have effectively no vapor pressure, and hence cannot emit volatile organic compounds. This feature makes ionic liquids excellent candidates as "green solvents" to replace their air-polluting counterparts in existing chemical processes.[57] In most circumstances, the upper limit of ILs' liquidus range is determined by their thermal decomposition temperature, which tends to be higher than 200˚C.[62] Because of the high thermal stabilities of ionic liquids, they could be used in high temperature processing conditions without any solvents degradation. Taking 1-akyl-3-methylimidzaolium salts for example, their glass transition temperatures are ranging

from -70 to -90˚C; and their thermal decomposition temperatures are in the range of 250 to 450 ˚C. Therefore, the liquid range for 1-akyl-3-methylimidzaolium salts is over 300˚C.[63] By contrast, the liquid range of water is 100 ˚C, and 164 ˚C for hexane.[64] Another fascinating feature of ionic liquid is that they are highly tunable. The properties of ionic liquids such as solubility, density, viscosity, liquid range, etc. can be adjusted by modifying their cations and anions with considerable ease.[65] In theory at least, ionic liquids can be designed to deliver almost any set of physical and chemical properties for almost any applications, therefore, ionic liquids are also known as "designer solvent".[57,63,65]

Of interest in this study, we would like to discuss ILs miscibility and solubility characteristics in greater details. Generally speaking, the miscibility of ILs with water depends strongly on the ion species. ILs with highly-fluorinated and charge-delocalised anions, such as $[Tf2N]^-$, $[PF_6]^-$ and $[BF_4]^-$ are usually immiscible with water.[7] On the other hand, smaller anions with higher surface charge concentration usually exhibit stronger interaction with water and thus tend to be miscible with water. For example, halides, such as Cl^- and Br^- are mostly miscible with water. At the same time, cations (the positively charged ions) also have great impacts on ILs miscibility. As the length of the alkyl chains on cations increases, the ionic liquid tends to become less miscible. For example, the hydrophobicity of the $[C_n mim][BF4]$ series of ionic liquids increases as the alkyl chain length increases. In this series, ionic liquids with n=2-5 are miscible with water at room temperature while those with n>5 are not.[63]

The prediction schemes for ILs solubility are less straightforward. Solvent polarity is the most commonly used solvent classification to determine whether the

solvent is polar (e.g. water) or nonpolar (e.g. benzene). However, the concept itself is complex and usually nebulous, even when just considering ordinary molecular solvents; it is poorly understood and often confused. The solvation taking place in ionic liquids are usually far more complicated, the interactions between ILs and solute could include ionic interactions, hydrogen bonding, dipole interaction, van der Walls fore, and aromatic interaction[66] at the same time. Taking imidazolium-based ionic liquids[67] for example, the charged imidazolium ring and anion could have coulombic interactions with counter-ions, meanwhile, its nonpolar aliphatic chain could interact with non-polar species, such as n-hexane. The polarity of ionic liquids is usually determined empirically by means of spectroscopic techniques,[63,68,69] and Ionic liquids are generally considered polar solvents because they consist of ions and are therefore electrically charged. However, ionic liquids usually can dissolve both polar and non-polar solutes and they tend to be more strongly solvating than conventional organic molecular solvents.[63] By far, the solubility data of ionic liquids are far from enough, and our knowledge of ILs solvation mechanisms are insufficient.

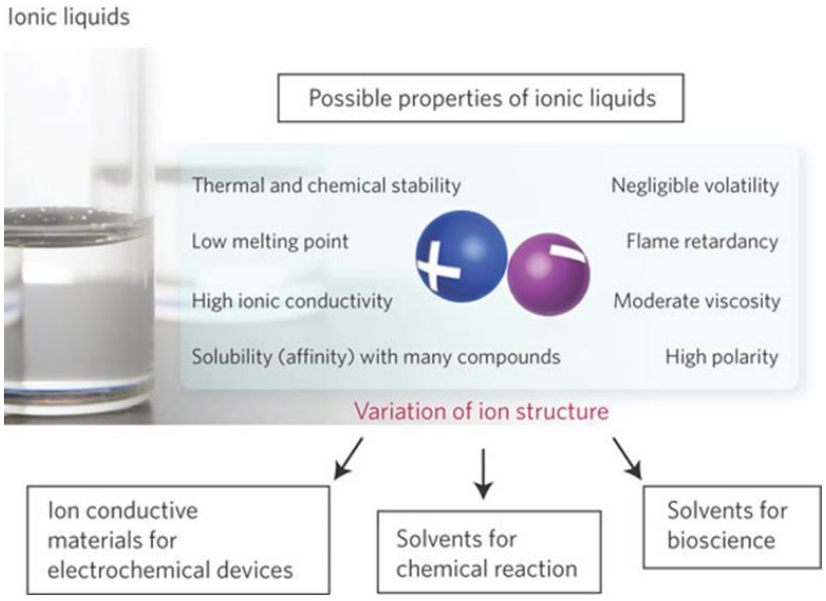

Figure 2-6 Schematic representation of ionic liquid-in-oil (IL/o) micro-emulsions containing drug molecules. Chemical structure of IL (b) and acyclovir (c). Adapted from reference 61.

As illustrated in Figure 2.6,[70] due to their unique physicochemical properties, ionic liquids have been explored for numerous applications, which range from energy storage and conversion to metal deposition, and can be used as reaction media in chemistry, biochemistry and even biomechanics.[70] One promising application of ILs is dissolution of natural biomaterials, especially of cellulose, one of the most abundant renewable resources in the world. Cellulose is produced at a rate of 10^{11} t /year in nature, dissolution of cellulose with ionic liquids allows the comprehensive utilization of cellulose by combining two major green chemistry principles: using environmentally preferable solvents and bio-renewable feed-stocks.[71] Cellulose consists of polydisperse linear glucose polymer chains which form hydrogen-bonded supramolecular structures; cellulose is insoluble in water and most common organic liquids.[72] Traditional cellulose dissolution processes, including the cuprammonium and xanthate processes, are often

cumbersome or expensive and require the use of unusual solvents, typically with high ionic strength and use relatively harsh conditions. Moreover, these processes sometimes cause serious environmental problems because these solvents cannot be recovered and reused[71]. Polar ionic liquids are promising solvents to solve these problems. Multiple studies on the preparation of polar liquids have shown that the key parameter for achieving the dissolution of cellulose is a strong hydrogen-bond-accepting ability of the selected ionic liquid.[70] This research indicated that 1-butyl-3-methylimidazolium chloride ($[C_4MIM]Cl$)[72] and 1-allyl-3-methylimidazolium chloride ([AMIM]Cl)[73] could be excellent solvents for processing cellulose.

In the past few years, ILs have also gained great interests for the application in pharmaceutical industry. For example, the association of water in otherwise water immiscible ionic liquids make them versatile materials for the containment of entrapped/solubilised drug, thus making them interesting reservoirs for controlled release.[74,75] Vikas Jaitely et al. explored the immiscible ILs /water system consisting of the hexafluorophosphate ($[PF6]^-$) salts of butyl, hexyl and octyl-3-methylimidazolium cations ($[BMIM]^+$, $[HMIM]^+$, $[OMIM]^+$, respectively) and found out the release of sucrose and dexametasone from ionic liquids reservoirs into water can be prolonged over 48 h, and the saturated solutions of these ionic liquids show little toxicity towards Caco-2 cells.[75] This research demonstrated the immiscible ILs/water system may serve as pharmaceutical excipients in a variety of scenarios. Ionic liquids also have been found to be particularly useful for the solubilization of poorly soluble drugs. Pharmaceutical industries have been posed challenges in the topical and transdermal administration of drugs which are poorly soluble or insoluble in water and most organic solvents, many

promising drugs never enter a formulation stage due to their poor solubility as well as difficulties in delivery. Moniruzzaman M. et al.[76] found that ionic liquid-in-oil micro-emulsion could be applied as a potential carrier of sparingly soluble drug. It demonstrated that the water/ILs micro-emulsion systems can dramatically enhance the formulation stability and permeation of acyclovir (a model for sparingly soluble drugs), meanwhile, the IL/water micro-emulsion system also provides low cytotoxicity. Taking these benefits together, IL/water micro-emulsion systems may serve as a versatile and efficient nano-delivery system for insoluble or sparingly soluble drug molecules that require solubilizing agents for delivery.

ILs represent a unique class of liquids and it has attracted great attention from various fields of studies. Research conducted on ionic liquids has grown rapidly over the last 15 years, new applications are proposed every year, and ILs are expected to be the "solvents of the future".[58] However, as previously mentioned, many fundamental aspects of ionic liquids are still poorly understood. For example, our knowledge of ILs solvation mechanisms is inadequate, especially when other solvents are also present at the same time, such as water. In the later chapters, we will use Molecular Dynamics simulations as our tool to investigate the impacts of IL on the diffusion and solvation behaviors of PNIPAM, a macromolecule, at immiscible ILs/water interface and in the miscible ILs-water mixtures. Atomic level details about the interactions between water, ionic liquids, and PNIPAM were revealed in our investigations. These computational results and atomic level analysis may provide some insights and explanations to the macroscopic solvation and diffusion behaviors of macromolecule in water-IL systems.

2.3. "Smart" Materials – Thermoresponsive Polymers

"Smart" materials, are designed materials which can show a dramatic change in properties in a controlled fashion upon a small or modest change of external stimuli. They are one of the most exciting merging classes of materials.[77–79] One of the main groups of "smart" materials is based on polymers because polymers are cheaper and more easily tailored than metals or ceramics.[80,81] Smart polymers or intelligent polymers exhibit significant property changes due to small changes of external factors in the environment including temperature, pH, light, magnetic or electric field, ionic factors, biological molecules, and so on.[78,79,81–87] Smart polymers have a wide variety of applications. By looking at only biomedical engineering, smart polymers have great potentials as delivery systems of therapeutic agents, tissue engineering scaffolds, cell culture supports, disoperation devices, sensors or actuators system.[81,83–85,88–91]

Thermo-responsive polymers are probably the most widely studied category among smart polymers. The normal body temperature of the human is 37°C, but under certain pathological conditions or in the presence of pyrogens, the body temperature deviates from normal. This change in temperature can be utilized as a stimulus for the delivery of drugs via temperature-responsive delivery systems.[89] Such polymers were usually introduced in the form of solution, enabling it to exhibit a volume phase transition at a certain temperature, which cause a sudden change in the solvation state.[81,88] If a thermo-responsive polymer solution is miscible below the critical temperature and becomes phase-separated upon heating. Such polymers have a lower critical solution temperature (LCST). If a polymer solution is phase-separated below the critical temperature and become miscible above the critical temperature, this kind of polymers are considered having an upper critical solution temperature (UCST).[81,88,92] A schematic

phase diagram to illustrate the concepts of LCST and UCST is indicated in Figure 2.7, which is adapted from the work of Mark A. Ward and Theoni K. Georgiou.[77]

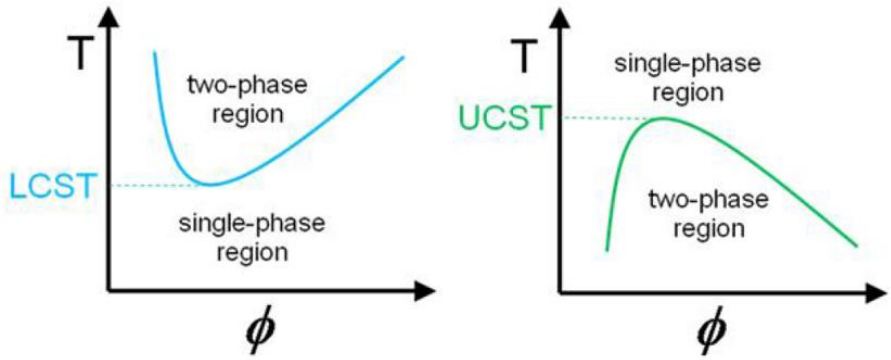

Figure 2-7 Phase diagram for a binary polymer-solvent mixture demonstrating (a) lower critical solution temperature (LCST) behavior and (b) upper critical solution temperature (UCST) behavior. Adapted from reference 68.

Most of the increased interests in thermos-responsive polymers are focused on those that exhibit LCST behavior in water due to their great potential in biomedical applications. These polymers are hydrophilic at low temperatures and turn to be hydrophobic at higher temperature. Below a certain temperature of the solution, the polymer is able to form hydrogen bonds with surrounding water molecules resulting in hydration. With the increased temperature, the hydrogen bonding strength is weakened and water molecules tend to be expelled from the polymer structure so that the polymer chains are partially dehydrated, which further promote the agglomeration of polymers. Since the phase separation is developed with the conformational changes of the polymer, a coil to globule transition can be observed in a thermos-responsive polymer immersed in water as shown in Figure 2.8.[93]

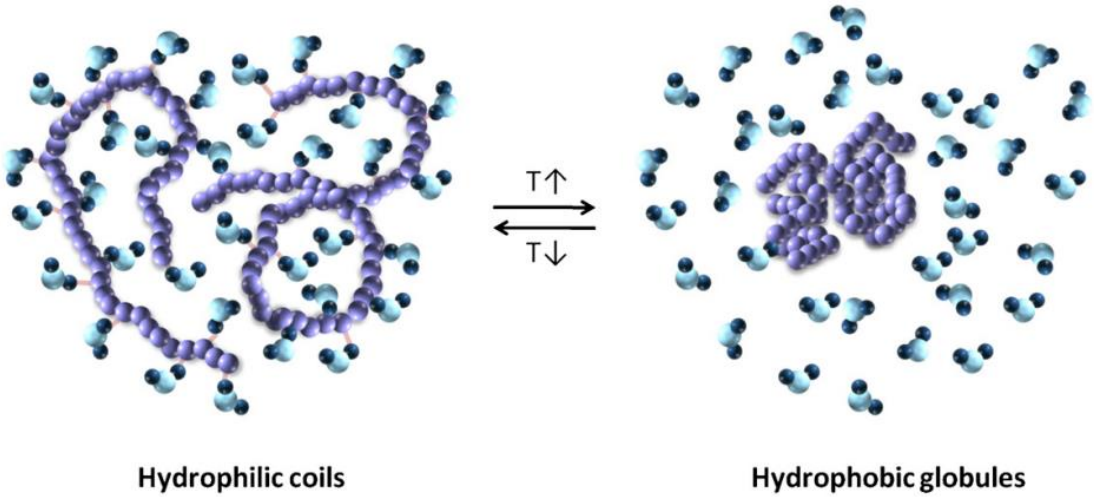

Figure 2-8 The reversible coil-to-globule transition in thermo-responsive polymers immersed in aqueous solution. Adapted from reference 82.

Among all reported thermo-responsive polymers, Poly(N-isopropylacrylamide) (PNIPAM) is one of the best-known and most intensively studied polymers. The aqueous solution of PNIPAM exhibit a reversible transition with a lower critical solution temperature (LCST) of 32˚C.[94] Below its LCST, this thermos-responsive polymer is hydrophilic and sustains a "swollen" or "extended" configuration; above its LCST, PNIPAM becomes hydrophobic and transformed into a "folded" or "coiled" structure. This sharp extended-to-coiled transition of PNIPAM was generally believed due to the presence of a hydrophilic amide group on the side chain and a hydrophobic isopropyl group in each N-isopropylacrylamide (NIPAM) unit as well as a hydrophobic carbon backbone.[88,95,96]

PNIPAM has a great potential for different applications.[81,83,84,87,97–103] Due to the importance of PNIPAM in both industrial and academic interests, numerous studies were conducted to investigate the diffusion and solvation behaviors of PNIPAM.[104–118] For example, in the study of Pang et al., solvation behaviors of a monomers of PNIPAM in

water/methanol mixtures with various component ratios are studied by molecular dynamics simulations.[104] It is found that the de-solvation process of PNIPAM will take place in the systems with methanol contents ranging from 0.25 to 0.80, in which the number of hydrogen bonding between PNIPAM and solvent molecules evidently decreases. Mukea et al. investigated PNIPAM hydrogels in water/ alcohol mixtures at 298.15 K. They measured the H-bonds between the hydrogel and the solvents with FTIR spectroscopy and found that the hydrogel is strongly dehydrated in the collapsed state.[116,118] Therefore, the hydrogel mainly interacts with itself when collapsed. Further, they measured a higher amount of alcohol in the hydrogel than in the bulk solvent, leading to a higher degree of swelling in several pure alcohols than in pure water at 298.15 K. This leads to the conclusion that methanol is the better solvent. Most of the previous studies were conducted in a pure water system or a homogeneous liquid system, which means the "third component" (besides water and PNIPAM) were either solutes (e.g. salts, surfactant) which are soluble in water, or co-solvents which are completely miscible with water. However, in reality, PNIPAM has been applied in the immiscible liquid-liquid system frequently. For example, PNIPAM based microgels have been widely used to stabilize environment responsive Pickering emulsion.[119–123] The diffusion and solvation behaviors of PNIPAM at a liquid-liquid interface have been barely reported, thus, a fundamental molecular level understanding of the interactions between PNIPAM and solvent molecules at liquid-liquid interface is still lacking.

In a later chapter, we will employ Molecular Dynamics (MD) Simulations to understand the detailed mechanism behind diffusion and solvation behaviors of PNIPAM at water/[BMIM][PF6] and water/[BMIM][TF2N] interfaces. A PNIPAM oligomers

consisting of 26 units were created for this study, in the validation part of our work, the extended-to-coiled transitions of PNIPAM were observed below and above its LCST in water phase. The gyration radius and the number of inter/intra-molecule hydrogen bonding of PNIPAM were calculated and compared with the previous studies, indicating our simulation results were consistent with experimental values and simulation results in the published works. The Radial Distribution Function g(r) between the cations/anions of the ionic liquids and amide O, N, as well as, isopropyl and carbon backbone of PNIPAM were examined. In addition, the equilibrium position of PNIPAM was obtained through simulation and explanations from the aspect of energy analysis and solute-solvent interactions at atomic level are provided in this report. To our best knowledge, it is the first molecular dynamics study which discussed the equilibrium position of PNIPAM at water/ionic interface below and above its LCST, and it is also the first report which provided an atomic level understanding of how cations and anions of ionic liquids interacts with different moieties of PNIPAM.

3. MOLECULAR DYNAMICS SIMULATION METHODOLOGY

Molecular Dynamics (MD) simulation has been a powerful tool to investigate the properties of assemblies of molecules in terms of their structure and the microscopic interactions between them. It serves as a bridge between microscopic length and time scales and the macroscopic world of the laboratory. Besides, MD simulation offers a unique opportunity to explore the microscopic world which cannot be studied by conventional experiments: the hidden details behind bulk measurement can be revealed by MD simulation.

All MD simulations in our investigation were performed using the GROMACS package, a widely used open-source and free software for dynamic simulations. It does not have a force field of its own, but is compatible with GROMOS, OPLS, AMBER, and ENCAD force fields. In addition, it can handle polarizable shell models and flexible constraints. The program is versatile, as force routines can be added by the user, tabulated functions can be specified, analyses can be easily customized, and a rich set of calculation types, preparation and analysis tools are provided by GROMACS package.[124,125]

3.1.Force Field

3.1.1. Gromos Force Fields

Gromos force fields have been broadly applied to MD simulations of proteins, nucleic acid, and organic molecules. In Chapter 3, nanoparticles and benzene were described by the Gromos53A6 force filed,[126–129] which was validated by the previous researchers[126] as a reasonably estimation of the real liquid benzene.

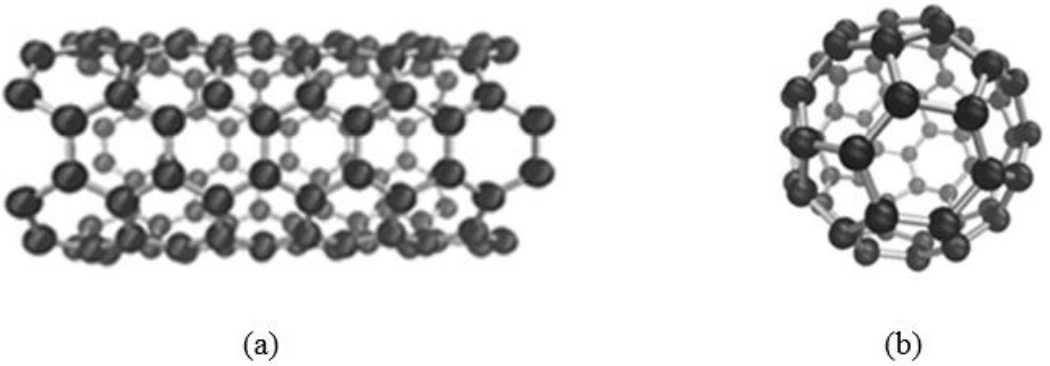

Figure 3-1 The (a) Single Walled Carbon Nanotube (SWCNT); (b) Bucky ball in the oil/water simulation system.

The geometrical structures of single-walled carbon nanotube (SWCNT) and buckyball were created by Nanotube Modeler, as shown in Figure 3.1. The Gromos54A7 forcefiled[129] was used to describe SWCNT[130,131] and buckyball.[132] We also performed simulation with Gromos53A6[127] and observed no changes in the systems behaviors.[133] The spherically modified hydrocarbon nanoparticles (0.6HCP, 1.2HCP), as shown in Figure 3.2 were formed by truncating a diamond-like lattice made of carbon atoms bonded in a non-planar hexagonal structure, and to increase the simulation efficiency, saturated with united CH, CH_2, and CH_3 atoms.[134,135] The force filed parameters for 0.6HCP and 1.2HCP were taken from the Gromos54A7 parameter set[127,129] to simulate rigid hydrophobic particles.[136,137] This structure has been used in previous simulation studies focused on interfacial self-assembly.[50,53,137–139]

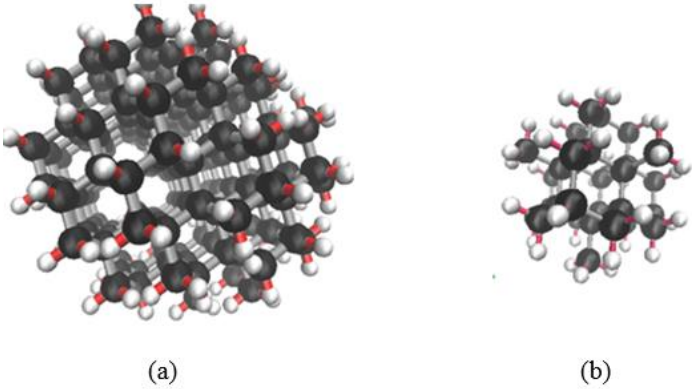

Figure 3-2 (a) Diameter = 1.2nm spherically modified hydrocarbon nanoparticles (1.2HCP); (b) diameter = 0.6nm spherically modified hydrocarbon nanoparticles (0.6HCP).

3.1.2. Optimized Potential for Liquid Simulations (OPLS)

OPLS (Optimized Potential for Liquid Simulations) is a set of force fields developed by Prof. William L. Jorgensen.[140] There are both united atom (OPLS-UA) and all atom (OPLS-AA) force fields. OPLS-UA includes hydrogen atoms next to carbon implicitly in the carbon parameters while OPLS-AA includes every atom explicitly. In our research, we created a 26-units PNIPAM oligomer (as shown in Figure 3.3) and applied OPLS-AA force field[141,142] to describe PNIPAM. OPLS-AA has been widely applied and validated by previous researchers[143–148] for the MD simulation of PNIPAM.

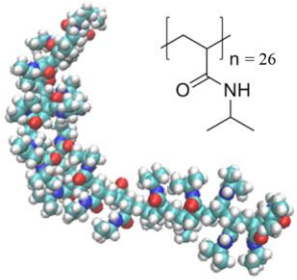

Figure 3-3 The 26-units PNIPAM oligomer (at extended status) employed in the simulation system.

For example, J. Walter et al. studied the conformation change of PNIPAM in water as a function of temperature both experimentally and by MD simulations.[148] Different force fields (GROMOS-87, GROMOS-96 53A6 and OPLS-AA) were applied to describe the PNIPAM-water system, and it turned out OPLS-AA well agreed with the experimental data. G. Kamath et al[147]. assessed four popular force field (AMBER, OPLS-AA, CHARMM and GROMOS) in terms of their ability to predict thermodynamic properties such as free energies of solvation, free energies of hydration and partition coefficient as a function of temperature, as well as densities and heats of vaporization of PNIPAM. They concluded that OPLS-AA can provide reasonable explanations of the mechanism behind the conformational change seen in the polymer across the lower critical solution temperature. E. Algaer and N. van der Vegt[143] studied PNIPAM in aqueous electrolyte solutions and link its "salting-in" and "salting-out" propensities to molecular-level structural details by using OPLS-AA force field. Aqueous solutions of NaF, NaCl, NaBr, NaI, $NaNO_3$, and $NaClO_4$ with PNIPAM were investigated. It was reported that all salts but NaI provoke a hydrophobic collapse transition of PNIPAM in water at 300 K, in qualitative agreement with experimentally measured salt effects on the lower critical solution temperature of this system.

The force field parameters applied on the ionic liquids in our simulation system (the chemical structures of the ILs cations and anions were illustrated in Figure 3.4) were also based on OPLS-AA force field, but some of the parameters were modified according to Bhargava and Balasubramanian's recommendation.[149,150] This set of force field parameters have been applied and validated by different publications,[53,54,151,152] in which

it has been confirmed that the force field not only provide reasonable values for ILs density but also gave accurate surface tensions and self-diffusion coefficients. Therefore, it is more suitable for modeling the interfacial behavior of ionic liquids. In this work, these optimized force field parameters were used to simulate the diffusion and solvation behaviors of PNIPAM at the ionic liquid-water interfaces and a miscible [BMIM][I]/water system. Table 3.1 listed more detailed information about the ionic liquids systems.

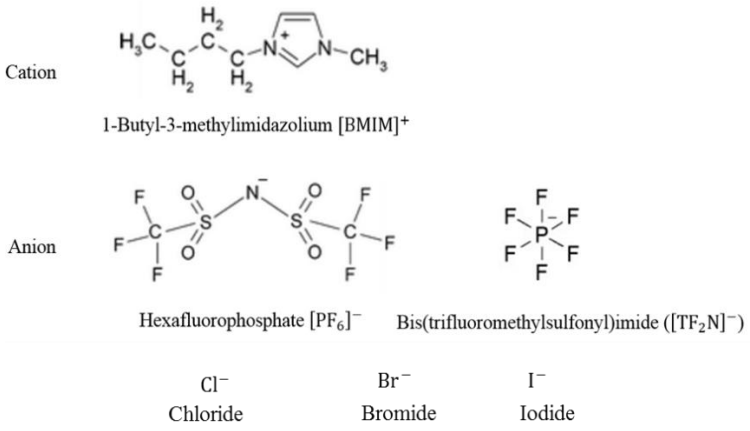

Figure 3-4 Chemical structure of the cation and anions of the ionic liquids in the water/miscible ILs solutions and water-immiscible ILs two phase simulation system.

Table 3-1 Summary of ionic liquid systems, with model source, and model verification

	# of IL Pairs	Force Field Parameters	Exp. ρ (kg/L)	Sim. ρ (kg/L)	% Error
[BMIM][PF_6]	350	Ref[149,153,154]	1.363	1.381	1.3%
[BMIM][Tf_2N]	250	Ref[150,155]	1.44	1.45	0.8%
10% [BMIM][I]/Water solution	300	Ref[140,155]	1.259	1.259	0.3%

3.2.Periodic Boundary Condition

Three-dimensional Periodic Boundary Condition (PBC) was applied in our simulation systems to remove the boundary effects caused by finite size of the simulation box. The simulation box was surrounded by virtually identical boxes in three dimensions, and the atoms in the simulation system can interact with those in the surrounding boxes, so the system would act more like an infinite one. A two-dimension system with Periodic Boundary Condition was illustrated in Figure 3.5. In the simulation, when a molecule moved in the central simulation box, all its periodic images in every simulation boxes moved with the same orientation and speed. Therefore, as a molecule leaves the central box, one of its images will enter through the opposite faces. There are no walls at the boundary of the central simulation box, the central simulation box simply provides a convenient coordinate system for measuring locations of the atoms in the simulation system.[156]

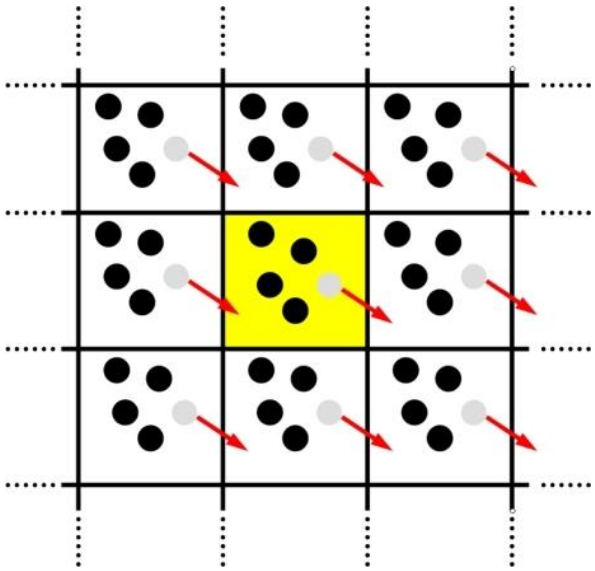

Figure 3-5 Two-dimensional schematic of periodic boundary conditions. The particle trajectories in the central simulation box are copied in every direction.[156]

3.3.Integration Method—Leap-frog Algorithm

Leap-frog algorithm was applied for the integration of the Newton's equations of motion. It is one of the most commonly used integration methods in MD simulations. The leap-frog algorithm uses positions r, at time t, and velocities v, at time $t - \frac{1}{2}\Delta t$; it updates positions and velocities using the forces F(t) determined by the positions at time t:[157]

$$\left(\boldsymbol{v} + \frac{\mathbf{1}}{\mathbf{2}}\boldsymbol{\Delta t}\right) = \mathbf{v}\left(\mathbf{t} - \frac{\mathbf{1}}{\mathbf{2}}\boldsymbol{\Delta t}\right) + \frac{\boldsymbol{\Delta t}}{\boldsymbol{m}}\boldsymbol{F}(\boldsymbol{t}) \qquad \text{(Equation 3-1)}$$

$$\boldsymbol{r}(\boldsymbol{t} + \boldsymbol{\Delta t})) = \boldsymbol{r}(\boldsymbol{t}) + \boldsymbol{\Delta t}\boldsymbol{v}\left(\boldsymbol{t} + \frac{\mathbf{1}}{\mathbf{2}}\boldsymbol{\Delta t}\right) \qquad \text{(Equation 3-2)}$$

The leap-from algorithm is visualized in Figure 3.6, and there are two primary strengths of leapfrog integration. First, it is time-reversible so that one can integrate forward n steps, and then reverse the direction of integration and integrate backwards n steps to arrive at the same starting position. The second strength is its symplectic nature, indicating that it conserves the energy of dynamical systems, even at relatively large time steps. Therefore, the computational time could be greatly decreased, and it is usually the method of choice in MD simulations. However, when extremely accurate velocities and positions are needed, the Verlet algorithm may be preferred.[157]

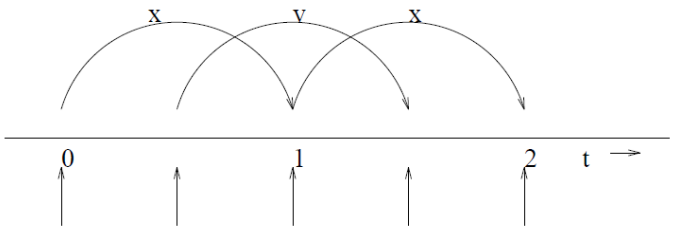

Figure 3-6 The Leap-Frog integration method. The algorithm is called Leap-Frog because r and v are leaping like frogs over each other's backs.[157]

3.4.NPT Ensemble

The experimental conditions in the lab usually include a fixed number of molecules N, constant pressure P, and constant temperature T. To mimic the reality, all our simulations were carried out under the NPT ensemble, which means in the simulation system there are constant number of molecules, and these molecules are under constant temperature and pressure.

In MD simulations, the temperature control can be realized by controlling the kinetic energy of the system. In our research, we applied "Berendsen thermostat"[158] to maintain the system's temperature. In this method, the system is weakly coupled to an external heat bath with given temperature T_0. The effect of this algorithm is that a deviation of the system temperature from T_0 is slowly corrected according to Equation 3-3:

$$\frac{dT}{dt} = \frac{T_0 - T}{\tau} \qquad \text{(Equation 3-3)}$$

where τ is the coupling parameter which determines how tightly the bath and the system are coupled together. It turns out that a temperature deviation decays exponentially with a time constant τ (Equation 3-4):

$$T = T_0 - Ce^{\frac{t}{\tau}} \qquad \text{(Equation 3-4)}$$

τ is used as an empirical parameter to adjust the strength of the coupling. Its value should be chosen with care. If the value τ is too big, such as $\tau \to \infty$, the Berendsen thermostat become inactive and the simulation is sampling a microcanonical ensemble (also termed "NVE" ensemble: constant number of molecules, constant system volume, and constant total energy). On the other hand, if the value of τ is too small, it will cause

unrealistically low temperature fluctuations. We choose τ=0.2ps, which is a typically value used in MD simulation[158].

The simulation systems' pressure was maintained by "Berendsen barostat".[158] The Berendsen algorithm controls the system's pressure by dynamically adjusting the size of the unit cell and rescaling all atomic coordinates during the simulation, as indicated in Equation 3-5

$$\frac{\boldsymbol{dP}}{\boldsymbol{dt}} = \frac{\boldsymbol{P_0 - P}}{\boldsymbol{\tau_P}} \qquad \text{(Equation 3-5)}$$

Where P is the instantaneous pressure, P_0 is the target pressure, and τ_P is the brostat relaxation time constant. In the isotropic implementation, at each step the cell volume is scaled by a factor, and coordinates and cell vectors by $\eta^{\frac{1}{3}}$:

$$\boldsymbol{\eta = 1 - \frac{\beta \Delta t}{\tau_P}(P_0 - P)} \qquad \text{(Equation 3-6)}$$

where β is the isothermal compressibility of the system, it is usually a specified constant which takes to be the isothermal compressibility of liquid water,[157] its exact value is not critical to the algorithm as it relies on the ratio $\frac{\beta}{\tau_P}$. τ_P is also termed pressure coupling time constant, and its value is usually recommended to be larger than 100 times the value of "time step" ($\tau_P > 100\Delta t$).[158] In our simulation, $\Delta t = 0.002ps$, and we chose 1ps as τ_P.

4. DIFFUSION OF NANOPARTICLES AT/ACROSS WATER-OIL INTERFACES

4.1.Introduction

The diffusion and self-assembly of nanoparticles at/across liquid-liquid interfaces are important in both natural and industrial applications. For example, the small size of the nanoparticles results in weak confinement of the nanoparticles at the liquid-liquid interface, which opens avenues to size-selective particle assembly.[8] Furthermore, there is a growing interest in solid-stabilized emulsions (Pickering emulsions) that use solid nanoparticles or microparticles as emulsion stabilizers: small particles can form a layer between the interface of the droplet (dispersed phase) and the continuous phase to inhibit the coalescence of droplets and generate kinetically stable emulsions.[25] However, the fundamentals of the diffusion and self-assembly of nanoparticles at/across liquid-liquid interfaces have not been fully explored. One of the remaining challenges is to understand multiphase interactions, self-assembly processes, and self-assembled structures of nanoparticles, especially when the size of the nanoparticles is comparable with the molecular dimension of the surrounding liquids.[50] For example, there are few reports on the effect of anisotropic particle shapes in Pickering emulsions.[26,159] In addition, the kinetics of particle adsorption onto liquid interfaces is also not completely understood.[26]

Molecular Dynamics (MD) simulations have been a powerful tool for understanding the properties of assemblies of molecules in terms of their structure and the microscopic interactions between them. It serves as a bridge between microscopic length and time scales and the macroscopic world of the laboratory. Besides, MD simulations offer a unique opportunity to explore the microscopic world which cannot be

studied by conventional experiments: the hidden details behind bulk measurement can be revealed by MD simulation. For example, Moreira and Skaf[160] reported a significant reduction of hydrogen bonds near the water/carbon tetrachloride interface and the dipole moments of water show preference of aligning along the interface. The work by Zhang et al.[52] suggest that there are inner and outer layers near the water - octane interface and that the water dipoles point in opposite directions at the different layers. Recently, Dai's research group has simulated the self-assembly and diffusion of nanoparticles in water-oil, ionic liquid-water, and ionic liquid-oil systems,[50,137,138,151,161] providing insights into the transport and interfacial behavior of nanoparticles in liquid-liquid systems. However, systematic numerical investigation of the effects of structural and chemical parameters of nanoparticles on diffusion kinetics at/across liquid-liquid interfaces has not been carried out and is thus the focus of this work. It is expected that a fundamental understanding of nanoparticle diffusion in liquid systems could be obtained from this study, and a microscopic mechanism theory could be proposed to explain macroscopic observations. In this study, we have demonstrated that MD simulations can provide insight into nanoparticle diffusion in a water-benzene model system. Furthermore, a detailed discussion including simulation system validation, and the effects of size, shape, and surface composition on the self-assembly and diffusion behaviors of nanoparticles at/across water-benzene interface is given.

4.2.Methodology

All MD simulations were performed using the GROMACS 4.5.4 package.[162] The initial simulation box for each interfacial system was approximately 5.0 × 5.0 × 10.0 nm.[163] After the initial configurations were obtained, 1000 energy minimization steps

were performed using the steepest descent method. The leapfrog algorithm was used for integrating Newton's equation of motion with a time step of 0.002 ps. We performed NVT ((constant number of molecules, constant volume, and constant temperature) simulations for calculating the surface tension of benzene/air and benzene/water interfaces, and the Berendsen thermostat[158] was applied to maintain the system's temperature at 300 K. For simulating the water/oil/nanoparticle system, the NPT (constant number of molecules, constant pressure, and constant temperature) ensemble was applied, with the Berendsen thermostat and Berendsen barostat[158] used to couple the system to a temperature and pressure bath at 300 K and 1 bar, respectively. Periodic boundary conditions (PBC) were applied to all three directions of the simulated boxes. The initial atomic velocities were generated with a Maxwellian distribution at the given absolute temperature. The Particle-Mesh Ewald (PME) method was used for the long-range electrostatic interactions. The cut-off distance for Lennard-Jones forces was set as r = 1.4 nm. After the simulation, the physical properties were characterized using the GROMACS analysis tools, and the structures were visualized by Visual Molecular Dynamics (VMD).[164]

Water was described with a single point charge (SPC) model, which has been proven to perform well in simulating the water-oil system.[138] The topology and structure of benzene were generated by Automated Topology Builder (ATB) and Repository version 2.1.[165] Benzene was described by the Gromos53A6 force filed,[126–129] which was validated by the previous researchers[126] as a reasonably estimation of the real liquid benzene. The geometrical structures of single-walled carbon nanotube (SWCNT) and buckyball were created by Nanotube Modeler. The Gromos54A7 forcefiled[129] was used

to describe SWCNT[130,131] and buckyball.[132] We also perform simulation with Gromos53A6[127] and observed no changes in the systems behaviors.[133] The spherically modified hydrocarbon nanoparticles (0.6HCP, 1.2HCP) were formed by truncating a diamond-like lattice made of carbon atoms bonded in a non-planar hexagonal structure, and to increase the simulation efficiency, saturated with united CH, CH_2, and CH_3 atoms.[135,138] The forcefield parameters for 0.6HCP and 1.2HCP were taken from the Gromos54A7 parameter set[127,129] to simulate rigid hydrophobic particles.[137,139] This structure has been used in previous simulation studies focused on interfacial self-assembly.[50,53,137–139]

The Potential of Mean Force (PMF) provides information on how the system's energy changes as a function of general "reaction coordinates".[166,167] In this report, PMF calculations were used to examine how the system's energy changed as a function of the nanoparticle being pulled from the center of the water phase to the center of the benzene phase with respect to the z direction. We took snap shots of this pulling process with the nanoparticle at every 0.15 nm in the z direction, for about 5 nm total. These snapshots were then equilibrated for 5 ns each while restraining the particle in its respective position. The force required to restrict the nanoparticle was calculated and analyzed via the weighted histogram analysis method (WHAM)[168–170] and the profile of the PMF of the system in the z direction was generated.

4.3.Results and Discussion

As presented in Figure 4.1, the influence of the size of the nanoparticles was investigated by studying two nanospheres with the same surface features (saturated

hydrocarbons) but different sizes, including two types of spherical modified hydrocarbon nanoparticles: 0.6 nm in diameter (0.6HCP) and 1.2 nm in diameter (1.2HCP). The shape effects on the liquid-liquid interface behavior of the nanoparticles were explored by comparing the buckyball and SWCNT, which had the same surface feature (graphene), comparable size (as indicated in Table 4.1), but the shape of buckyball was symmetrical whereas the shape of the SWCNT was directional. Detailed information for the nanoparticles is shown in Table 4.1 Finally, the effects of the nanoparticle's surface composition were investigated by comparing the buckyball and 0.6HCP. Both nanoparticles have the same size and shape. However, the surface of the buckyball consisted of sp^2 carbon atoms, while the surface of 0.6HCP was composed of saturated hydrocarbons.

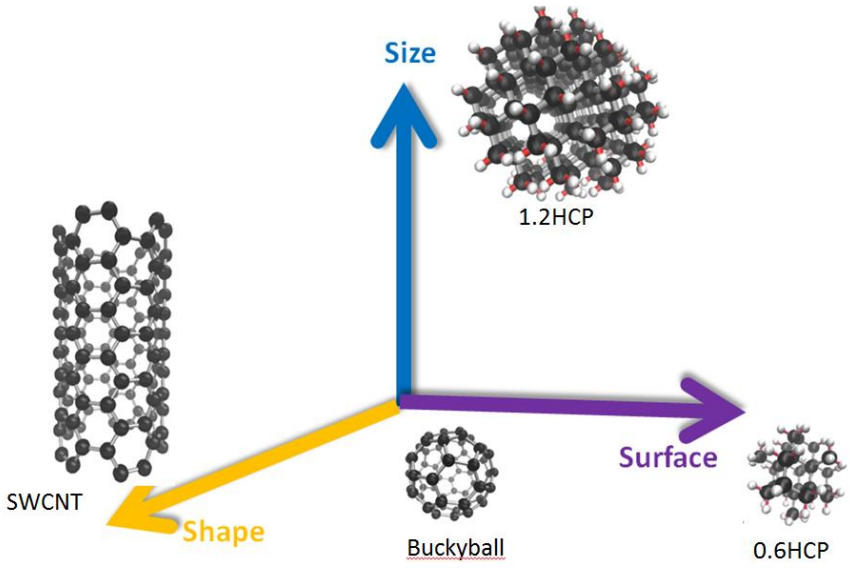

Figure 4-1 Schematic of the SWCNT, buckyball, and hydrocarbon particles used to investigate the effect of shape, size, and surface composition on the diffusion and self-assembly process of nanoparticles at a liquid-liquid interface.

Table 4-1 Detailed information of the studied nanoparticles.

Nanoparticle	Dimension		Carbon Number	Hydrogen Number
	Radius (nm)	Length (nm)		
SWCNT	0.32	1.2	120	0
Buckyball	0.34	-	60	0
0.6HCP	0.33	-	30	40
1.2HCP	0.62	-	171	128

4.3.1. Validation of the Simulation System

The liquid-liquid interfaces were simulated by placing a cubic water simulation box adjacent to a cubic benzene simulation box. The Gromacs 4.5.4 package contains a pre-equilibrated coordinate file for SPC water, and the water simulation box was verified by previous researchers;[50,138,163,171] so it was unnecessary to again equilibrate and validate the water simulation box.

The benzene boxes were equilibrated under NPT conditions (constant number of molecules, constant pressure, and constant temperature) for 5 ns. The purpose of this step was to make sure that the benzene box had correct density at1 bar and 300 K. Our simulation indicated that the benzene box achieved equilibrium after 3.7 ns, and the equilibrium density of the benzene box was 859.95 kg/m^3. Compared with the experimental value, 873.8 kg/m^3 in the literature[172], the error is within 2%, which suggests that our simulation system can provide reasonably accurate predictions of reality

The simulation system was also examined by calculating the surface tension of the benzene/air and benzene/water interface. We calculated the surface tensions of

benzene/air by doubling the z vector of the equilibrated boxes to form a liquid/gas surface, and then perform a 10 ns NVT MD simulation. The simulated value of surface tension of benzene/air was 27.0 ± 2.1 mN/m, which is comparable to the experimental value of 28.22 mN/m,[172] indicating a reasonable value of surface tension. To calculate the interfacial tension of benzene/water, we put an equilibrated benzene box adjacent to an equilibrated water box, and then performed a 10 ns NVT simulation. The simulation result of the benzene/water interfacial tension was 35.2 ± 2.7 mN/m. The surface tension measured by Cupple et. al.[173] was 32.67 ± 0.05 mN/m, which further indicated our simulation systems were a reasonably approximation to the real system and its interfacial behavior.

4.3.2. Effect of Nanoparticle Size

We investigated the effect of size by comparing the 0.6HCP and 1.2HCP. The diffusion coefficients of nanoparticles are estimated by monitoring the Mean Square Displacement (MSD) as a function of time, using the Einstein relation,[174] $\lim_{n\to\infty}\langle|r_i(t) - r_i(0)|^2\rangle = 6D_A t$, where $r_i(t)$ is the center of the mass position of the nanoparticle i at time t. The diffusion coefficients of the nanoparticles are calculated by taking the linear regression of the mean square displacement as a function of time. The comparison of the nanoparticles' MSD plots at z direction in water box are indicated in Figure 4.2, the inset table lists all the diffusion coefficient calculated from their MSD plots.

Table 4-2 Comparison of the nanoparticle diffusion coefficients in the water phase for the MD simulation and the SE equation, respectively

	D_{MD} $(10^{-5}\,cm^2/s)$	D_{SE} $(10^{-5}\,cm^2/s)$
0.6HCP	3.61 ± 0.08	2.52
1.2HCP	4.33 ± 0.15	1.26

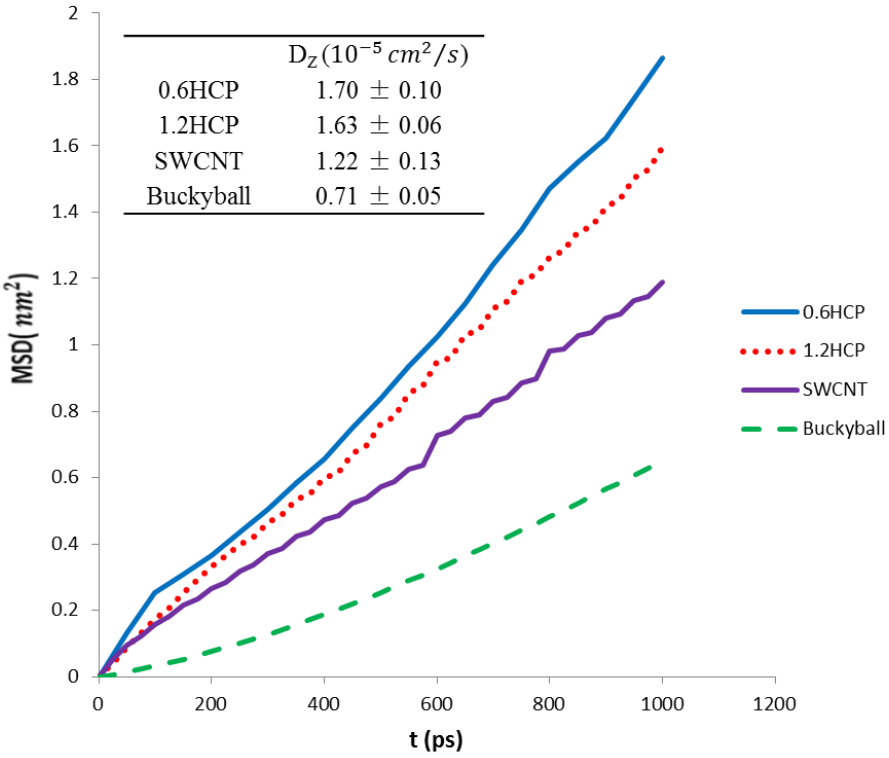

Figure 4-2 Mean Square displacement (MSD) plots of nanoparticles at z direction in water phase within the first 1ns. The 0.6HCP is indicated by a solid blue line, 1.2HCP by a dotted red line, SWCNT by a solid purple line and buckyball by a dashed green line. The inset table indicated the diffusion coefficient calculated from the slope of the mean square displacement plots

The most common basis for estimating diffusion coefficients of particles in liquids is the Stokes-Einstein (SE) equation,[174] $D = \frac{k_B T}{6\pi\eta a}$, where D is the diffusion coefficient, k_B is the Boltzmann's constant, T is the absolute temperature, η is the

viscosity of the fluid, and a is the particle radius. In our simulation system, the viscosity of SPC water is 0.30±0.05cp and we used the simulated viscosities of water to estimate the diffusion coefficients since the nanoparticles are immersed in such media.[137] Table 4.2 shows that the simulated diffusion coefficients in z direction were larger than those calculated from the SE equation. Previous studies also showed that the diffusion coefficient of nanoparticles was larger than that predicted by the SE equation. For example, Cadmium Selenide nanoparticles were found to diffuse 200 times faster in a polymeric liquid than predicted by the SE equation due to the small size of the nanoparticles.[175] One possible explanation for the failure of the SE equation is that the SE equation is derived by assuming a rigid solute sphere diffusing in a continuum of solvent. When the solute radius is less than five times that of the solvent, the SE equation usually breaks down.[176] The effectiveness of the SE equation may even become worse as the solute size becomes smaller and smaller.[177] In our simulation, 1.2HCP is approximately 4 times larger than the water molecule (0.27 nm) and the 0.6HCP is about the same size of water molecule. In addition, the SE equation assumes that the interaction between the particles and the liquids is isotropic. However, in our system, there is a water/benzene interface, which is not isotropic in all three directions. We may indicate how anisotropic our system is by the profile of the PMF: Figure 4.3 (a) shows the calculation of the PMF with respect to the z direction for both 0.6HCP and 1.2HCP, with the approximate position of the water/benzene interface at z = 0 nm. The PMF decreases dramatically as the particle approaches the interface. This suggests that our system is directional, that there is a driving force pointing toward the benzene direction. The first derivatives of the PMF are plotted in Figure 4.3 (b), and two observations can be made from Figure 4.3 (b).

First, the absolute value of the first derivative of PMF, d(PMF)/dz is larger for 1.2HCP than for 0.6HCP, indicating a stronger driving force on 1.2HCP. According to the estimation of SE equation, the diffusion coefficient of 1.2HCP should be half of 0.6 HCP. However, this study demonstrates that the diffusion coefficients of 1.2HCP and 0.6HCP are very close to each other, as shown in Figure 4.2. Second, the minimum value of the PMF appears near the interface of benzene/water at the benzene side, which is similar to the calculations of Frost et al. for the hexane/ionic liquid and water/ionic liquid systems.[151] In the referenced simulations, the minimum value of the PMF also approached the liquid/liquid interface and the nanoparticles eventually equilibrated at positions which correspondent to the minimum value of the PMF.

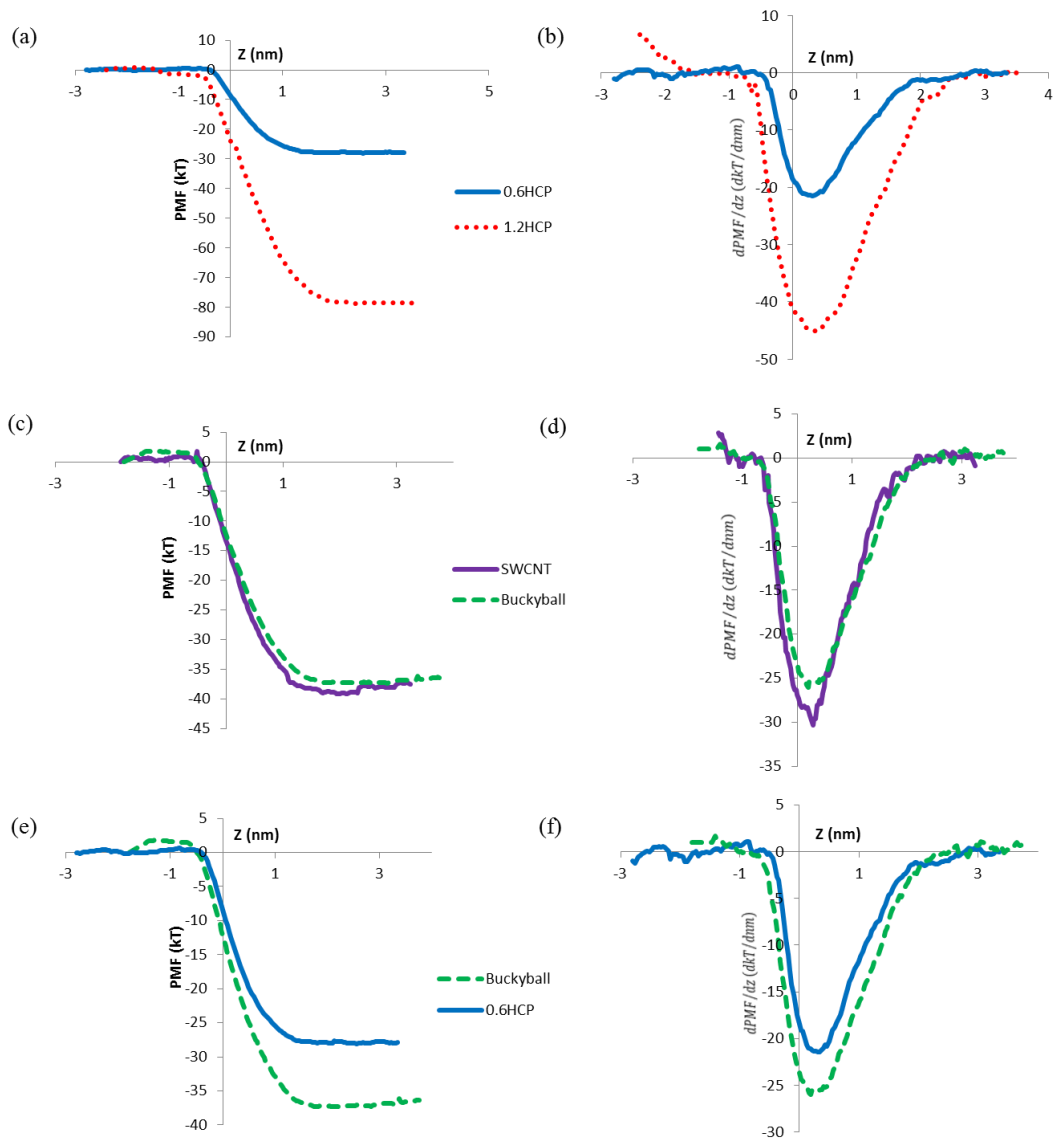

Figure 4-3 Plots on the left (a, c, e) illustrate comparisons of the Potential of Mean Force (PMF) and plots on the right (b, d, f) show the corresponding first derivatives of the PMF for 0.6HCP *vs* 1.2HCP, buckyball *vs* SWCNT, and buckyball *vs* 0.6HCP. The 0.6HCP is indicated by a solid blue line, the 1.2HCP by a dotted red line, SWCNT by a solid purple line and the buckyball by a dashed green line. The water/benzene interface is at z = 0 nm.

Another interesting observation is that when the nanoparticles pass through the interface, the speed of the large nanoparticles seems to decrease, lingering around the interface at the benzene side for a while. However, the small nanoparticle seems to pass

through the interface quite smoothly. Figure 4.4 shows snapshots of the 0.6HCP and 1.2HCP at various times, indicating the time necessary for the 0.6HCP and 1.2HCP to pass through the interface and to the center of the benzene phase. The 1.2HCP "vibrated" and moved laterally near the interface, and it took 4,800 ps to move from the interface to the center of the benzene phase. While for the small particle, it moved to the center of the benzene phase in a quite straightforward manner and it only took 1,000 ps. This phenomena maybe explained by the particles' desorption energy (Equation 4-1)[178]:

$$\Delta G = \pi a^2 \gamma_{ow} (1 \pm cos\theta)^2 \qquad \text{(Equation 4-1)}$$

where a is the particle radius, γ_{ow} is the oil-water interfacial tension, and θ is the three-phase contact angle measured through the water phase. The sign inside the bracket is positive for absorption into or desorption from oil and negative for absorption into or desorption from water. This calculation for particle desorption energy quantifies how strongly particles are held at the interface. According to a previous study,[26] for particles with intermediate hydrophobicity in the size range from several nanometers to several microns, the desorption energy is significantly higher than the thermal energy of 1 kT, so the particles are attached at the interface irreversibly.[30] For extremely small particles (radius $\leq$ 1 nm), the desorption energy becomes comparable to the thermal energy (kT) and the particles might detach from the interface.[179] In our simulation, the radius of 1.2HCP is 0.6 nm, thus the effect of the desorption energy is about 9.7 kT,[26] which starts to show its influence, while for the 0.6HCP, the desorption energy is only about 2.4 kT,[26] which is comparable to the thermal energy, so no "hesitation" is observed when the 0.6HCP passes through the interface.

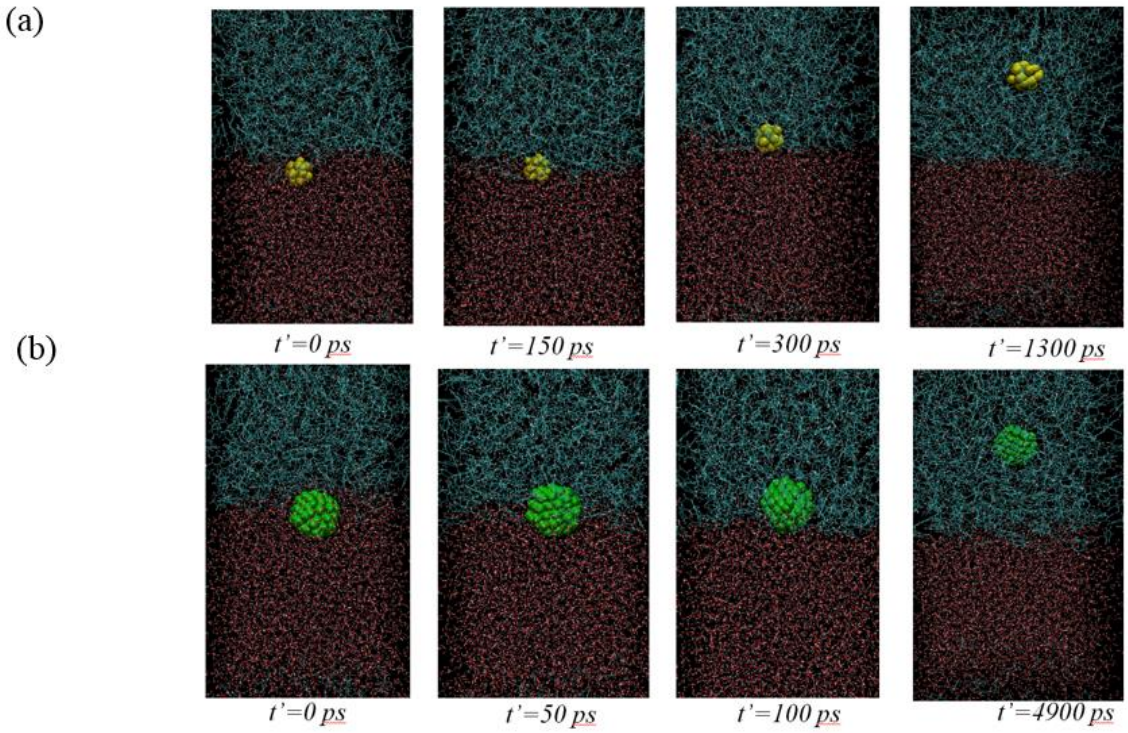

Figure 4-4 Snap shots of the nanoparticles at various times. The time was rescaled to compare the time for the movement of the (a) 1.2HCP and (b) 0.6HCP to travel from the water/benzene interface to the approximate center of the benzene phase. The 1.2HCP and 0.6HCP were represented by green and yellow ball, and the water and benzene molecules were represented by the red and blue molecules, respectively.

4.3.3. Effects of Nanoparticle Shape Configuration

The effect of a nanoparticle's shape configuration was investigated by comparing buckyball and SWCNT. Both of them have comparable dimensions (as indicated in Table 4.1) and the same surface composition (graphene), but the shape of a buckyball is totally symmetrical, while the shape of a SWCNT directional. If we compare the MSD of the buckyball and SWCNT in Figure 4.2, it is obvious that the diffusion coefficient of SWCNT in the z direction is much larger than that of the buckyball. We calculated the PMF and the numerical differentiation of the PMF for both SWCNT and buckyball. As

illustrated in Figure 4.3 (c) and (d), we can see that the absolute value of the dPMF/dz of the SWCNT is quite close to that of the buckyball. Therefore, we cannot explain the bigger diffusion coefficient of SWCNT by the difference of the driving force on them.

However, if we compare the radial distribution (rdf) functions of the water molecules with respect to the center of mass of the buckyball and SWCNT in the water phase, we can see that there is a notable difference between the buckyball and SWCNT in the rdf plot: as indicated in Figure 4.5 (a zoomed-in view of the comparison between buckyball and SWCNT isillustrated in inset (a)) there is a sharp peak in the rdf plot of the buckyball in water, which indicates an accumulation of solvent molecules surrounding the surface of the buckyball, and also suggests a better-defined solvent layer for the buckyball. The solvent layers around water-solvated species (solvation shell, or hydration shells) have been studied both theoretically and experimentally[180] with particularly focus on solvated proteins.[181,182] A few studies have reported the solvation shells around colloidal particles in both water[183] and oil[184] and suggested that the shells originate from weak interactions between the particle surface and the solvent molecules. We hypothesize that the formation of better-defined solvent layers for the buckyball is due to its shape and the carbon distribution on its surface. Because of the perfect spherical shape of the buckyball, solvent molecules can be packed closely as a spherical shell surrounding its surface. Additionally, because carbon atoms are evenly distributed on the surface of the buckyball, the interaction force between the buckyball and solvent molecules can also form a perfect spherical shell, while for the carbon nanotube there are two open ends, and this uneven distribution of carbon could deform the interaction force field between the carbon nanotube and the solvent molecules and destroy the structure of the “solvent

shell" as well. Therefore, the smaller diffusion coefficient of the buckyball may be explained by the formation of the solvent shell: when the buckyball migrates in the solvent, a thickened layer of solvent travels with it. Thus, its "effective radius" (e.g., the radius associated with the "solvent shell") is actually larger than the radius of the particle itself.

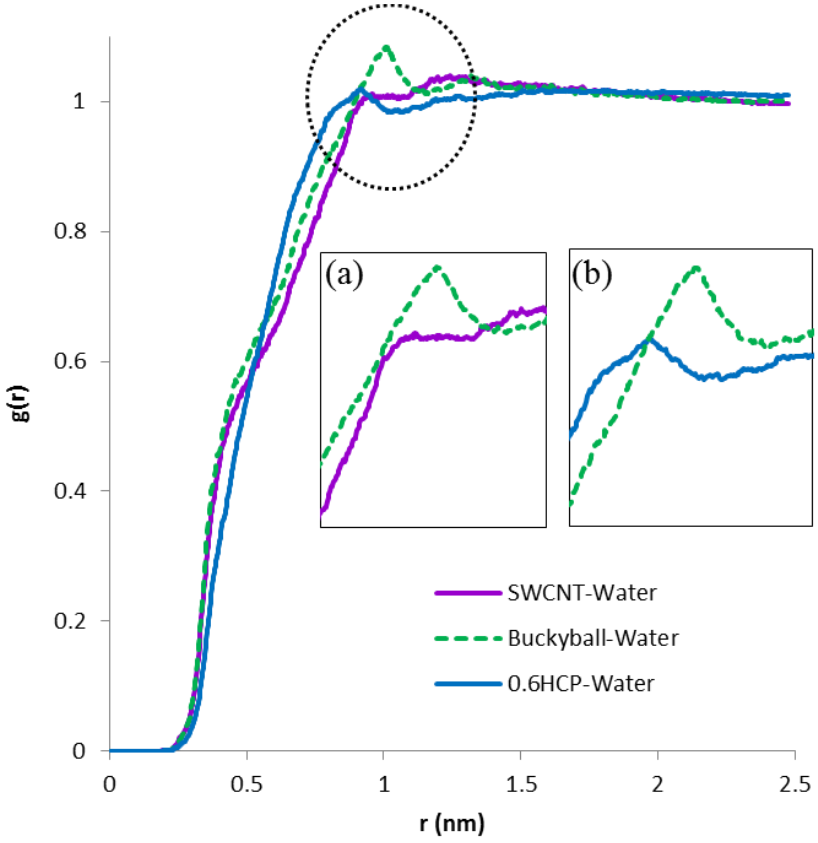

Figure 4-5 Radial distribution function (rdf) of: water molecules around the buckyball in the water phase, water molecules around the SWCNT in the water phase and water molecules around 0.6HCP in the water phase. Inserts (a) and (b) are zoomed-in comparisons of buckyball vs SWCNT and buckyball vs 0.6HCP. The SWCNT is indicated by the solid purple line, buckyball by the dashed green line, and 0.6HCP by the solid blue line.

4.3.4. Effect of Nanoparticle Surface Composition

The effect of the surface composition was studied by comparing the buckyball and 0.6HCP, which have a similar shape (spheres) and similar diameters (d ≈ 0.6 nm), but the surface of the buckyball is made of graphene, while the surface of 0.6HCP is composed of saturated hydrocarbons. As indicated in Figure 4.2, although the 0.6HCP and buckyball have a similar shape and size, the diffusion coefficient of the 0.6HCP is significant larger than that of the buckyball in water. The PMF of the 0.6HCP and buckyball is depicted in Figure 4.3 (e), with the numerical differentiation of the PMF illustrated in Figure 4.3 (f). As we can see, the absolute value of the PMF of the 0.6HCP and buckyball is quite close when they are in the water phase. The most noticeable difference between the 0.6HCP and buckyball system is again in their radial distribution function. As illustrated in Figure 4.5 (the detailed comparison between buckyball and 0.6HCP isillustrated in inset (b)), the peaks of the radial distribution of water molecules for 0.6HCP areweaker than those of the buckyball. Unlike the surface of the buckyball, the atoms on the surface of the 0.6HCP are not all the same and evenly distributed, which results in the asymmetry of the interaction force field, and thus perturb and distort the structure of the solvation shell. Although the buckyball and 0.6HCP have the similar sizes, the solvent layers make the effective radius of the buckyball larger than that of the 0.6HCP causing a smaller diffusion coefficient of the buckyball compared to the 0.6HCP.

4.4.Conclusion

In this paper, we have systematically investigated the effects of size, shape, and surface composition on the diffusive behaviors of nanoparticles at/across water-oil

interfaces via molecular dynamics simulations. Specifically, four different types of nanoparticles were studied. We found that the diffusion coefficients of the 0.6HCP and 1.2HCP are larger than that predicted by the SE equation. We attribute the deviation from the SE equation to two reasons: first, because the particle size is comparable to the size of the solvent molecules, the viscosity in the original SE equation is overestimated and certain modifications are needed; second, the anisotropy of the system also makes the diffusion coefficients for the nanoparticles different from the estimation of the SE equation. We then proposed that the first derivative of the PMF (d(PMF)/dz) serves as a driving force in the z direction. In addition, the simulation indicates that the solvation shell of the nanoparticles is influenced by their shape and surface geometry. A highly symmetrical nanoparticle with uniform surface such as a buckyball may lead to a uniform interaction force filed with the solvent molecules, so that a better defined solvation shell is formed, and this solvation shell makes the "effective radius" of the nanoparticle larger than its own radius, which causes a decrease in the diffusion coefficient. We will further investigate this hypothesis by conducting simulations of nanoparticles with different shapes and surface chemistries.

5. INTERFACIAL BEHAVIOR OF PNIPAM AT WATER-ILS INTERFACES

5.1.Introduction

As we introduced in Chapter 1, the aqueous solution of PNIPAM exhibit a reversible transition with a lower critical solution temperature (LCST) of 32˚C.[94] The sharp extended-to-coiled transition of PNIPAM is caused by the presence of a hydrophilic amide group on the side chain and a hydrophobic isopropyl group in each N-isopropylacrylamide (NIPAM) unit as well as a hydrophobic carbon backbone as seen from the chemical structure of PNIPAM in Figure 5.1.[88,95,96]

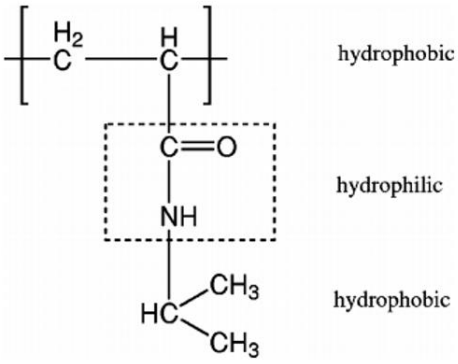

Figure 5-1 The chemical structure of PNIPAM including the hydrophobic carbon backbone and an isopropyl group and a hydrophilic amide group in each repeat unit.

It is most widely accepted that entropy effect is the mechanism to explain this thermal-induced phase behavior of PNIPAM; when the temperature is below its LCST, hydrogen bonds are formed between the amide groups and the water molecules, so the negative enthalpy term from hydrogen bonding donates the free energy (Equation 5.1). In this case PNIPAM is highly solvated and possesses a hydrophilic extended status. However, once the temperature is elevated, the hydrogen-bonding between the water

molecules and polymer becomes broken, at the same time, the water molecules are less ordered, so the entropy of this polymer-water system dominates (second term in Equation 5-1), therefore PNIPAM exhibits a hydrophobic coiled structure in aqueous solution.[81,94,185]

$$\Delta G = \Delta H - T\Delta S \qquad \text{(Equation 5-1)}$$

PNIPAM is a highly versatile polymer, and it can be adapted to microgels, liposomes, micelle, and membranes. By adding additives and copolymerization, PNIPAM-based products can be not only responsive to temperature but also various environmental stimuli such as PH, electric and magnetic field, and ionic strength.[186–192]

For example, Dai's and Jiang's research groups have demonstrated the capability of integrating PNIPAM hydrogel with thin film silicon ribbons, and enable the stiff silicon ribbons to become adaptive and drivable by the soft environmentally sensitive substrate.[193,194] This integration provides a means of mechanical buckling of the thin silicon film due to changes in environmental stimuli (e.g., temperature, pH). Shen, et al.[103] proposed a PNIPAM based novel drug delivery system to perform cancer treatment. The conventional cancer therapy has serious adverse effects, such as the indiscriminate distribution of cytotoxic drug in the body without targeting, insufficient local drug concentration in the tumor and poor controlled drug release. In Shen et al.'s study,[103] a novel PNIPAM based drug delivery system was fabricated to address these shortcomings. The magnetic Fe_3O_4 nanoparticles (MNP) and anticancer drug 5-Fu were encapsulated by PNIPAM and mesoporous silica film. These nanoscale drug-delivery vehicles can be directly implanted or injected into the tumor sites. When the temperature was below the LCST, the PNIPAM chains were expanded and the drug was mainly stored in the

composite. On the other hand, when they were subjected to an alternating magnetic field, the magnetic energy would be transformed to thermal energy by the Fe_3O_4 nanoparticles, and the temperature of the tumor would be locally elevated above LCST, so the polymer chains would shrink and then the drug would be excreted from the Fe_3O_4/PNIPAM/5-Fu@mSiO_2 composite. The tumor cell can be killed in an isolated fashion by this novel drug delivery system. In the field of tissue engineering, Okano and co-workers have produced "cell sheet" by growing cells (e.g. endothelial cells) on PINIPAM thin films.[195] Traditionally, cells were usually dissociated from a culture surface by using digestive enzymes and chelating agents, which would destroy cell–cell junctions and can only produce single cell suspensions. In Okano's study, the cells, which surfaces were hydrophobic were initially spread and proliferated on the PNIPAM-grafted surface at 37˚C, which was also hydrophobic above LCST. After the cells on the film reaching confluency, the sample was cooled down to 20˚C, so the PNIPAM-grafted surface became hydrophilic and the cells would detach from it as a piece of "cell sheet"— a contiguous intact monolayers of cells. This method allows cell confluency maintenance post-harvest in large area sheets and these monolayers of cells have also maintained basal surface extracellular matrix proteins after detachment.

Recently, there are growing interests in the diffusion and solvation behaviors of PNIPAM-based products at liquid-liquid interface due to remarkable features of PNIPAM. For example, In T. Ngai et al.'s study,[186,187,192] PNIPAM-based microgel was applied as the emulsion stabilizer between liquid-liquid interface, and it found out that PNIPAM-based microgel particles behave distinctly differently from the conventional solid particles at the liquid-liquid interface, one unique feature is that the stability of

emulsions can be triggered by changing the environmental conditions such as temperature, pH, or ionic strength.[186–189,192] This tunable stabilizing property is especially desirable in industrial applications such as fuel production and oil transportation processes where the emulsions can be prepared and broken on demand.[187] In Zhifeng Bai et al.'s study,[196] a PNIPAM-based "micelle shuttle" was reported: at room temperature, the PNIPAM-PEO copolymers reside preferentially in the water phase, upon heating, the micelles were formed, and they transferred spontaneously to the hydrophobic ionic liquid phase. And the entire process was totally reversible by cooling down the system. Therefore, a controllable micellization/demicellization were realized by changing the environmental temperature. This interesting phenomenon could have potential applications in various fields of study. For example, it could enable recycling of valuable payloads such as catalysts. In addition, this PNIPAM-based micelle system could realize loading/releasing active ingredients via external stimuli such as temperature and PH for drug delivery.

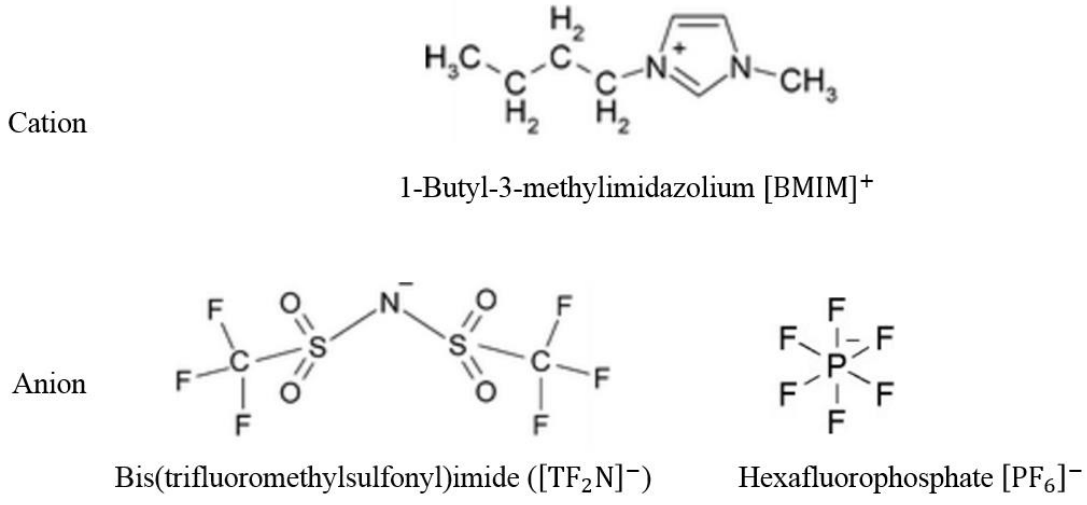

Figure 5-2 Chemical structure of the cation and anions of the ionic liquids in the simulation system.

Although PNIPAM and PNIPAM-based products have drawn numerous attentions both from academia and industry for many years, our understanding of diffusion and solvation behavior of PNIPAM at liquid-liquid interfaces is far from clear. Very few experimental and simulation work have been conducted to investigate the interactions between solvent molecules and PNIAPM at liquid-liquid interface. Particularly, we know nothing about configuration and diffusion of PNIPAM at/across water/ionic liquid interface. Ionic liquids (ILs) represent a unique class of liquids and it has attracted intensive investigations from various industries. There are some remarkable properties of ionic liquids. For example, ILs have negligible vapor pressure, high thermal stability, and their physiochemical properties are highly tunable by modifying their cations and anions. Thus, ionic liquids are often referred as "green solvents", and "designer solvents". In this study, a chain of PNIPAM polymer was investigated by Molecular Dynamics (MD) simulations in its extended and coiled status at the interface of water with [BMIM][PF_6], and with [BMIM][TF_2N]. Figure 5.2 illustrated the chemical structures of the ionic liquids, these two ILs have the same cation, and both are immiscible with water but their anions exhibit starkly different morphology and hydrophobicity: $[Tf_2N]^-$is long and nonisotropic in shape, whereas $[PF_6]^-$ is smaller and perfectly symmetrical, as a result, $[Tf_2N]^-$ is more hydrophobic than $[PF_6]^-$.

Molecular Dynamics (MD) simulations have been a powerful tool for understanding the properties of assemblies of molecules in terms of their structure and the microscopic interactions between them. It serves as a bridge between microscopic length and time scales and the macroscopic world of the laboratory. For example, in the study of Pang et al.[104], solvation behaviors of a monomer of PNIPAM in water/methanol

mixtures with various component ratios are studied by molecular dynamics simulations. It was found that the de-solvation process of PNIPAM took place in the systems with methanol contents ranging from 0.25 to 0.80, in which the number of hydrogen bonding between NIPAM and solvent molecules evidently decreased. Honbo Du et al.[197] studied the effects of salt on the LCST of PNIPAM. MD simulations of PNIPAM in 1 M of NaCl, NaBr, NaI, and KCl were carried out to elucidate the interactions between salt ions and PNIPAM. Their results suggested that cations had a much stronger affinity with the polymer, whereas anions bind weakly with the polymer. Moreover, the cation−polymer binding affinity was inversely correlated with the cation−anion contact pair association constant in solution.

In our study, we have employed Molecular Dynamics (MD) Simulations to investigate the detailed mechanism behind diffusion and solvation behaviors of PNIPAM at water/ [BMIM][PF6] and water/[BMIM][TF2N] interfaces. A PNIPAM oligomers consisting of 26 units were created for this study, in the "validation" part, the extended-to-coiled transitions of PNIPAM were observed below and above its LCST in water phase via MD simulation. The gyration radius and the number of inter/intra-molecule hydrogen bonding of PNIPAM were calculated and compared with the previous studies, indicating our simulation results were consistent with experimental values and previous simulation results in the published works. The Radial Distribution Functions (RDF) between the cations/anions of the ionic liquids and amide O, N, as well as, isopropyl and carbon backbone of PNIPAM were examined. In addition, the equilibrium positions of extended/coiled PNIPAM were obtained through simulation, and explanations from the aspect of energy and molecular interactions at atomic level were provided in this report.

To our best knowledge, it is the first molecular dynamics study which discussed the equilibrium position of PNIPAM at water/ionic interface below and above its LCST, at the same time, it is also the first report which provided atomic level of understanding about how cations and anions of ionic liquids interacts with different moieties of PNIPAM in a water-ILs biphasic system.

5.2.Methodology

All MD simulations in our investigation were performed using the GROMACS package, a widely used open-source and free software for dynamic simulations. The water-ILs interfaces were created by placing a cubic box of water adjacent to a cubic box of an IL and the initial simulation box for each interfacial system was approximately 5.0 × 5.0 × 10.0 nm.[163] After the initial configurations were obtained, 1000 energy minimization steps were performed using the steepest descent method. The leapfrog algorithm was used for integrating Newton's equation of motion with a time step of 0.002 ps.

We employed NPT (constant number of molecules, constant pressure, and constant temperature) ensemble to simulate the PNIPAM-Water-ILs system. Berendsen barostat[158] was applied to maintain the system's pressure at 1bar, and Berendsen thermostat[158] was employed to keep the system's temperature below PNIPAM's LCST (32˚C) and above LCST respectively. Periodic boundary conditions (PBC) were applied to all three directions of the simulated boxes. The initial atomic velocities were generated with a Maxwellian distribution at the given absolute temperature. The Particle-Mesh Ewald (PME) method was used for the long-range electrostatic interactions. The cut-off

distance for Lennard-Jones forces was set as r = 1.2 nm as was done by the developers of the force field.[155] After the simulation, the physical properties were characterized using the GROMACS analysis tools, and the structures were visualized by Visual Molecular Dynamics (VMD).[164]

Table 5-1 The source of force filed parameters for the ionic liquids in our simulation system

Ionic Liquids	Cation Force Field	Anion Force Field	Charge Scale
[BMIM][PF_6]	Ref[3,5]	Ref[7]	±0.8
[BMIM][Tf_2N]	Ref[3,5]	Ref[7]	±0.75

Water was described by the extended simple point-charge model (SPC/E), which has been demonstrated to perform well in the water/IL system[54,151]. A 26 units PNIPAM oligomer was created and OPLS-AA force field was employed to describe PNIPAM. OPLS-AA has been widely used and validated by previous researchers[143,144,146–148,198] for the simulation of PNIPAM. As for the ionic liquids, we have one cation—1-butyl-3-methylimidazolium (BMIM), and two different anions—hexaflurophosphate (PF_6) and bis(trifluoromethylsulfonylimide) (Tf_2N)—combined into two different ionic liquids in our simulation system. The model to describe ionic liquids were also based on the OPLS-AA force field, but their force filed parameters were modified based on Lopes et al.[150,155] and Bhargava et al.'s[149] publications. Table 5.1 provided more detailed information about the force field parameters of ionic liquids in our simulation system. The IL models were adapted for the specific systems studied by scaling partial atomic charges to give non-

integer total ion charges[54,154]. The technique of scaling charges in this manner has been extensively used to capture the effect of charge transfer between cation and anion in ionic liquids when using a non-polarizable force field[54,154,199]. This set of force filed parameters for ionic liquids were also carefully examined and validated by multiple researchers in Dai's group[53,54,151,152], and it has been proved not only lead to reasonable values for ILs density but also gave accurate surface tensions and self-diffusion coefficients[54,149,199], therefore, it is more suitable for modeling the interfacial behavior of ionic liquids, thus, we employed this optimized force field parameters to simulate the diffusion and solvation behaviors of PNIPAM at the ionic liquid-water interface.

5.3.Results and Discussion

The PNIPAM oligomer consisted of 26 monomers, and the extended and coiled configurations of PNIPAM were obtained by equilibrating the oligomer in the water box below and above its LCST for 15ns,. The extended and coiled PNIPAM were initially dispersed in the water phase and then, a 20-25ns MD simulation were performed to make sure the system had achieved the equilibrated status. More details of the simulation systems were indicated in Table 5.2.

Table 5-2 Summary of simulation systems with PNIPAM configuration, temperature, numbers of IL pairs, numbers of water molecules, simulation time and number of parallel runs

PNIPAM State	Temperature (K)	Ionic Liquid Phase	# of IL Pairs	# Water Molecules	Simulation Time (ns)	# of Parallel runs
Extended	300	[BMIM][PF_6]	350	3968	20	4
Extended	300	[BMIM][Tf_2N]	250	3966	20	4
Coiled	342	[BMIM][PF_6]	350	3968	20	4
Coiled	342	[BMIM][Tf_2N]	250	3968	20	4

Table 5-3 Comparison of the experimental value vs. simulation value of IL's density at 1bar, 300K.

Ionic liquids	Exp. ρ (kg/L)	Sim. ρ (kg/L)	% Error
[BMIM][PF_6]	1.364[200]	1.381	1.2%
[BMIM][Tf_2N]	1.44[201]	1.45	0.8%

5.3.1. Validation of the Simulation Systems

The Gromacs 4.5.4 package contains a pre-equilibrated coordinate file for SPC/E water, and the water simulation box was verified by previous researchers;[50,138,163,171] so it was unnecessary to again equilibrate and validate the water simulation box. The IL boxes were equilibrated under NPT conditions (constant number of molecules, constant pressure, and constant temperature) for 5 ns. The purpose of this step was to make sure

that the IL box had correct density at 1 bar and 300 K. As shown in Table 5.3, the equilibrium density of [BMIM][PF_6] and [BMIM][Tf_2N] boxes was 1.381 kg/L and 1.45kg/L respectively, compared to the experimental value, 1.364 kg/L and 1.44 kg/L [202] in the literature, the error was within 1.5%, which suggested that our simulation system can provide reasonably accurate predictions of reality.

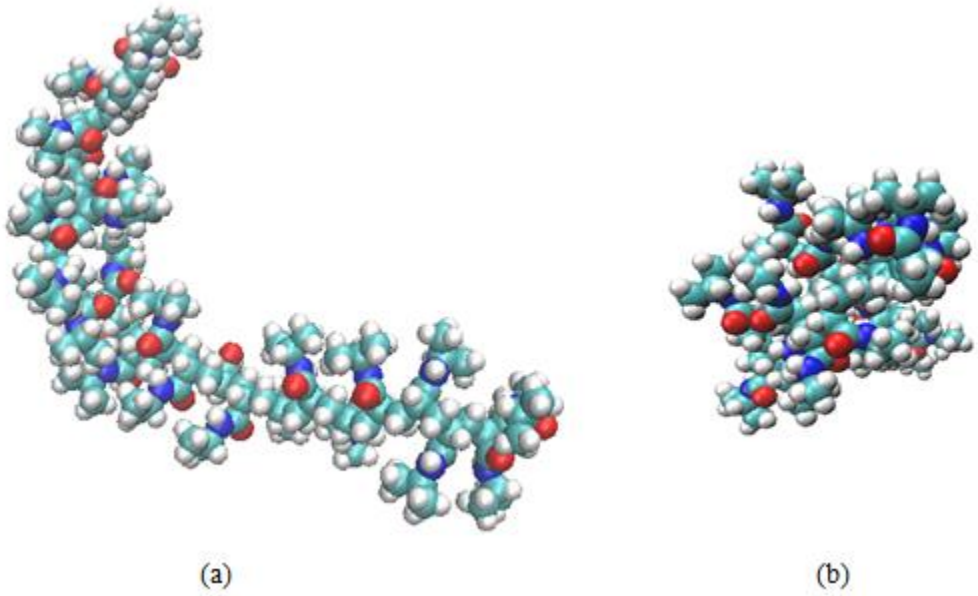

Figure 5-3 The configurations of the 26-units PNIPAM oligomer (a) extended structure at 295K; (b) coiled structure at 320K.

The simulation system was also examined by simulating the phase behavior of PNIPAM in water phase and compared our simulated results with the previous experimental and simulated data. First, as shown in Figure 5.3, PNIPAM exhibited similar phase behavior when comparing with experimental results. Below its LCST at 295K PNIPAM was extended, above the LCST, 320K, PNIPAM was coiled. To further validate the model, the Radius of gyration (R_g), the number of inter-molecule and intra-

molecule hydrogen bonds and the Radial Distribution Function (RDF) of water molecule around PNIPAM were calculated.

Radius of gyration described the dimensions of a polymer chain. Figure 5.4 indicated the evolution of the R_g during the 15 ns of simulation. As shown in Figure 5.4, the radius of gyration for PNIPAM at 320 K started to decrease at the beginning of the simulation and achieved equilibrium at about 4.8 ns, and the equilibrated Rg was about 1nm. On the other hand, the radius of gyration at 295 K decreased slightly during the simulation, and reached approximately 1.5 nm at equilibrated status. This result agreed with the previous simulation work of Honbo Du et al.[197] and Sanket A. et al[109].

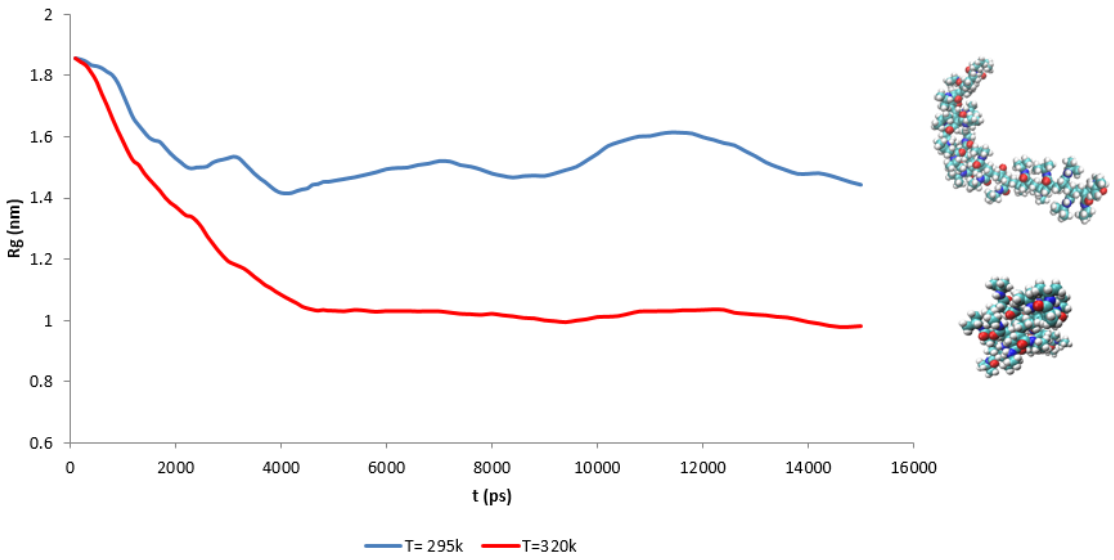

Figure 5-4 Time evolution of the Radius of Gyration (R_g) of PNIPAM in water at 295K (blue line), 320K (red line) respectively, during the 15ns MD simulation.

Two types of hydrogen bonding were analyzed to evaluate the hydrophilic-hydrophobic transition of the PNIPAM polymer below and above its LCST. These types

of hydrogen bonding included the intra-molecule hydrogen bonding within PNIPAM, and inter-molecule hydrogen bonding between the polymer and water molecules. The criterion used to determine the presence of a hydrogen bond was illustrated in the inset picture of Figure 5.5 Hydrogen bond length between two heavy atoms D, A (O or N in PNIPAM and O in water molecules) is greater or equal to 3.5Å, and that the cut-off for the hydrogen bond angle is 30˚.

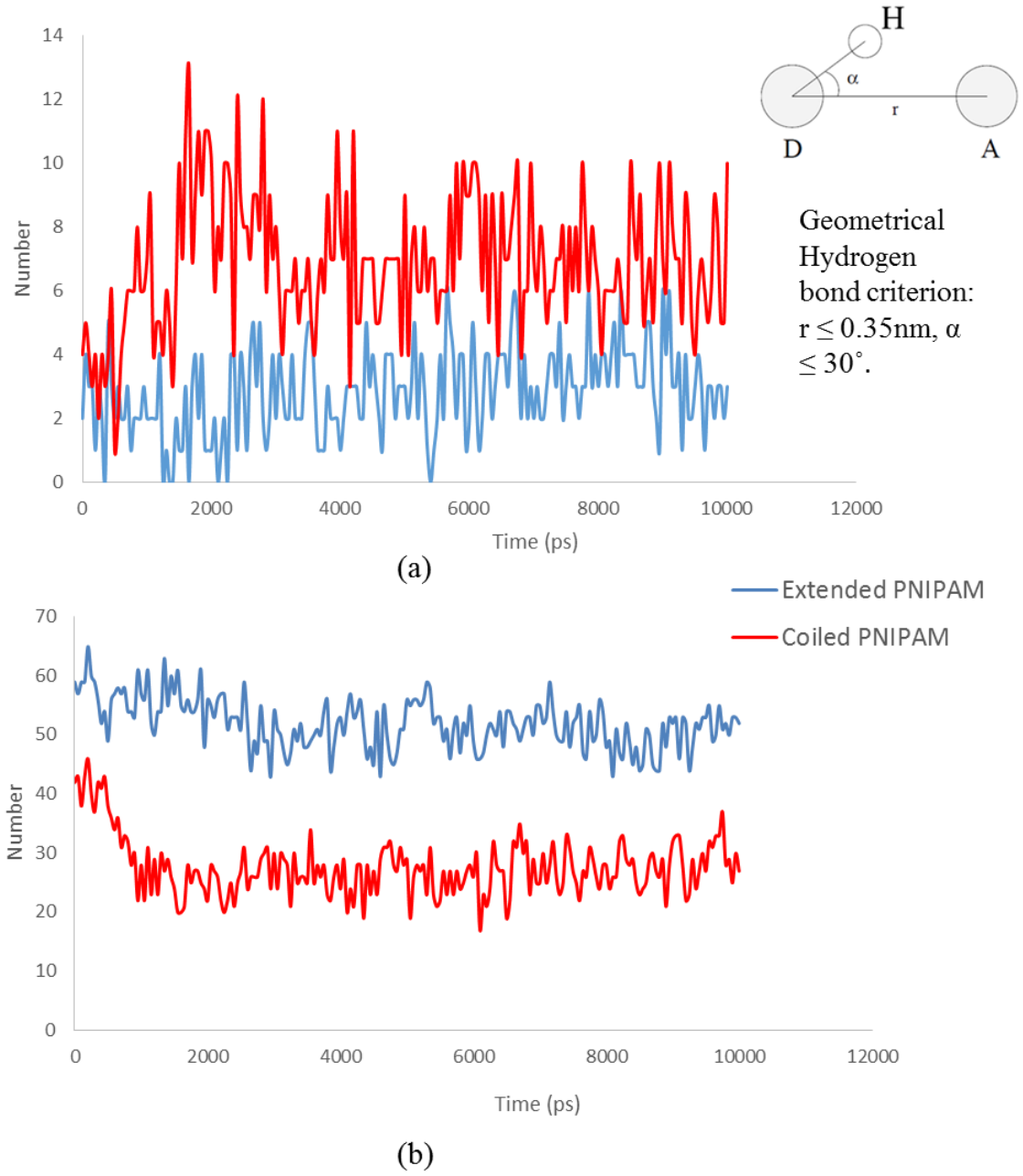

Figure 5-5 (a) the intrachain hydrogen bond numbers of PNIPAM (b) The intermolecular hydrogen bond numbers between PNIPAM and water; inset picture is the geometric criterion for hydrogen bond.

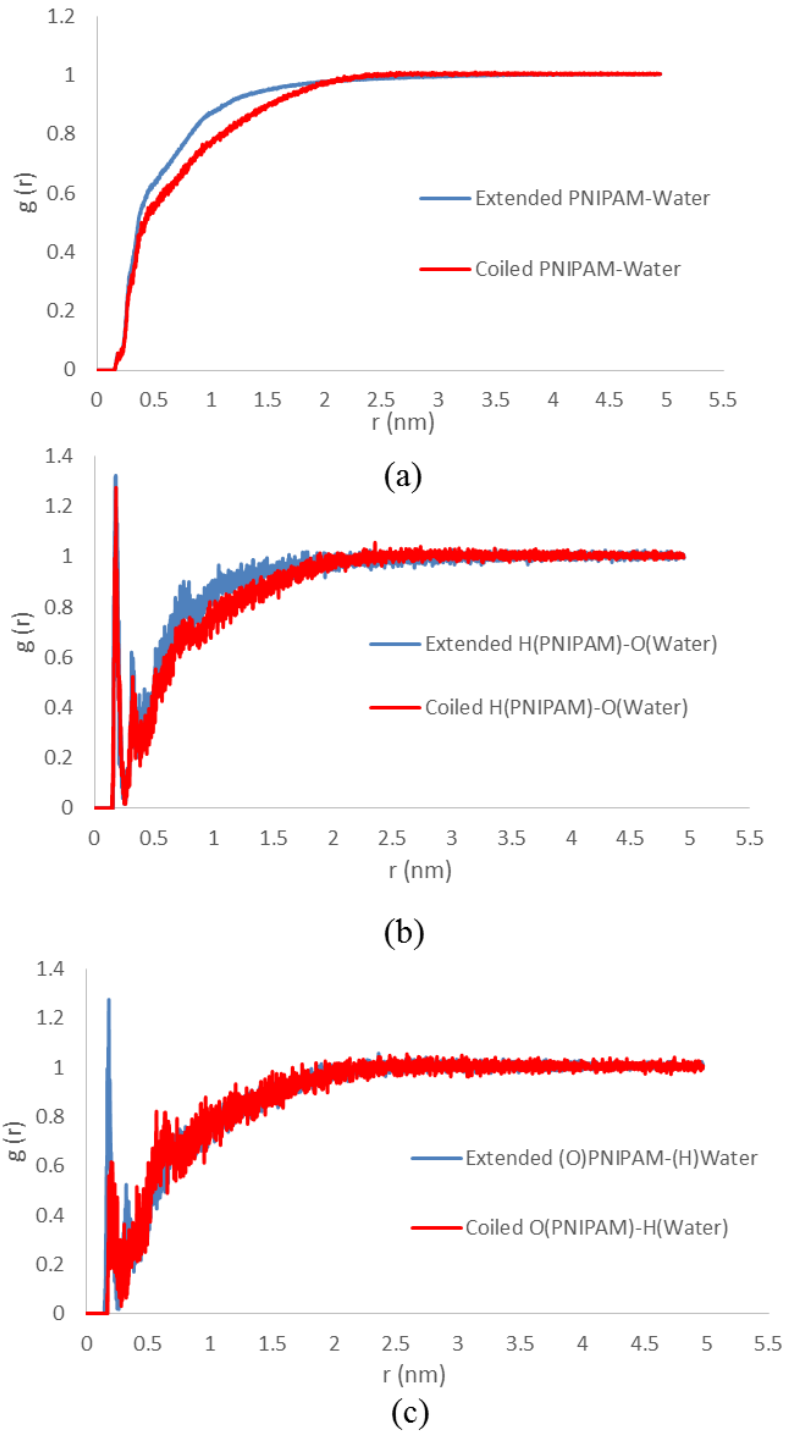

Figure 5-6 Radial Distribution Function of (a) water molecule around PNIPAM molecule; (b) hydrogen of water around the carbonyl oxygen of PINIPAM; (c) oxygen atom of water around the amide hydrogen of PNIPAM.

The time evolution of hydrogen bonds of extended and coiled PNIPAM along the simulations at 295K and 320K in water is showed in Figure 5.5. For the simulation of the intra-molecule hydrogen bonds as shown in Figure 5.5 (a), the number of intra-molecule hydrogen bonds for the extended PNIPAM fluctuated around 4 at 295K, while at 320K, the number of intra-molecule hydrogen bonds of the coiled PNIPAM fluctuated at about 8. Therefore, when the PNIPAM was at coiled status above its LCST, the number of intra-molecule hydrogen bonds increased. As for the number of inter-molecule hydrogen bonds the trend was opposite, as seen in Figure 5.5 (b), at 295K, the number of inter-molecule hydrogen bonds between the extended PNIPAM and water molecule fluctuated around 52. On the other hand, at higher temperature, the number of inter-molecule hydrogen bonds between the coiled PNIPAM and water fluctuated at about 25. Due to the difference in the length of the polymer chain and other simulation conditions, such as temperature, the accurate number of hydrogen bonds was incomparable with the data in the existing publications. However, the pattern of our simulation results was qualitatively consistent both with the previous simulation works[111,197] and experimental hypothesis.[94,203]

Radial Distribution Functions (RDF) were calculated after the phase transition was observed and the system achieved equilibrium. The Radial Distribution Functions were averaged for the last 5ns of simulation time for each case. Figure 5.6 (a) shows the radial distribution function between PNIPAM polymer and water molecules at temperatures above and below LCST. It suggests that water molecules had stronger interaction with the extended PNIPAM. Figure 5.6 (b) and Figure 5.6 (c) reveals more atomic details of the interactions between PNIPAM and water molecules: Figure 5.6 (b)

is the RDF of water oxygen with respect to the mass center of PNIPAM amide hydrogen, from which it can be seen that the RDF plot for the extended and coiled PNIPAM were quite similar. On the other hand, the interactions between water hydrogen and carbonyl oxygen of PNIPAM were quite different for extended and coiled PNIPAM, as shown in Figure 5.6 (c), the peak at r = 0.2 nm for the extended PNIPAM were obviously shaper and higher than the coiled PNIPAM, which indicated a much stronger affinity between water hydrogen and carbonyl oxygen for the extended PNIPAM. Therefore, we may assume that PNIPAM oxygen played a more important role in the formation of hydrogen bonding between PNIPAM and water. This hypothesis is consistent with the calculations of Juan Pan et al.[104]

In summary, the calculations of gyration radius, hydrogen bonding, and RDF were all consistent with the previous simulation studies. Particularly, the results of hydrogen bond numbers and Radial Distribution Functions for the extended and coiled PNIPAM suggested that the polymer were more hydrophilic and better solvated at extended status, which agreed with the observations and hypothesis in the previous experimental works.

5.3.2. PNIPAM in the Water-Ionic Liquids (ILs) System

We will first discuss the interfacial equilibrium simulations. Figure 5.7 shows the snapshot of the equilibrated positions of the extended PNIPAM and coiled PNIPAM in the water-[BMIM][PF_6] system (Figure 5.7 (a), (b)) and water [BMIM][TF_2N] system (Figure 5.7 (c), (d)) with an accompanying density profile, which was averaged across all simulation runs. The extended and coiled PNIPAM were simulated at 295K and 340K

respectively. In the water-[BMIM][PF_6] system, the extended PNIPAM exhibited more hydrophilic behavior. Figure 5.7 (a) shows that only a small part of the extended PNIPAM adsorbed to the IL /water interface, most of it remained in the water phase. In contrast, for the coiled PNIPAM (see Figure 5.7 (b)), most of it equilibrated at the IL side of the interface. These observations were confirmed by the corresponding density profiles, which are provided to present an average of all four parallel runs. Thus, in comparison to the extended PNIPAM, the phase preferences of the coiled PNIPAM at the water-[BMIM][PF_6] interface was qualitatively opposite. We can expect the [BMIM][PF_6] to respond to these two different configurations of PNIPAM in different ways. However, in the water-[BMIM][TF_2N] system, the phase preference for the extended or coiled PNIPAM was not as clear as that in water-[BMIM][PF_6] system (see Figure 5.7 (c), (d)). Unlike the solvation behavior of the extended PNIPAM in the water-[BMIM][PF6] interface, In the water-[BMIM][TF_2N] system, the extended PNIPAM almost totally entered the water-IL interface and most of it equilibrated in the IL side of the interface. As shown in Figure 5.7 (d), the coiled PNIPAM also equilibrated in the IL side of the system. Thus, in the water-[BMIM][TF_2N] system, both extended PNIPAM and coiled PNIPAM tended to stay at the IL side of the interface.

Interaction energy between PNIPAM and different species in the solvents at their equilibrated positions were examined for these two water-IL systems. Table 5.4 (a) and (b) summarizes the Lennard-Jones (LJ) and Coulombic interaction (Coul) energies for the water-[BMIM][PF_6] system and the water-[BMIM][TF_2N] system respectively, averaged over the last 5 ns of simulation. The values of the interaction energies of the extended PNIPAM and coiled PNIPAM between water and IL were illustrated in Figure 5.8.

Figure 5.8 (a) shows that in the water-[BMIM][PF_6] system, the interaction energy between extended PNIPAM and water was much lower than its interaction energy with IL, thus, extended PNIPAM was more energetically favorable to water phase. On the other hand, the coiled PNIPAM's interaction energy with [BMIM][PF_6] was lower than its interaction energy with water. This may explain why the coiled PNIPAM preferred to the IL side of the interface in the water-[BMIM][PF_6] system. Figure 5.8 (b) shows the interaction energies of extended and coiled PNIPAM in the water-[BMIM][TF_2N] system. Obviously, the pattern of PNIPAM's interaction energies in the water-[BMIM][TF_2N] system was quite different from that of the water-[BMIM][PF_6] system: for both extended and coiled configurations, PNIPAM's interaction energies with [BMIM][TF_2N] were lower than its interaction energy with water. Thus, both the extended and coiled PNIPAM in the water-[BMIM][TF_2N] system energetically favored the IL side of the interface.

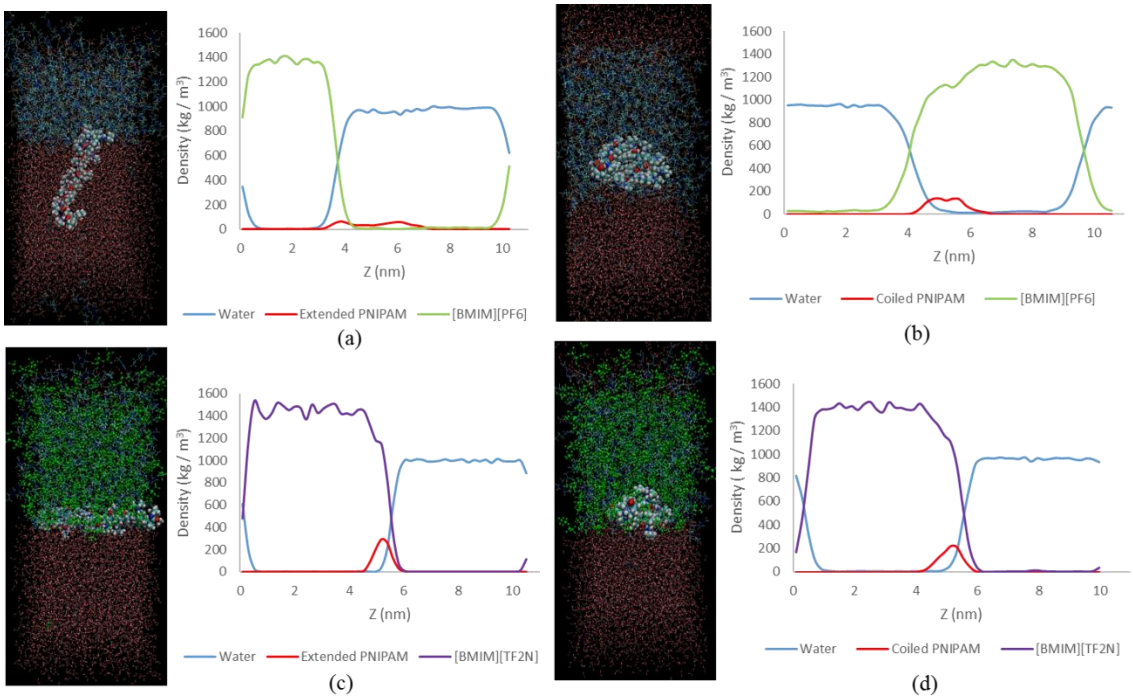

Figure 5-7 The snapshots and density profiles of the equilibrated positions of extended and coiled PNIPAM (a) extended PNIPAM at 295K in in water-[BMIM][PF_6] system; (b) coiled PNIPAM at 342K in in water-[BMIM][PF_6] system;(c) extended PNIPAM at 295K in in water-[BMIM][TF_2N] system; (d) coiled PNIPAM at 342K in in water-[BMIM][TF_2N] system.

Table 5-4 (a) The interaction energies (defined as Lennard-Jones potential energy plus Coulombic potential energy) of extended vs. coiled PNIPAM in water-[BMIM][PF_6] system

	Extended PNIPAM	**Coiled PNIPAM**				
Interacting Species with PNIPAM	**Coul (kJ/mol)**	**LJ (kJ/mol)**	**Interaction energy (kJ/mol)**	**Coul (kJ/mol)**	**LJ (kJ/mol)**	**Interaction Energy (kJ/mol)**
Water	1354.73 ±41.0	-700.51 ±14.0	-2055.24 ±30.0	-339.82 ±24.0	-74.92 ±9.9	-414.74 ±18.4
$[BMIM]^+$	-13.80 ±7.2	-119.02 ±19.0	-249.94 ±10.8	-67.19 ±7.3	-670.13 ±19.0	-1281.26 ±11.4
$[PF6]^-$	-55.20 ±4.7	-61.92 ±5.4		-253.71 ±6.9	-290.24 ±7.9	

Table 5-4 (b) The interaction energies of extended vs. coiled PNIPAM in water-[BMIM][TF_2N] system

	Extended PNIPAM			**Coiled PNIPAM**		
Interacting Species	**Coulomb (kJ/mol)**	**LJ (kJ/mol)**	**Interaction energy (kJ/mol)**	**Coulomb (kJ/mol)**	**LJ (kJ/mol)**	**Interaction Energy (kJ/mol)**
Water	-719.58±14.0	-276.16±2.4	-995.74±10.0	-589.84±9.3	-191.64±4.4	-781.47±7.3
$[BMIM]^+$	-42.93±4.5	-361.37±6.2	-1238.29±6.6	-23.02±5.4	-362.44±5.7	-1089.26±6.1
$[TF2N]^-$	-251.47±9.8	-582.50±4.4		-208.40±4.8	-495.41±8.0	

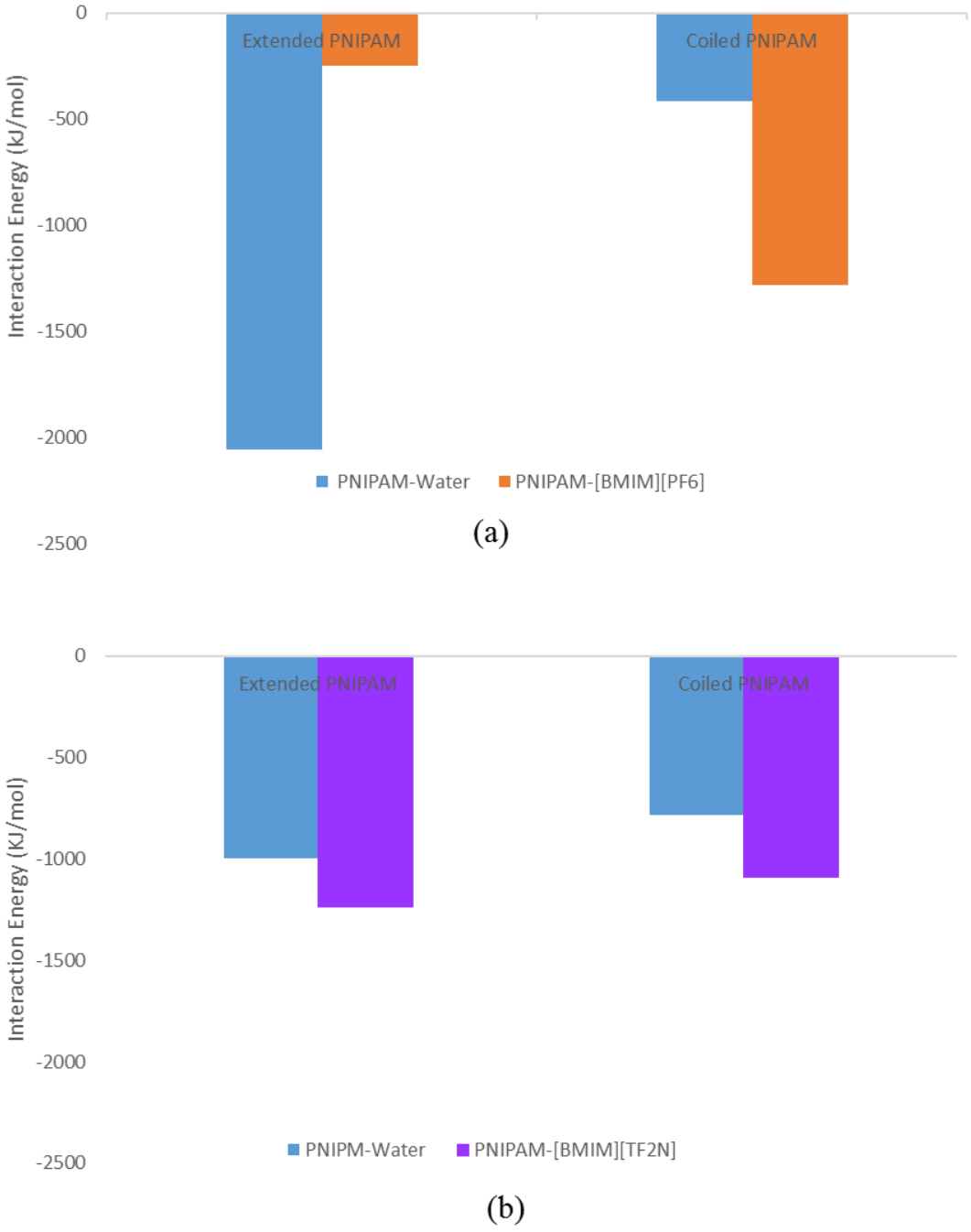

Figure 5-8 Compare the Interaction energies of PNIPAM-water and PNIPAM-Ionic liquid for extended vs. coiled status at their equilibrated position (a) in the water-[BMIM][PF_6] system;(b) in the water-[BMIM][TF_2N] system.

Each Coulombic and LJ potentials composing the interaction energies for PNIPAM in the water-[BMIM][PF_6] system and water-[BMIM][TF_2N] system was illustrated in Figure 5.9. Figure 5.9 (a) shows that in the water-[BMIM][PF_6] system when PNIPAM was extended, its Coulombic potential with water was significant lower than other energies, thus the electrostatic force between water and PNIPAM may play the major role in attracting the extended PNIPAM. On the other hand, when PNIPAM was coiled, the LJ potential between PNIPAM and BMIM cation most notably reduced, indicating that BMIM cation may be mainly responsible for extracting the coiled PNIPAM into the [BMIM][PF_6] side of the interface. In the water-[BMIM][TF_2N] system (see Figure 5.9 (b)), we noticed that (1) the change of Columbic and LJ potentials of interacting pairs from the extended to the coiled status for PNIPAM was not as significant as that in the water-[BMIM][PF_6] system. (2) TF_2N anion played a more significant role than BMIM cation in attracting PNIPAM to the IL phase.

To quantify our observation, the percentage of each component making up the interaction energies of PNIPAM at the equilibrated positions in the water-[BMIM][PF_6] and water-[BMIM][TF_2N] systems were calculated (see Table 5-5) and illustrated in Figure 5.10. In the water-[BMIM][PF_6] system (see Figure 5.10 (a), (b)), the Columbic potential of water-PNIPAM account for 58.8% (in magnitude) of the total interaction energy for extended PNIPAM, while for the coiled PNIPAM the biggest contribution to the interaction energy came from the LJ potential between the coiled PNIPAM and BMIM cation (39.5% of the total interaction energy for coiled status).In Figure 5.10 (c) and (d), It can be seen in contrast to the water-[BMIM][PF6] system, the anion (TF_2N) always played a more important role than BMIM cation for attracting PNIPAM: the LJ

potential of [TF_2N]-PNIPAM accounted 26.1% and 26.5% of the total interaction energy for extended and coiled PNIPAM respectively, compared to 16.2% and 19.4% contribution from the [BMIM]-PNIPAM LJ interactions.

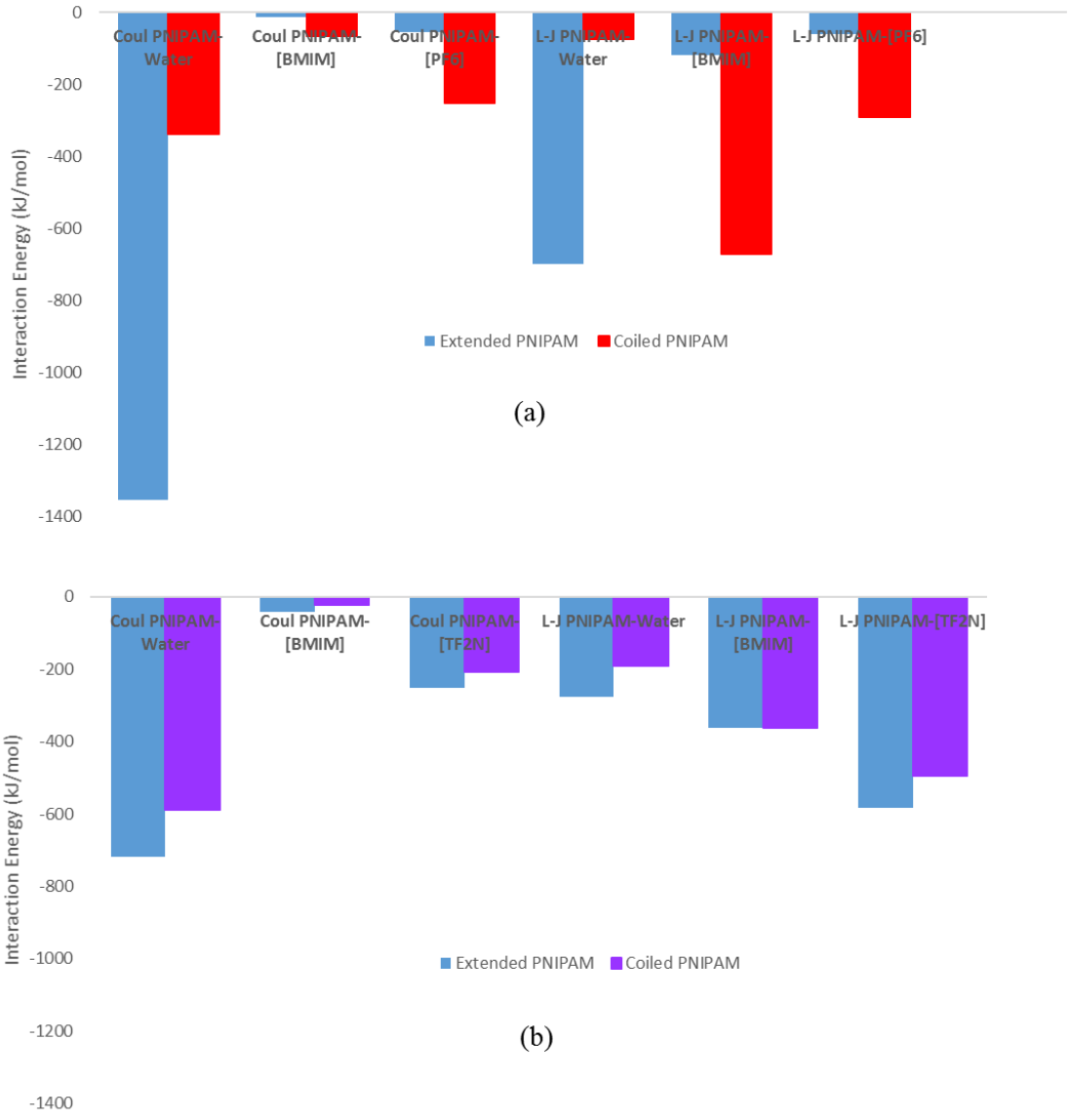

Figure 5-9 Comparison of the Coulombic potential and Lennard-Jones potential of PNIPAM-water, PNIPAM-$[BMIM]^+$ and PNIPAM-anions for extended vs. coiled status at the equilibrated position (a) in the water-[BMIM][PF6] system; (b) in the water-[BMIM][TF_2N] system.

Table 5-5 (a) Percentage of each component making up the interaction energy of PNIPAM at the equilibrated position in water-[BMIM][PF_6] system.

	Coul PNIPAM-Water	Coul PNIPAM-[BMIM]	Coul PNIPAM-[PF_6]	L-J PNIPAM-Water	L-J PNIPAM-[BMIM]	L-J PNIPAM-[PF_6]
Extended PNIPAM	58.8%	0.6%	2.4%	30.4%	5.2%	2.7%
Coiled PNIPAM	20.0%	4.0%	15.0%	4.4%	39.5%	17.1%

Table 5.5 (b) Percentage of each component making up the interaction energy of PNIPAM at the equilibrated position in water-[BMIM][TF_2N] system.

	Coul PNIPAM-Water	Coul PNIPAM-[BMIM]	Coul PNIPAM-[TF_2N]	L-J PNIPAM-Water	L-J PNIPAM-[BMIM]	L-J PNIPAM-[TF_2N]
Extended PNIPAM	32.2%	1.9%	11.3%	12.4%	16.2%	26.1%
Coiled PNIPAM	31.5%	1.2%	11.1%	10.2%	19.4%	26.5%

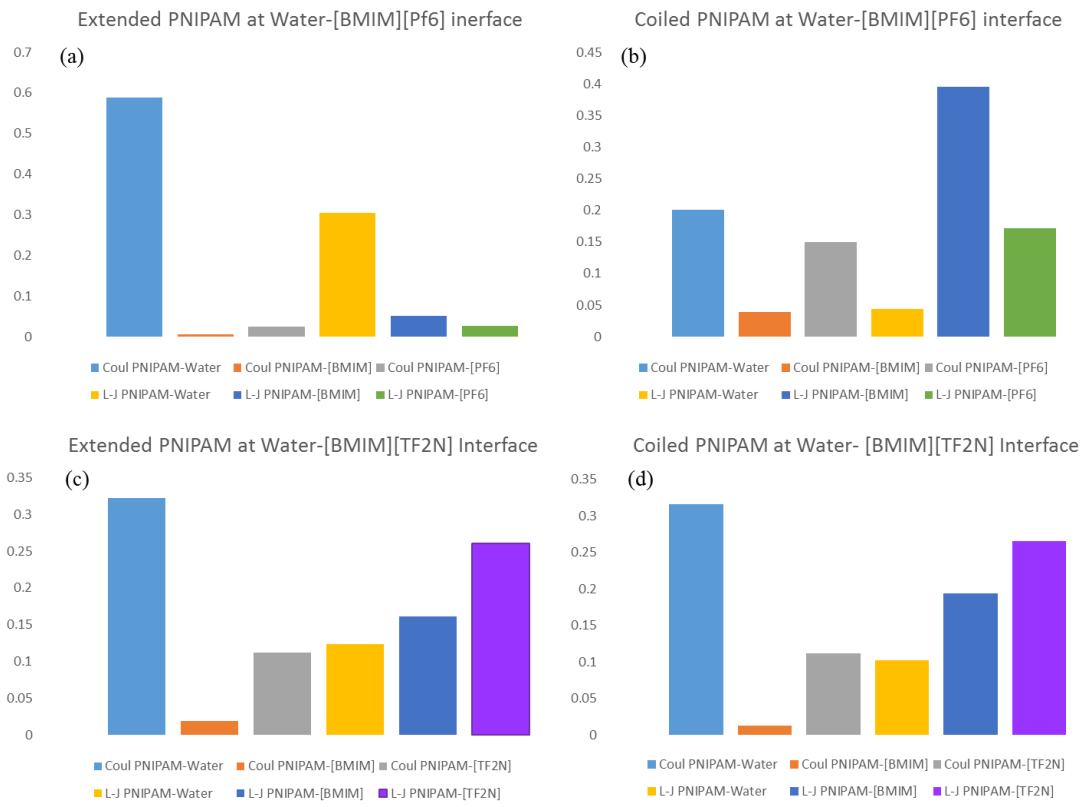

Figure 5-10 The percentage of each Coulombic and Lenard-Jones potentials that constitute the total interaction energy at the equilibrated position for (a) extended PNIPAM in the water -[BMIM][PF_6] system; (b) coiled PNIPAM in the water -[BMIM][PF_6] system; (c) extended PNIPAM in the water-[BMIM][TF_2N] system; (d) coiled PNIPAM in the water-[BMIM][TF_2N] system.

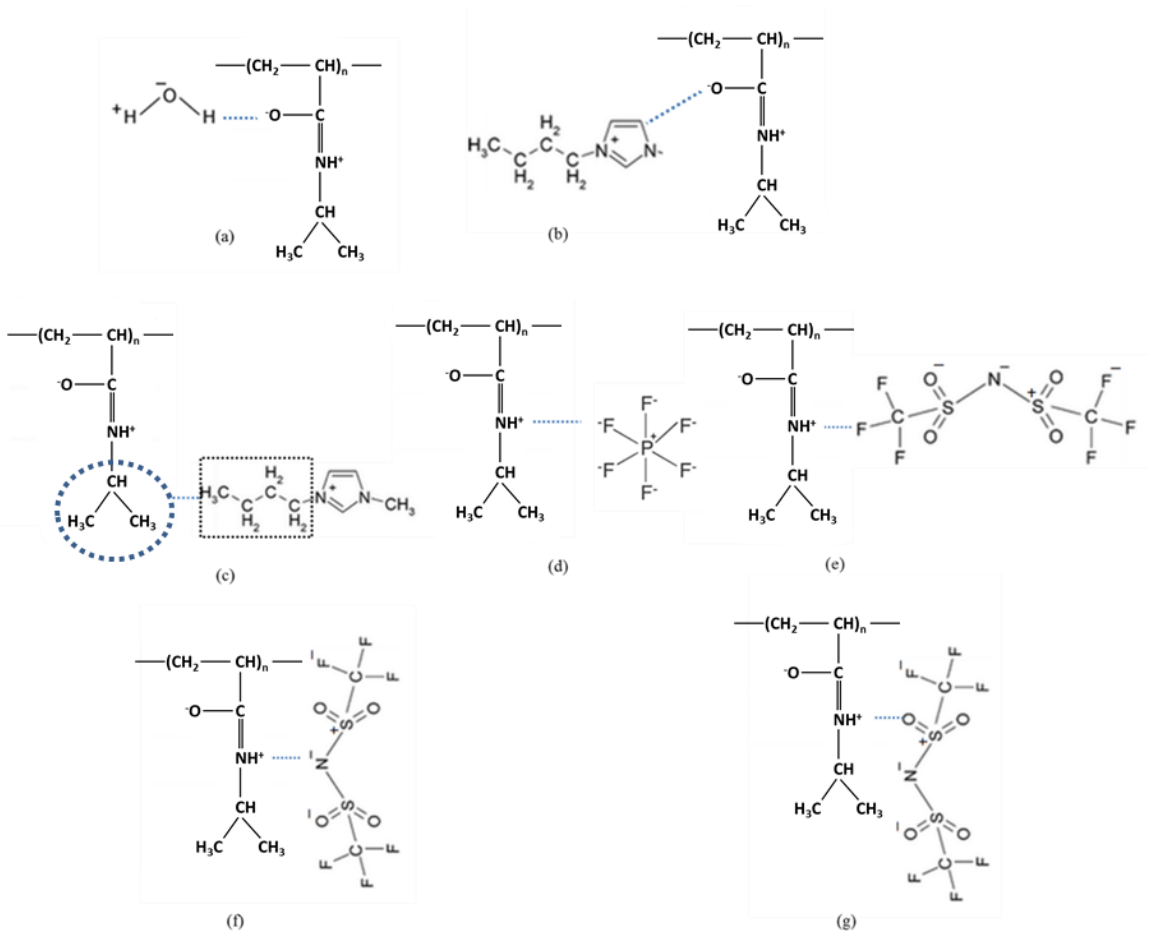

Figure 5-11 The Radial Distribution Functions discussed in this research (a) water hydrogen with respect to carbonyl oxygen of PNIPAM; (b) imidazolium ring of the BMIM cation with respect to the amide hydrogen of PNIPAM; (c) butyl group of the BMIM cation with respect to the isopropyl group of PNIPAM; (d) fluorine of PF_6 anion with respect to amide hydrogen of PNIPAM; (e) fluorine of TF_2N anion with respect to the amide hydrogen of PNIPAM; (f) nitrogen of TF_2N anion with respect to the amide hydrogen of PNIPAM; (g) oxygen of TF_2N anion with respect to the amide hydrogen of PNIPAM.

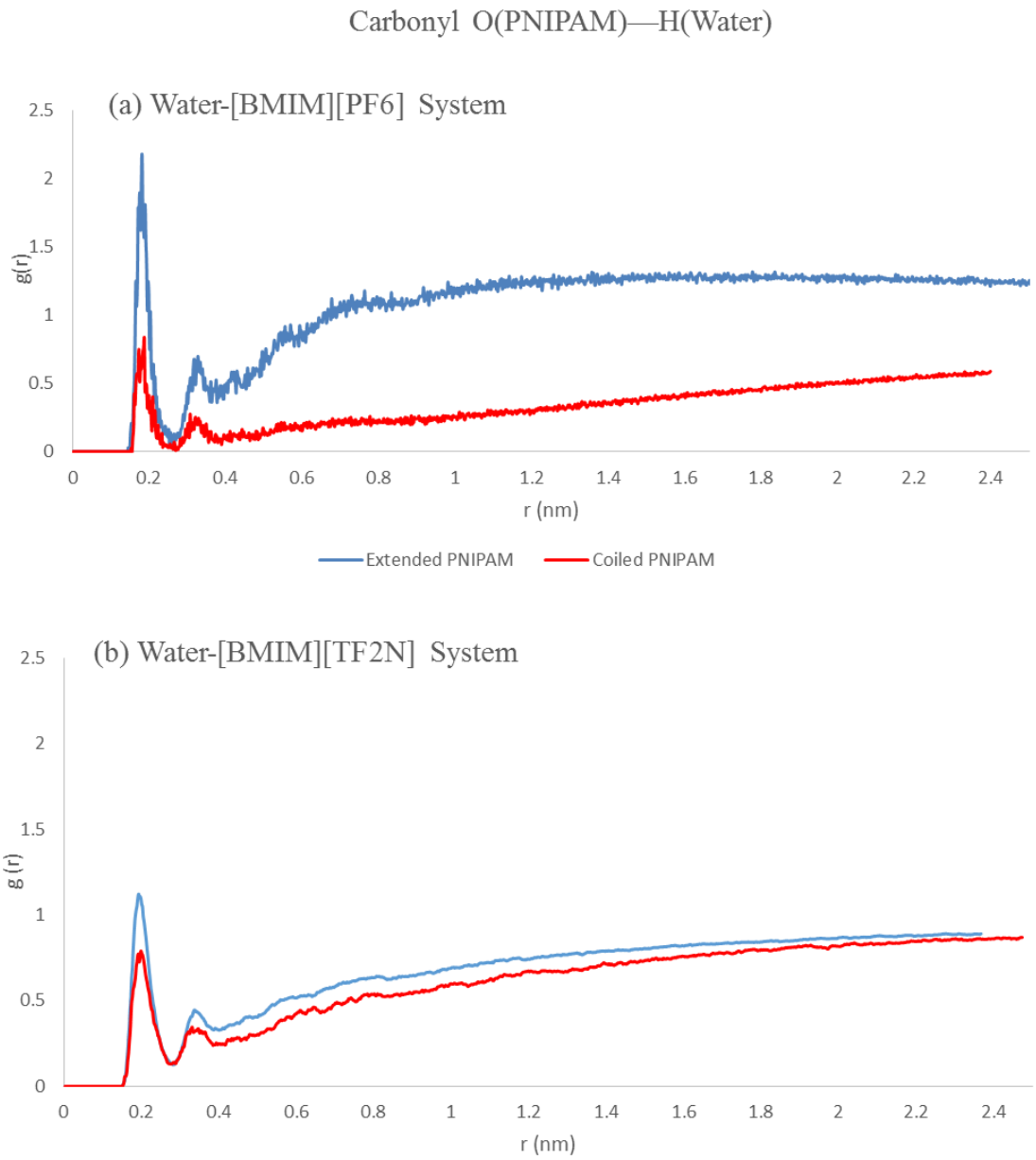

Figure 5-12 Radial Distribution Functions (RDF) of water hydrogen around carbonyl oxygen of PNIPAM in the (a) water - [BMIM][PF_6] system; (b) water-[BMIM][TF_2N] system.

To further explore the atomic scale interactions between PNIPAM and the solvent molecules, the radial distribution functions (RDF) were applied to probe the distribution of solvent molecules around the extended or coiled PNIPAM. We investigated the

interactions between the effectively charged parts of the molecules, such as the carbonyl oxygen (-) and amide hydrogen (+) of PNIPAM, the imidazolium ring (+) of BMIM cation, the fluorine (-) of PF_6 anion, and the oxygen (-) of TF_2N anion etc, which are supposed to significantly contribute to the overall interaction energy. In addition, the interaction between the nonpolar species such as the isopropyl group of PNIPAM and the butyl group of BMIM cation were also explored. More details were illustrated in Figure 5.11. In each case, the RDF was averaged for the last 5 ns of simulation time.

Figure 5.12 describes the interactions between the water and PNIPAM. Figure 5.12 (a) and Figure 5.12 (b) are the RDF of water hydrogen with respect to the mass center of carbonyl oxygen of PNIPAM in the water-[BMIM][PF_6] and the water-[BMIM][TF_2N] system respectively. In Figure 5.12 (a), it is obviously that the peak at 0.18 nm for the extended PNIPAM is much higher and sharper than that of the coiled PNIPAM, indicating a better-defined hydration shell around the carbonyl oxygen of the extended PNIPAM. On the other hand, in the water-[BMIM][TF_2N] system, as shown in Figure 5.12 (b) the height and shape of the peak for the extended and coiled PNIPAM were quite alike, indicating the distribution of water molecules around the PNIPAM was similar for the extended and coiled PNIPAM. This result is consistent with the previous energy analysis as shown in Figure 5.9. The change of interaction energies (including Columbic potential and LJ potential) between PNIPAM and water is very prominent as the polymer switched its configurations in the water-[BMIM][PF_6] system, while in the water-[BMIM][TF_2N] system, the difference of interaction energies with water between extended and coiled PNIPAM was relatively insignificant.

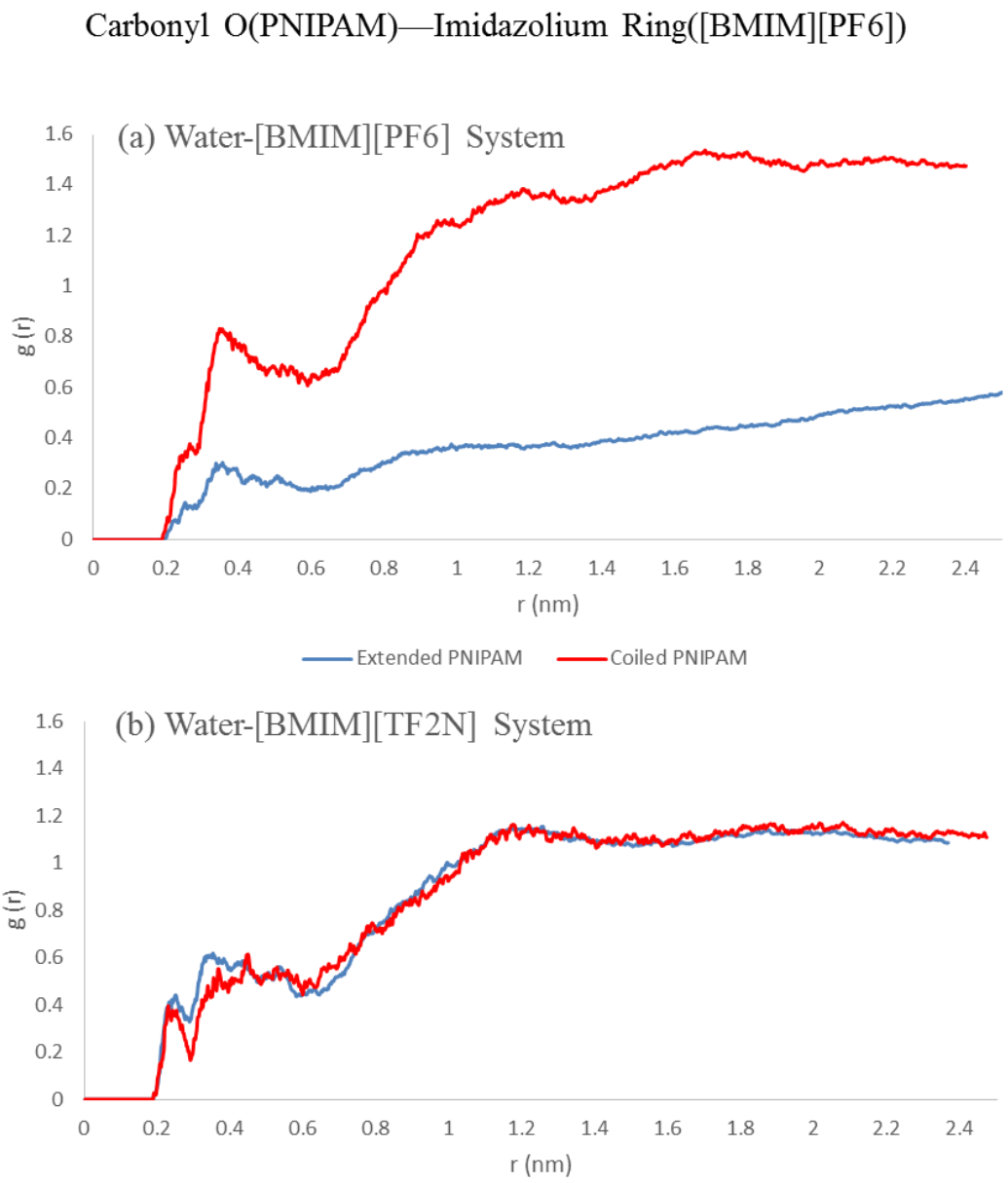

Figure 5-13 Radial Distribution Functions (RDF) of the imidazolium ring of BMIM cation around carbonyl oxygen of PNIPAM in the (a) water - [BMIM][PF_6] system; (b) water-[BMIM][TF_2N] system.

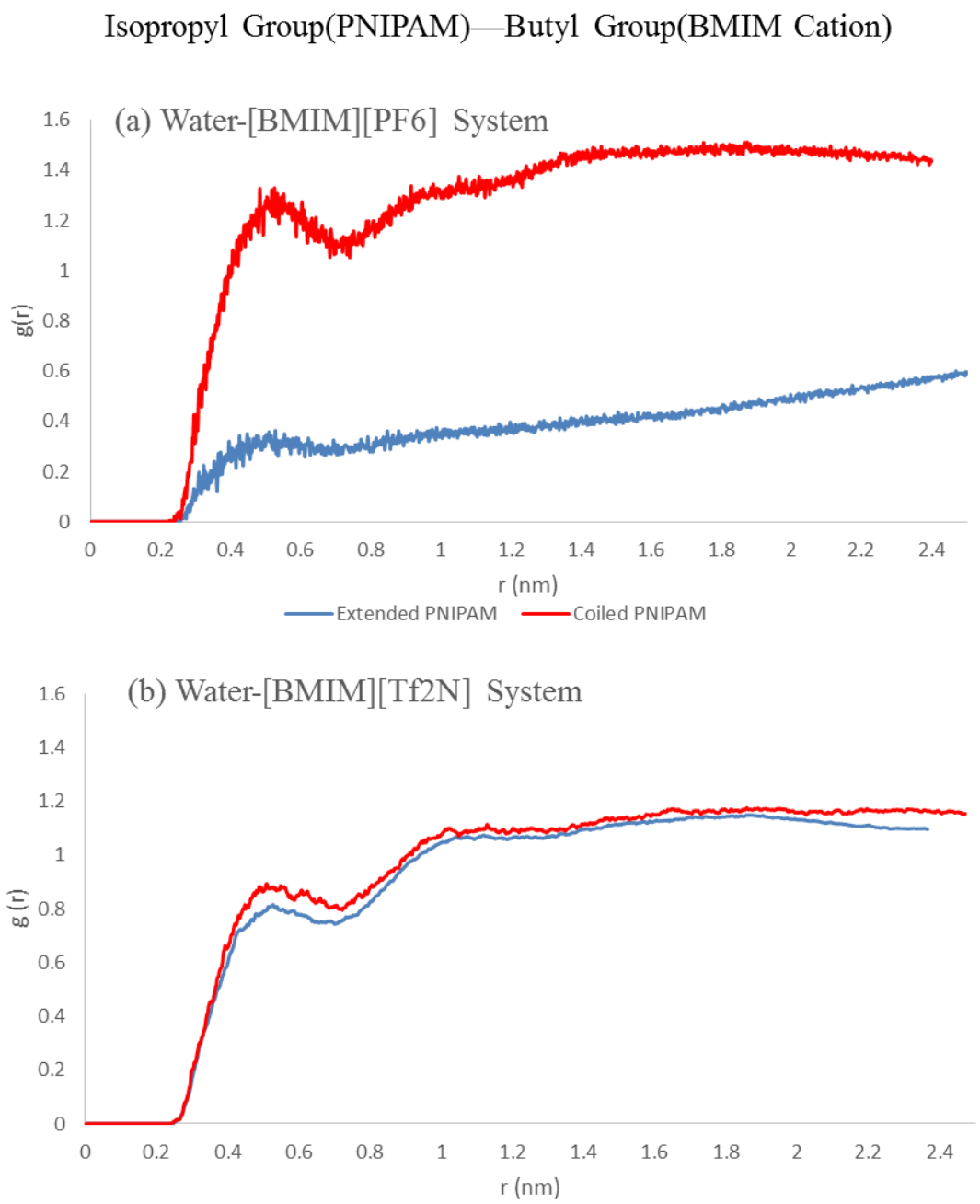

Figure 5-14 Radial Distribution Functions (RDF) of the butyl group of BMIM cation around the isopropyl group of PNIPAM in the (a) water - [BMIM][PF_6] system; (b) water-[BMIM][TF_2N] system.

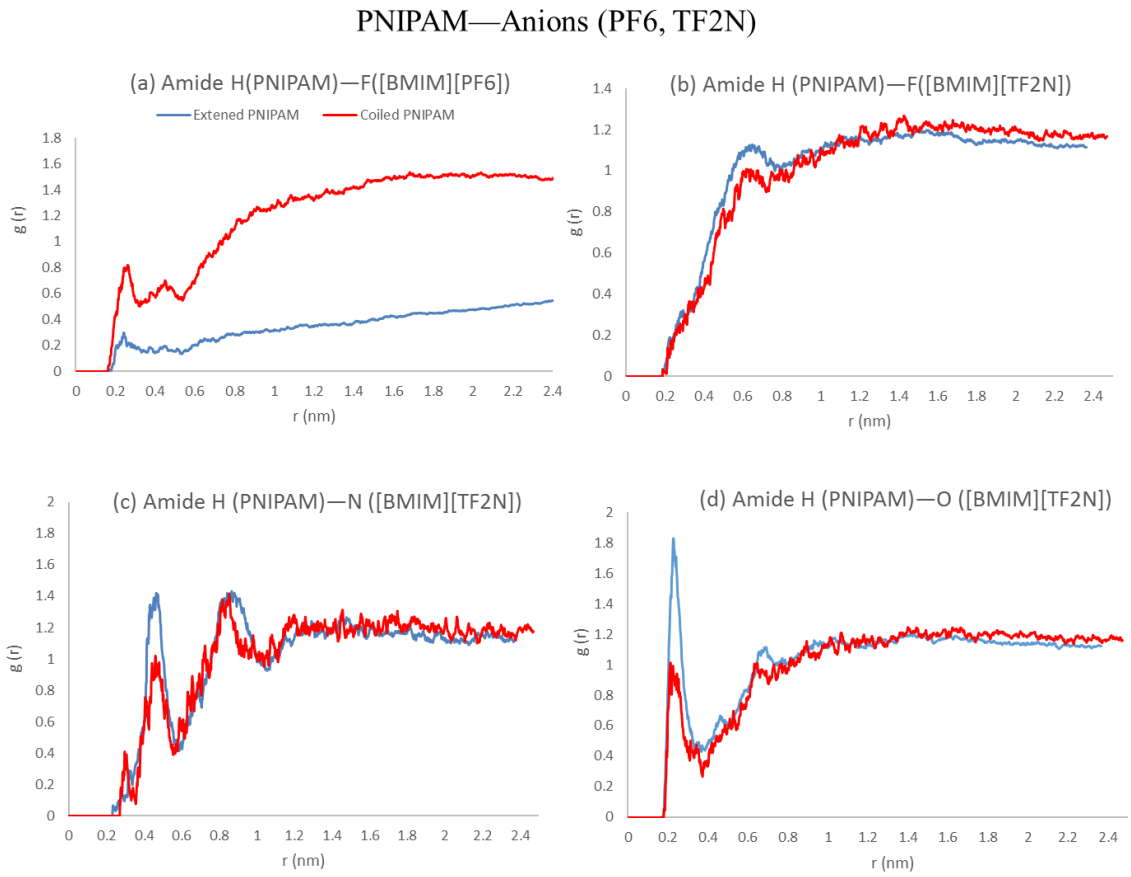

Figure 5-15 Radial Distribution Functions (RDF) of (a) the fluorine of PF_6 anion around the amide hydrogen of PNIPAM in the water - [BMIM][PF_6] system; (b),(c) (d) fluorine, nitrogen and oxygen of TF_2N anion around the amide hydrogen of PNIPAM in the water-[BMIM][TF_2N] system.

Figure 5.13 and Figure 5.14 describe the interactions between BMIM cation and PNIPAM. Figure 5.13 shows the distribution of the positively charged imidazolium ring of BMIM cation around the negatively charged carbonyl oxygen of PNIPAM. In Figure 5.13 (a) it can be seen that in the water-[BMIM][PF_6] system, the interaction between the carbonyl oxygen and the imidazolium ring for the coiled PNIPAM is much stronger than that for the extended PNIPAM. While in the water-[BMIM][TF_2N] system (see Figure

5.13 (b)), this trend was not very obvious. For both the extended and coiled PNIPAM, the shape of the RDF plots is alike, indicating their carbonyl oxygen had similar interactions with the imidazolium ring of BMIM cation. Figure 5.14 shows the RDF for the butyl group of BMIM cation with respect to the isopropyl group of PNIPAM. In the water-[BMIM][PF_6] system (Figure 5.14 (a)), the remarkable higher and stronger peak in the RDF plot for the coiled PNIPAM indicating that the affinity between these two nonpolar groups were much stronger for the coiled PNIPAM than that for the extended PNIPAM. Again, in the water-[BMIM][TF_2N] system (Figure 5.14 (b)) such prominent difference cannot be observed, suggesting that not only the interactions between the charged groups of PNIPAM and BMIM cation for different polymer configurations were similar, the affinities between the nonpolar groups for both extended and coiled status of PNIPAM were also alike in the water-[BMIM][TF_2N] system.

Figure 5.15 depicts the interactions between PNIPAM and the anions of the ionic liquids ($[PF_6]^-$, $[TF_2N]^-$). Figure 5.15 (a) indicates that the amide hydrogen of the coiled PNIPAM has stronger interaction with the fluorine of PF_6 anion than that of the extended PNIPAM in the water-[BMIM][PF_6] system. Figure 5.15 (b), (c), (d) shows the RDF plots of the fluorine, nitrogen and oxygen of TF_2N anion with respect to the mass center of amide hydrogen of PNIPAM in the water-[BMIM][TF_2N] system. As we can see for all of these three plots, the negatively charged moieties in the TF_2N anion have stronger affinity with the amide hydrogen of the extended PNIPAM than that of the coiled PNIPAM. Especially in Figure 5.15 (d), the prominent peak at 0.23 nm for the extended PNIPAM indicates that the amide hydrogen of the extended PNIPAM strongly interacted with the oxygen of TF_2N anion.

Therefore, in the water-[BMIM][PF_6] system, the coiled PNIPAM has stronger interaction with both the cation and anion of the ionic liquid than that of the extended PNIPAM. While in the water-[BMIM][TF_2N] system, the interactions between cation and PNIPAM were alike for the extended and coiled configuration, whereas, the anion tended to interact more strongly with the extended PNIPAM.

5.4.Conclusion

In this work, we have carried out extensive high fidelity molecular dynamics simulations to investigate the behavior of PNIPAM macromolecules on different liquid-liquid interfaces, including both the water-[BMIM][PF_6] system and water-[BMIM][TF_2N] system. In the water-[BMIM][PF_6] system, PNIPAM exhibited a clear phase preference for different configurations. Specifically, for the extended state (equilibrium state at lower temperatures), PNIPAM preferred the water phase, as evidenced by our observation that the PNIPAM macromolecule's tendency to stay in the water phase during the MD simulations. For the coiled PNIPAM (equilibrium state at high temperatures) tends to move forwards to the IL side of the interface, indicating its preference of the IL phase. On the other hand, in the water-[BMIM][TF_2N] system, we found that the phase preference is independent of PNIPAM macromolecule configurations, i.e., both extended and coiled PNIPAM tend to stay in IL phase close to the interface.

To further understand the thermodynamic origin of observed PNIPAM behaviors at different interfaces, we performed a detailed analysis of the interaction energy between PNIPAM macromolecules (the solute macromolecules), as well as detailed structural

quantification via the radial distribution functions to precisely determine the interacting atomic groups on different macromolecules. We found that in the water-[BMIM][PF_6] system, interactions between the extended PNIPAM and water molecules (amide oxygen of PNIPAM and water hydrogen) are much stronger than the interactions between PNIPAM and IL. However, when PNIPAM is coiled, the imidazolium ring and butyl group of the BMIM cation played the most important role in attracting the coiled PNIPAM to the BMIM] [PF_6] side of the interface.

On the other hand, in the water-[BMIM][TF_2N] system, PNIPAM had similar level of interaction with water and IL for both extended and coiled status. It is probably mainly due to the influence of the Tf_2N anion: both extended and coiled PNIPAM had strong interaction with Tf_2N anion, this make its interaction energies with IL were always lower than its interaction energy with water. Thus, PNIPAM always stay at the IL side of the interface in the water-[BMIM][TF_2N] system.

6. EFFECTS OF HYDROPHILIC IONIC LIQUIDS ON THE LOWER CRITICAL SOLUTION TEMPERATURE OF PNIPAM

6.1.Introduction

The Lower Critical Solution Temperature (LCST) of PNIPAM can be influenced by the presence of other "ingredients" in its aqueous solution. Such ingredients could include surfactants,[204–208] salts,[203,209,210] co-solvents,[117,211,212] and so on. For example, previous investigations show that salt ions have significant impacts on the LCST of PNIPAM. Eeckman and coworkers' investigation[213] shows the addition of salts can lead to a significant decrease of PNIPAM's LCST; i.e., a 1 M NaCl solution leads to a decrease of the PNIPAM's LCST by about 12 K from approximate 305 K in pure water to about 293 K, while a 0.2 M Na_2SO_4 solution decreases its LCST by about 10 K. It appears that the salt type, concentration, valence and size of the anions play important roles in influencing the LCST of PNIPAM. Recent studies have shown that certain imidazolium based ionic liquids can influence the LCST of PNIPAM aqueous solution by hydrophobic collapse/aggregation of the PNIPAM chains. For example, P. M. Reddy, et al[112]. investigated the effects of 1-benzyl-3-methylimidazolium tetrafluoroborate ([Bzmim][BF_4]) on the LCST of PNIPAM in the aqueous solution by using fluorescence, viscometric, and dynamic light scattering (DLS) techniques. It indicated that the addition of [Bzmim][BF_4] can significantly decrease the LCST of PNIPAM, and the IL's concentration is the most important factor on the phase transition PNIPAM.

So far our understanding of the interactions between PNIPAM and the other 'ingredients' in the aqueous solution are still very limited and the exact nature of these interactions remains to be elucidated. For example, in the study of the effects of salts (e.g.

NaI, NaCl) on the LCST of PNIPAM in aqueous solutions, Molecular Dynamic simulation studies[105,143,214,215] showed that salt may impact the LCST of PNIPAM through direct binding between the amide group of PNIPAM and salt cations (e.g. Na^+, K^+). Salt anions had very weak or no interaction with PNIPAM. However, similar experimental studies[203,209,213,216–218] suggest that salts affect the LCST of PNIPAM mostly due to the interactions between PNIPAM and salt anions (e.g. I^-, Cl^-), while the influence of cations was negligible. Our understanding about the interactions between PNIPAM and ions in ionic liquid/water systems is even more limited. To the best of our knowledge, no systematic studies have been carried out to elucidate the mechanisms for the observed reduction of LCST of PNIPAM in ionic liquid/water solutions. Therefore, the goal of our work is to understand how ionic liquids interact with PNIPAM in aqueous solutions and affect its LCST behaviors via high fidelity molecular dynamics simulations.

A pure water system and two miscible ionic liquids/water systems, [BMIM][I]/water and [BMIM][Cl]/water systems were created for our study. Energy analysis was performed to understand the thermodynamic origin of the phase behaviors in different systems. Detailed structural quantification via Radial Distribution Functions (RDF) was applied to reveal the interacting functional groups on different molecules in our simulation systems. We also compared our simulation results with the previous simulation and experimental studies of PNIPAM in salt solutions to better understand the similarities/differences of PNIPAM-ion interactions in these systems and their effects on the LCST behaviors.

To our best knowledge, this work is the first systematic molecular dynamics study that leads to a comprehensive understanding of how cations and anions of the ionic

liquids interact with different moieties of PNIPAM at atomic level. It is also the first report discussing the resemblance and distinctions of PNIPAM in ionic liquid/water systems from PNIPAM in salt solutions.

6.2.Methodology

MD simulations were conducted using the Gromacs package.[124,162] Three simulation systems were created for our investigation: PNIPAM in pure water system, 10 mol % [BMIM][I]/water system, and 10 mol % [BMIM][Cl]/water system. The dimension of the simulation boxes was approximately 5.5 × 5.5 × 5.5 nm^3. More details about the simulation systems are described in Table 6.1. In each system, PNIPAM was placed in the center of the simulation box. After the initial configurations were obtained, 1000 energy minimization steps were performed using the steepest descent method. The leapfrog algorithm was used for integrating Newton's equation of motion with a time step of 0.002 ps.

Table 6-1 Summary of simulation systems with simulation temperatures, numbers of PNIPAM, IL pairs, and water molecules

Simulation System	Simulation Temp (K)	# of PNIPAM	# of IL Pairs	# of Water Molecules
Pure Water	295K, 350K	1	0	6692
[BMIM][I]/Water	295K,350K	1	300	2700
[BMIM][Cl]/Water	295K,350K	1	300	2700

NPT (constant number of molecules, constant pressure, and constant temperature) ensemble was employed to simulate the PNIPAM-Water-ILs system. Berendsen barostat[158] was applied to maintain the systems' pressure at 1bar, and Berendsen thermostat[158] was employed to keep the systems' temperature below PNIPAM's LCST at 295K and above LCST at 350K respectively. Periodic boundary conditions (PBC) were applied to all three directions of the simulated boxes. The initial atomic velocities were generated with a Maxwellian distribution at the given absolute temperature. The Particle-Mesh Ewald (PME) method was used for the long-range electrostatic interactions. The cut-off distance for Lennard-Jones forces was set as r = 1.2 nm as was done by the developers of the force field.[155] After the simulation, the physical properties were characterized using the GROMACS analysis tools, and the structures were visualized by Visual Molecular Dynamics (VMD).[164]

Water was described by the extended simple point-charge model (SPC/E), which has been demonstrated to perform well in the water/IL system.[54,151] A 26 units PNIPAM oligomer was created and OPLS-AA force field was employed to describe PNIPAM. OPLS-AA has been widely used and validated by previous researchers[143,144,146–148,198] for the simulation of PNIPAM. The model to describe [BMIM][I] and [BMIM][Cl] was also based on the OPLS-AA force field, but their force filed parameters were modified based on Lopes et al.[150,155] and Bhargava et al.'s[149] publications. Table 6.2 provides more detailed information about the force field parameters of ionic liquids in our simulation systems. The IL models were adapted for the specific systems studied by scaling partial atomic charges to give non-integer total ion charges.[54,154] The technique of scaling charges in this manner has been extensively used to capture the effect of charge transfer

between cation and anion in ionic liquids when using a non-polarizable force field[54,154,199]. Models with scaled charges have been found to simulate the density and diffusivity of ionic liquids better than models using charges of ±1.[149,152,219,220] Moreover, this set of force field parameters for ionic liquids were also carefully investigated and validated by various researchers in Dai's group.[53,54,151,152]

Table 6-2 The source of force filed parameters for the ionic liquids in our simulation system

Ionic Liquids	Cation Force Field	Anion Force Field	Charge Scale
[BMIM][I]	Ref[149,153]	Ref[140]	±0.5[152]
[BMIM][Cl]	Ref[149,153]	Ref[153]	±0.8

6.3.Results and Discussion

The Gromacs 5.0.4 package contains a pre-equilibrated coordinate file for SPC/E water, and the water simulation box was verified by previous researchers;[50,138,163,171] so it was unnecessary to equilibrate and validate the water simulation box again in this work. The IL boxes were equilibrated under constant NPT conditions (constant number of molecules N, pressure P, and temperature T) for 5 ns. The purpose of this step was to verify that the IL box possessed correct density at 1 bar and 300 K in order to validate the force field parameters for the IL. As shown in Table 6.3, the equilibrium densities of [BMIM][I] and [BMIM][Cl] boxes were 1.465 kg/L and 1.116kg/L respectively.

Comparing the corresponding values to the experimental value, 1.489 kg/L[152] and 1.079 kg/L[221] in the literature, we found the errors for both densities were within 3.5%, which indicated the validity of the choice of the force filed parameters.

Table 6-3 Comparison of the experimental value vs. simulation value of IL's density at 1bar, 300K.

Ionic liquids	Exp. ρ (kg/L)	Sim. ρ (kg/L)	% Error
[BMIM][I]	1.489 [152]	1.465±0.013	1.6%
[BMIM][Cl]	1.079 [221]	1.116±0.092	3.4%

Table 6-4 Summary of simulation boxes with simulation temperatures, simulation time and number of parallel runs

Simulation System	Temperature (K)	Simulation Time (ns)	# of Parallel runs	Equilibrated Status of PNIPAM
Pure Water	295	10	3	Extended
Pure Water	350	10	3	Coiled
[BMIM][I]/Water	295	15	3	Extended
[BMIM][I]/Water	350	15	3	Coiled
[BMIM][Cl]/Water	295	15	3	Extended
[BMIM][Cl]/Water	350	15	3	Coiled

PNIPAM macromolecules were dispersed in the center of the simulation boxes. Simulations were performed for 10-15 ns at 295K and 350K respectively to make sure the systems had achieved equilibrium. More details of the simulation systems were provided in Table 6.4. For all three simulation systems, PNIPAM possessed an extended configuration at 295K, and a coiled configuration at 350K (Figure 6.1). These results were consistent with the experimental observations in the previous studies.[94,112,222,223]

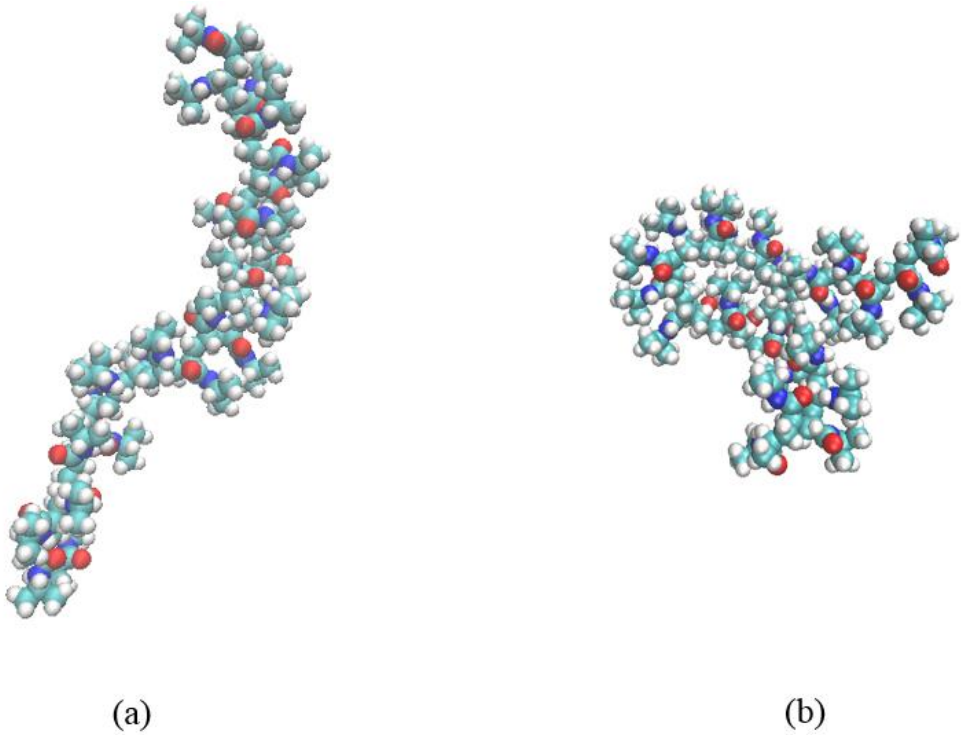

Figure 6-1 The configurations of the 26-units PNIPAM oligomer (a) extended structure at 295K; (b) coiled structure at 350K. (for the reason of concision, only the configurations in the [BMIM][I]/Water system was indicated here)

6.3.1. Trend of the LCST in Different Systems

The enthalpy associated with the PNIPAM under different conditions was calculated as its interaction energy with the solvent molecules by averaging over the last 10 ns of the simulations. Table 6.5 summarizes the values of enthalpy for each system at 295K and 350K. The difference of the enthalpy at high vs. low temperatures roughly indicates the "enthalpy contribution" to the free energy change associated with the extended-to-coiled transition of a single PNIPAM due the temperature change. As illustrated in Figure 6.2, we can see that the PNIPAM in the pure water system possessed the highest enthalpy increase after the extended-to-coiled transition. For the two hydrophilic ionic liquids/water systems, the increase of enthalpy was significantly lower.

Table 6-5 Enthalpies and enthalpy change of PNIPAM in water, [BMIM][I]/water and [BMIM][Cl]/water systems at 295K vs. 350K

Simulation System	H_{295K}	H_{350K}	ΔH
Pure Water	-2272.2±64.2	-1829.6±71.1	442.6±67.4
[BMIM][I]/Water	-1982.7±40.4	-1708.2±34.5	274.51±37.3
[BMIM][Cl]/Water	-2155.5±35.0	-1875.3±36.9	280.2±36.0

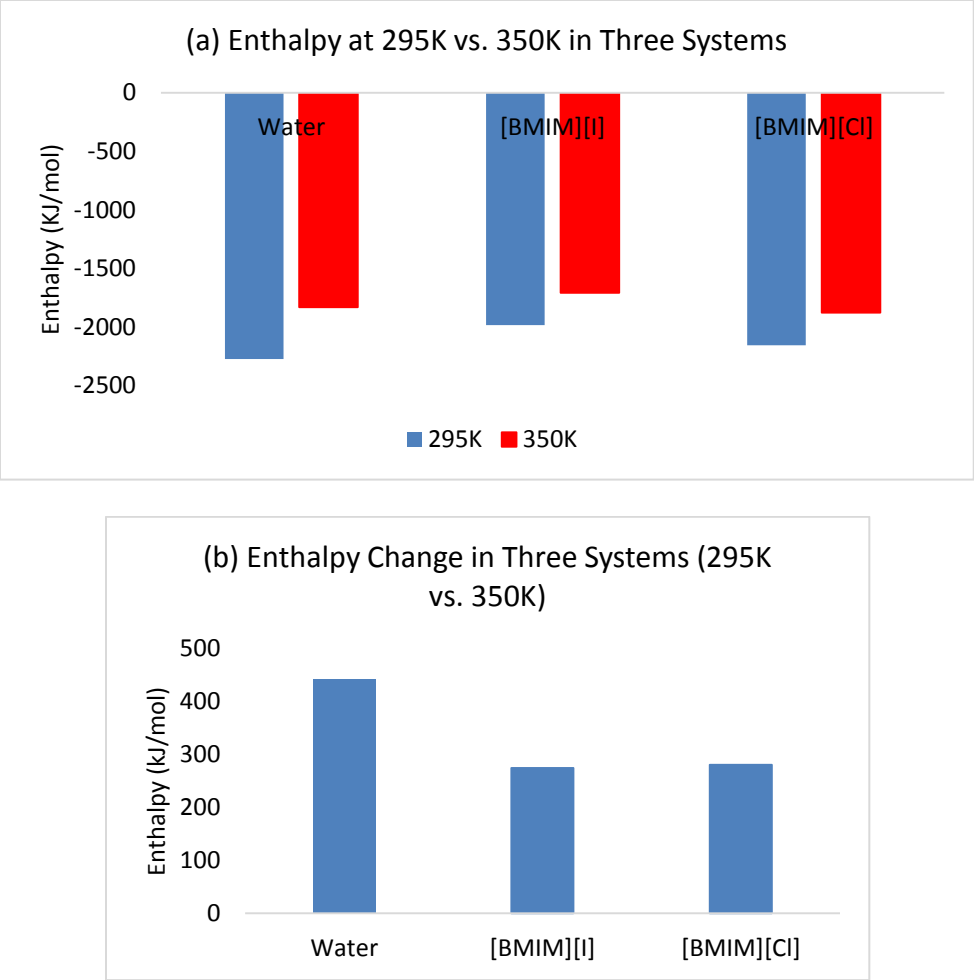

Figure 6-2 (a) The enthalpies of PNIPAM in water, [BMIM][I]/Water, and [BMIM][Cl]/water systems at 295K vs. 350K; (b) the enthalpy change of PNIPAM at 350K vs. 295K in three systems.

We now provide a thermodynamics argument based on these observations to predict the trend of LCST in these systems. In order for the coiled configuration to be stable at high temperatures, the overall change of the free energy ΔG for the extended-to-coiled transition should be negative, i.e.,

$$\Delta G = \Delta H - T_c \Delta S < 0$$

where ΔH and ΔS respectively indicate the change of enthalpy and entropy, and T_c is the LCST. Since for all three system, the corresponding low and high temperature PINIPAM configurations are statistically identical, thus, the entropy change ΔS in all three systems are roughly the same. This suggests that the system with a larger enthalpy increase $\Delta H>0$ for the transition requires a highly T_c to compensate the larger increase of ΔG due to this enthalpy contribution. Therefore, we argue that PNIPAM would possess a lower LCST for the extended-to-coiled transition in the [BMIM][I]/water and [BMIM][Cl]/water systems than the pure water system.

6.3.2. Effects of Hydrogen Bonding on the LCST

Inter-molecular hydrogen bonds between the PNIPAM and water molecules were calculated to investigate the hydrophilic-hydrophobic transition of the PNIPAM polymer at 295K and 350K in three systems (Table 6.6). The criterion used to determine the presence of a hydrogen bond was illustrated in the inset picture of Figure 5.5 in Chapter 5. The hydrogen bond length between two heavy atoms D, A (O or N in PNIPAM and O in water molecules) is greater or equal to 3.5Å, and that the cut-off for the hydrogen bond angle is 30˚. The temporal evolution of hydrogen bonds of PNIPAM in the simulations at 295K and 320K in three systems is illustrated in Figure 6.3. Two observations can be made from the calculations of hydrogen bonds: first, the number of hydrogen bonds between PNIPAM and water reduced at higher temperature in all three simulation systems, indicating that PNIPAM was less hydrated at higher temperature. This result is in agreement with the previous experimental observations and hypothesis.[94,218] Second, for both [BMIM][I]/water and [BMIM][Cl]/water systems, the number of hydrogen bonds between PNIPAM and water was significant lower than the pure water system at

the same temperature. This suggests that during the extended-to-coiled configuration transition in the miscible ionic liquids/water systems, fewer hydrogen bonds were broken between PNIPAM and water than that in the pure water system. This observation may also explain why PNIPAM tended to precipitate at a lower temperature in [BMIM][I]/water and [BMIM][Cl]/water systems than pure water.

Table 6-6 Number of Inter-molecular hydrogen bonds between PNIPAM and Water in pure water, [BMIM][I]/water and [BMIM][Cl]/water systems at 295K vs. 350K

Simulation System	# of HB, 295K	# of HB, 350K
Pure Water	53.56±3.68	43.55±4.46
[BMIM][I]/Water	26.46±4.19	21.97±4.42
[BMIM][Cl]/Water	32.03±3.0.	25.46±4.14

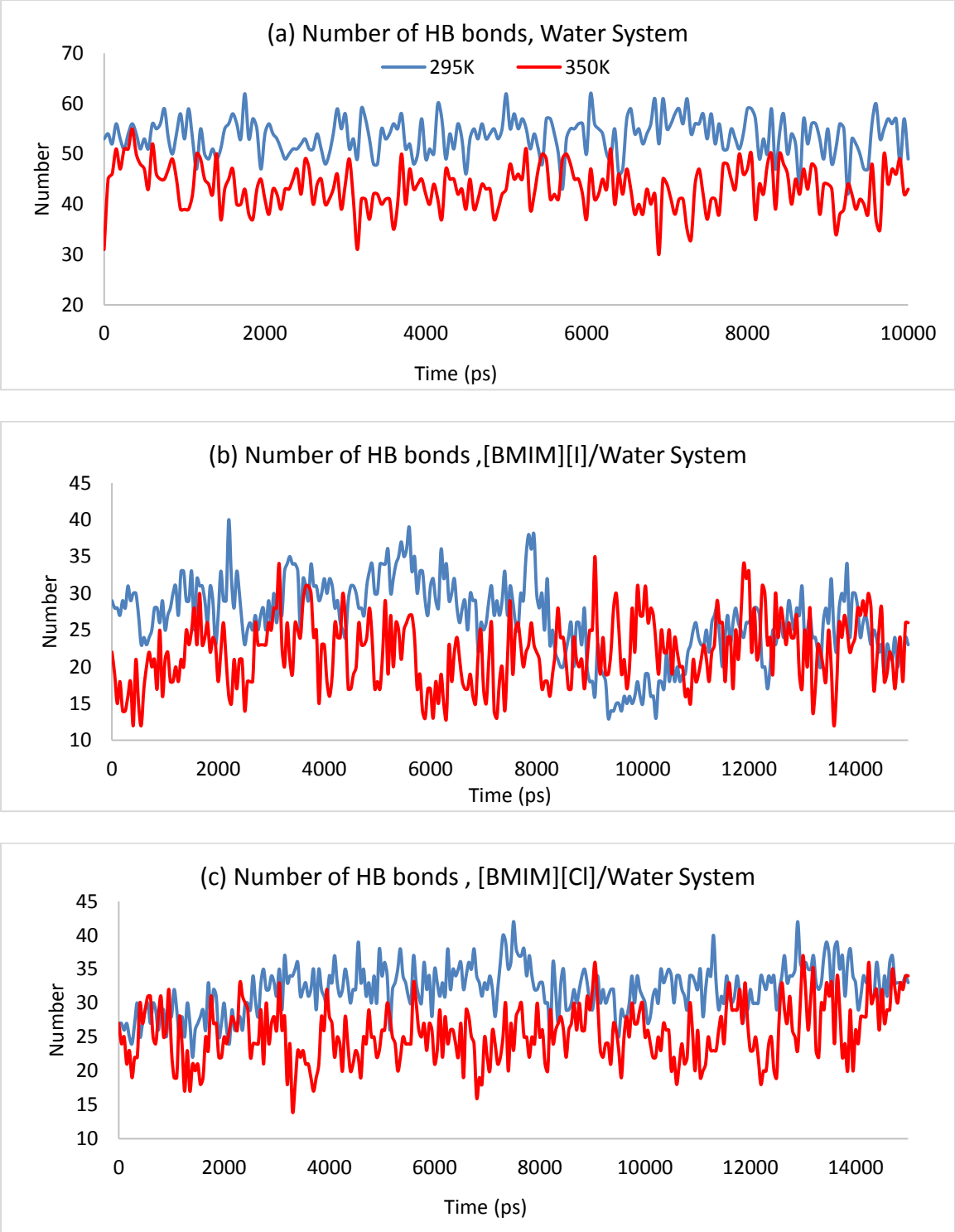

Figure 6-3 The intermolecular hydrogen bond numbers between PNIPAM and water at 295K vs. 350K in (a) pure water system, (b) [BMIM][I]/water system, and (c) [BMIM][Cl]/water system.

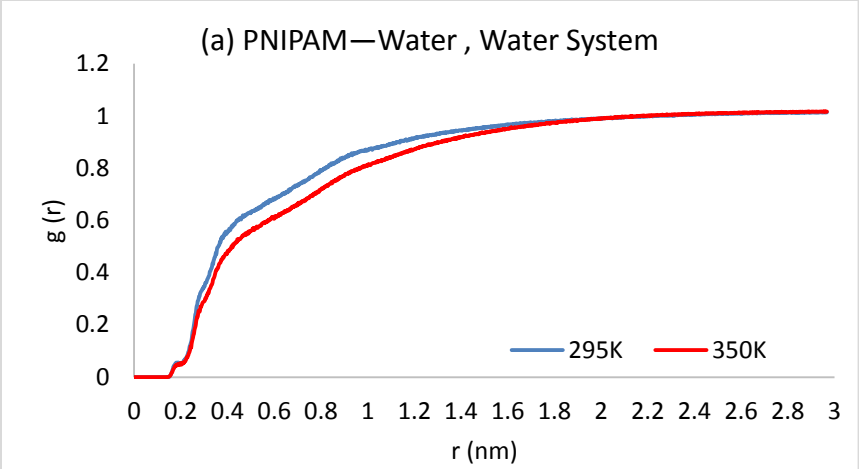

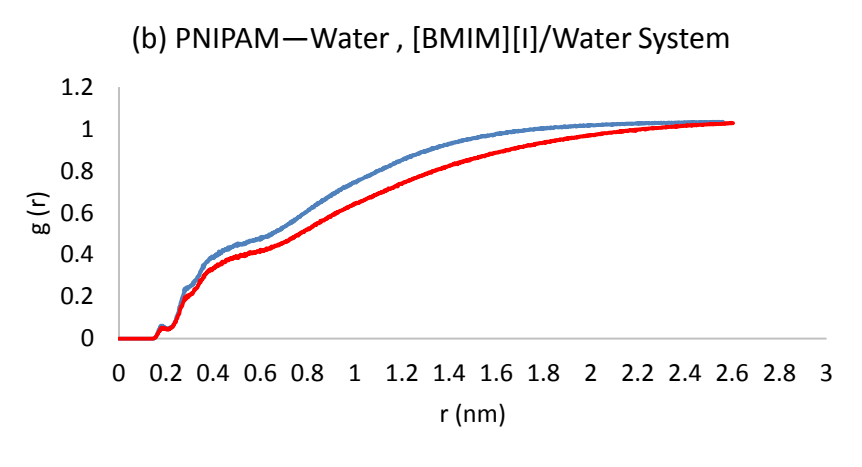

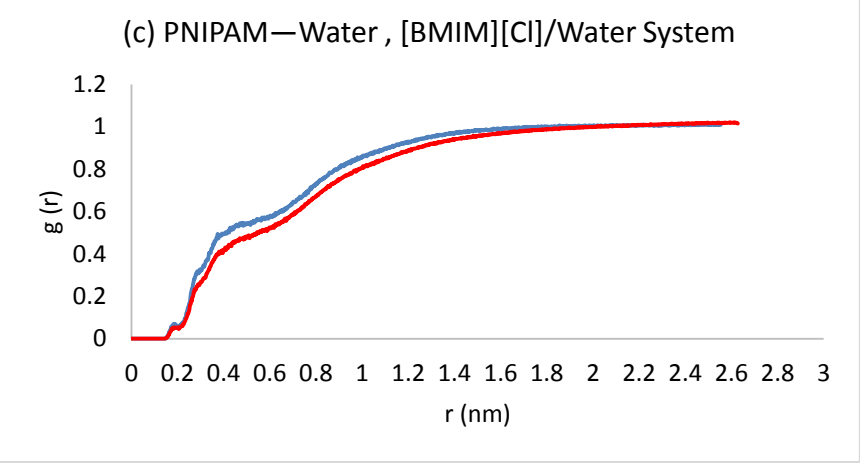

Figure 6-4 Radial Distribution Function of water molecules around PNIPAM molecule in (a) pure water system, (b) [BMIM][I]/water system, and (c) [BMIM][Cl]/water system.

To further explore the structural precursor for the interactions (i.e., hydrogen bonding) between PNIPAM and water, the Radial Distribution Function (RDF) between PNIPAM and water molecules were calculated. As shown in Figure 6.4, PNIPAM had stronger affinity with water molecule at lower temperature in all the three systems. This indicates that PNIPAM was better solvated at lower temperature. In addition, the "strength" of the interactions between PNIPAM and water molecule of different systems were assessed by comparing the PNIPAM-water RDF at the same temperatures. As shown in Figure 6.5, at both lower and higher temperatures, PNIPAM had the strongest interaction with water molecules in the pure water system, while in the two miscible ionic liquids/water systems, such interaction was significantly weaker. These results are perfectly consistent with the aforementioned direct hydrogen-bond counting and analysis.

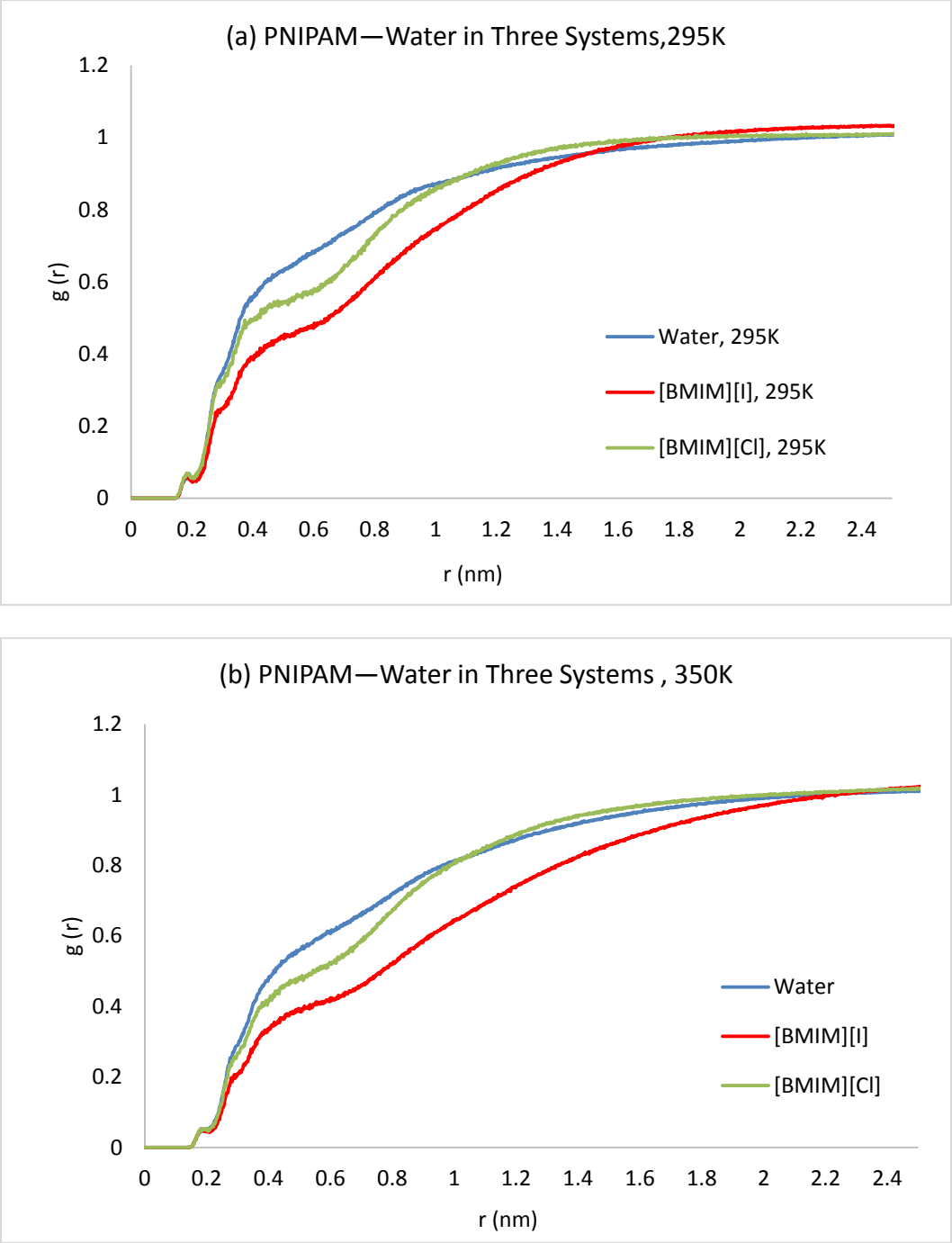

Figure 6-5 Comparison of Radial Distribution Function (RDF) of water molecules around PNIPAM molecule in pure water, [BMIM][I]/water and [BMIM][Cl]/water system at (a) 295K, (b) 350K.

6.3.3. Effects of Ions on the LCST

To elucidate the effects of ions on the LCST of PNIPAM, RDF was applied to probe the distribution of solvent species around PNIPAM in the [BMIM][I]/water and [BMIM][Cl] simulation systems. Interactions were investigated between the most effectively charged parts of the molecules, such as the carbonyl oxygen (-) and amide hydrogen (+) of PNIPAM, the imidazolium ring (+) of BMIM cation, the iodide (-) and chloride (-) anions. The interactions between the nonpolar species such as the isopropyl sidechain of PNIPAM and the butyl group of BMIM cation were explored as well. In each case, the RDF was averaged for the last 5 ns of simulation time.

Figure 6.6 and Figure 6.7 illustrate the interactions between PNIPAM and BMIM cation. Figure 6.6 shows the distribution of the positively charged imidazolium ring of BMIM cation around the negatively charged carbonyl oxygen. Figure 6.7 depicts the RDF for the non-polar butyl group of BMIM cation with respect to the isopropyl group of PNIPAM. Comparing Figure 6.6 and Figure 6.7, the remarkably sharp peak at around 0.55nm in Figure 6.7 indicates the isopropyl sidechain of PNIPAM had strong association with the butyl group of BMIM cation. While in Figure 6.6, such peaks cannot be clearly observed, suggesting the affinity between the charged moiety, carbonyl oxygen of PNIPAM and imidazolium ring of BMIM cation was weak. To further substantiate this observation, each Coulombic and Lenard-Jones component in the interaction energies of PNIPAM in the [BMIM][I]/water system and [BMIM][Cl]/water system was calculated (Table 6.7) and graphically presented in Figure 6.8. As shown in Figure 6.8, the magnitude of Lennard-Jones interaction of PNIPAM-BMIM cation was much greater than that of the Coulombic interaction of PNIPAM-BMIM cation at the same temperature

for both [BMIM][I]/water and [BMIM][Cl]/water systems. Thus, combing the calculation of RDF and energy analysis, we may conclude that the major interactions between PNIPAM and BMIM cation originated from the hydrophobic effects between two non-polar moieties, i.e., isopropyl group of PNIPAM and the butyl group of BMIM cation.

Table 6-7 (a) The Lennard-Jones potential energies and Coulombic potential energies of PNIPAM at 295K vs. 350K in [BMIM][I]/water system

	295K		**350 K**	
Interacting Species with PNIPAM	**Coul (kJ/mol)**	**LJ (kJ/mol)**	**Coul (kJ/mol)**	**LJ (kJ/mol)**
Water	-668.7±52	-224.2±44.7	-549.7±40.0	-183.9±37.9
$[BMIM]^+$	-4.2±2.7	-837.7±66.7	-6.0±0.8	-772.3±56.6
$[I]^-$	-220.1±57.2	-27.8±11.1	-169.6±40.7	-26.7±10.4

Table 6.7 (b) The Lennard-Jones potential energies and Coulombic potential energies of PNIPAM at 295K vs. 350K in [BMIM][Cl]/water system

	295K		**350 K**	
Interacting Species with PNIPAM	**Coul (kJ/mol)**	**LJ (kJ/mol)**	**Coul (kJ/mol)**	**LJ (kJ/mol)**
Water	-845.5±28.0	-321.2±34.0	-645.9±16	-277.8±33
$[BMIM]^+$	-10.2±5.5	-772.2±45.9	-37.7±4.3	-717.2±40.5
$[Cl]^-$	-161.0±50.1	-45.4±9.5	-156.6±49.8	-40.0±9.0

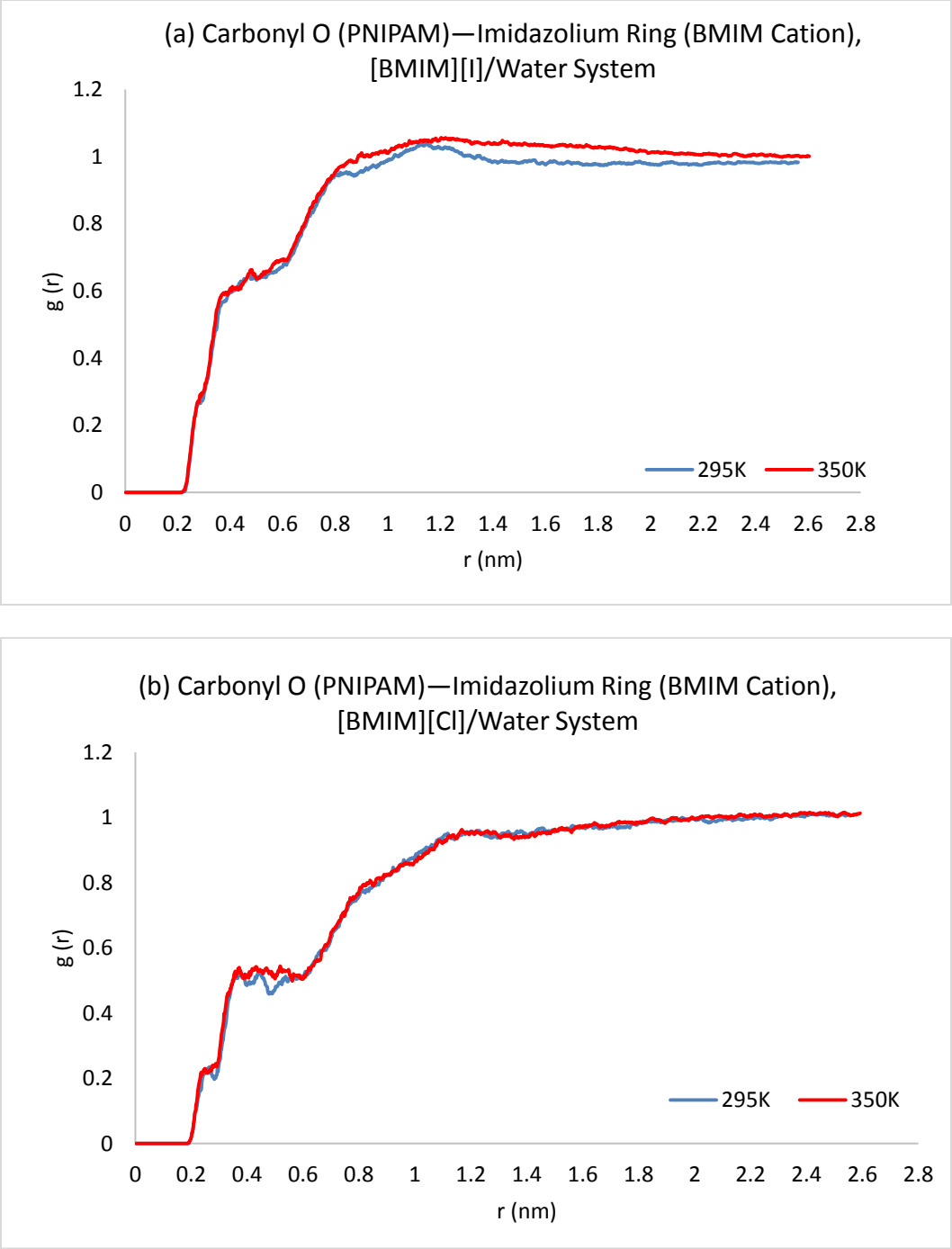

Figure 6-6 Radial Distribution Functions (RDF) of the imidazolium ring of BMIM cation around carbonyl oxygen of PNIPAM in the (a) [BMIM][I]/water system; (b) [BMIM][Cl]/Water system

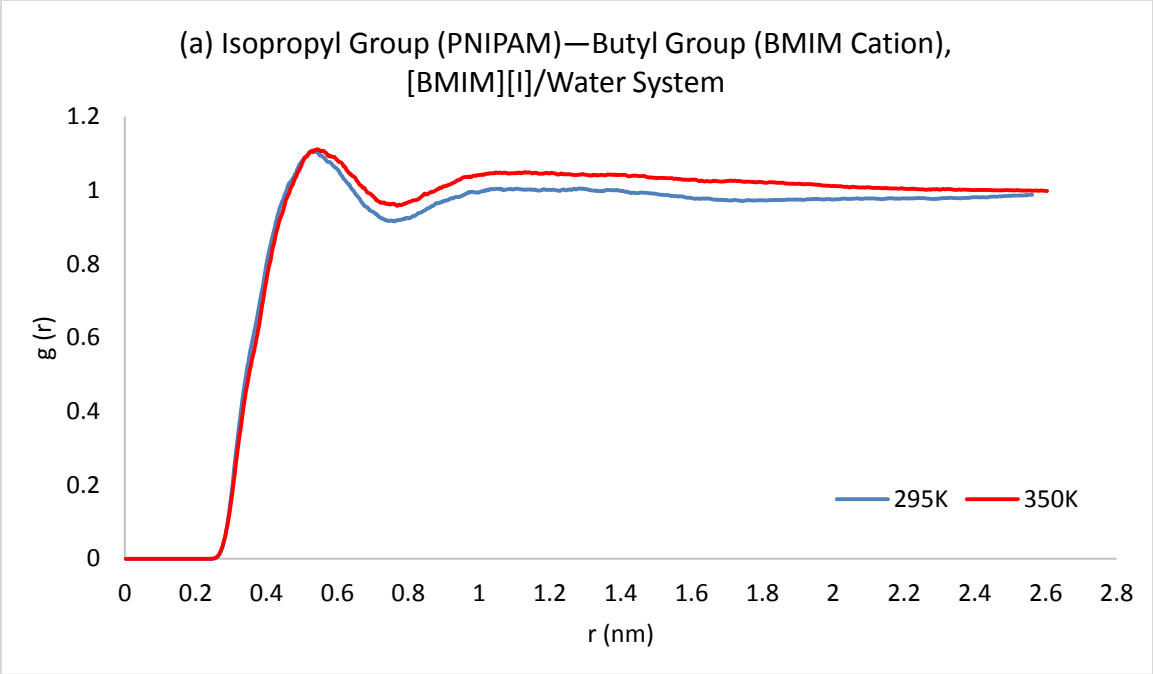

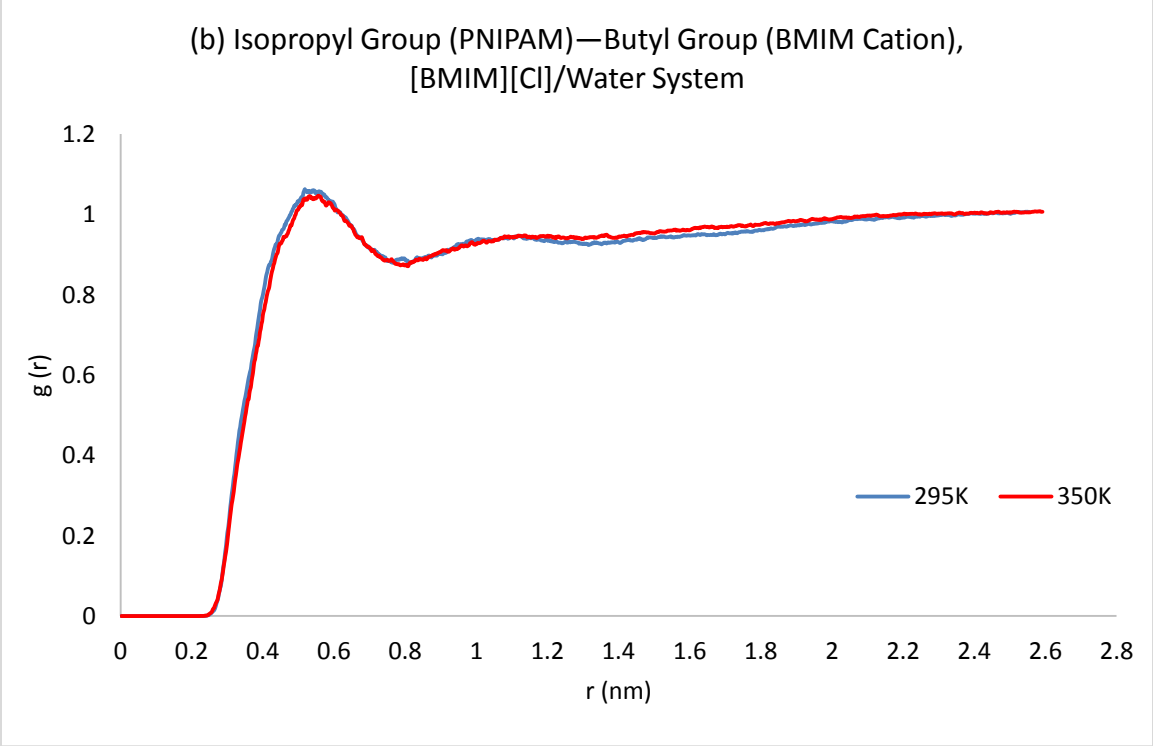

Figure 6-7 Radial Distribution Functions (RDF) of the butyl group of BMIM cation around the isopropyl group of PNIPAM in the (a) [BMIM][I]/water system; (b) [BMIM] [Cl]/water system.

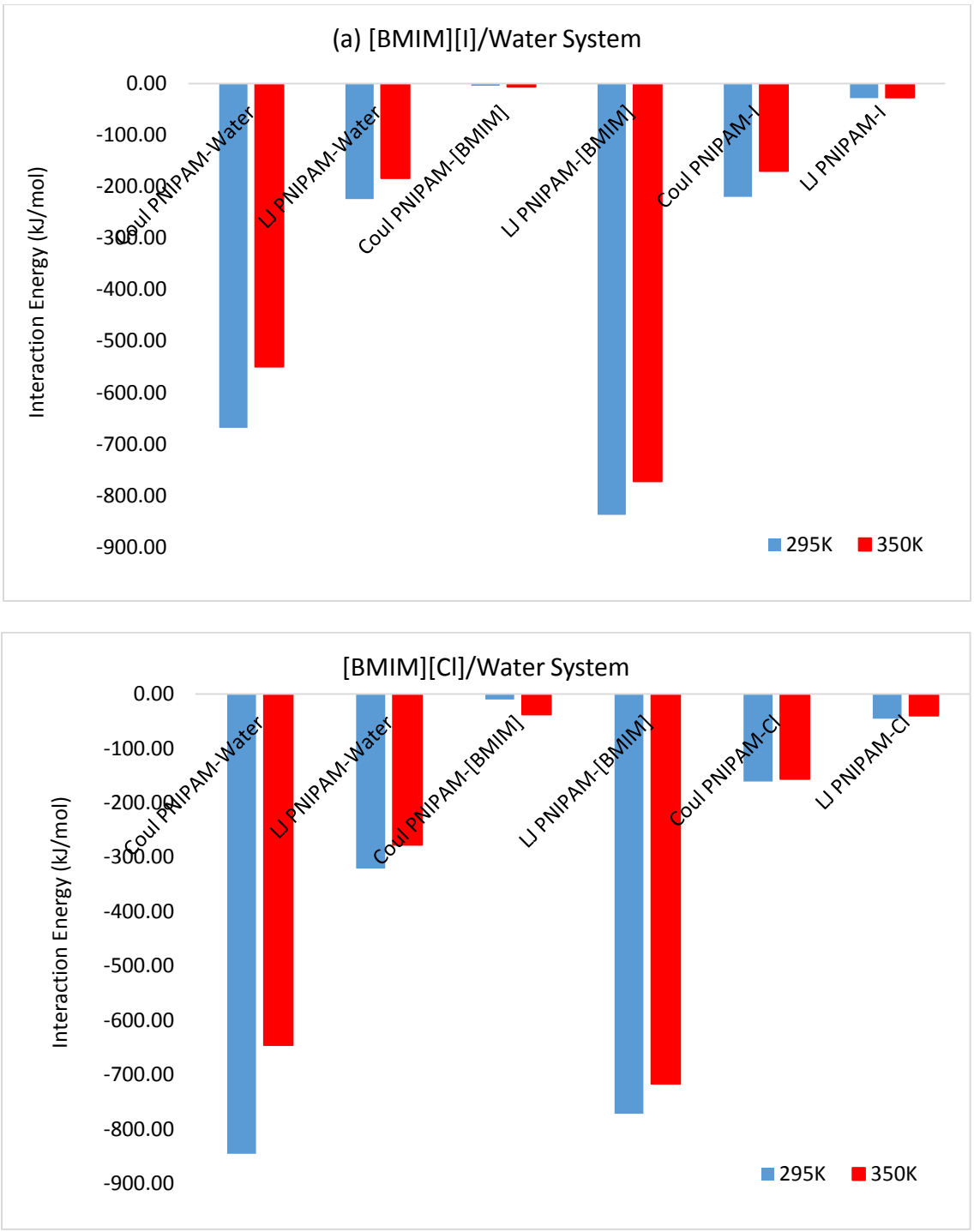

Figure 6-8 Coulombic potential (Coul) and Lennard-Jones potential (LJ) of PNIPAM-water, PNIPAM-$[BMIM]^+$ and PNIPAM-anions (I^- or Cl^-) at 295K and 350K in the (a) [BMIM][I]/water system; (b) [BMIM][Cl]/water system.

Figure 6.9 and 6.10 describe the interactions between PNIPAM and anions of the ionic liquids (I^-, Cl^-). Figure 6.9 is the RDF plots of the anions (I^-, Cl^-) with respect to the mass center of amide hydrogen of PNIPAM in [BMIM][I]/water and [BMIM][Cl[/water systems respectively. Figure 6.10 shows the RDF of anions (I^-, Cl^-) around the mass center of carbonyl carbon of PNIPAM in the ionic liquid/water systems. The well-defined peaks in Figure 6.9 and Figure 6.10 indicates both the amide hydrogen and carbonyl carbon of PNIPAM had strong affinity with the anions. Besides, if we compare the interaction strength between PNIPAM and anions by overlaying the RDF plots at the same temperature (Figure 6.11 and Figure 6.12), it can be found that I^- had much stronger interaction with amide hydrogen and carbonyl carbon of PNIPAM than Cl^-.

Table 6-8 Interaction energies of $[BMIM]^+$–Cl^- and $[BMIM]^+$–I^- at 300K

Interacting Species	**Coulomb (kJ/mol)**	**LJ (kJ/mol)**	**Interaction Energy (kJ/mol)**
$[BMIM]^+$—I^-	-19917.1±126.6	-1694.0±86.9	-21611.1±105.1
$[BMIM]^+$—Cl^-	-66772.8±241.3	-1329.0±127.3	-68101.8±174.9

In order to interpret the different binding strength between PNIPAM and anions, a series of energy analysis and RDF calculations were performed. Figure 6.13 illustrates the cation-anion interactions of [BMIM][I] vs. [BMIM][Cl] at 300K. It indicates at the same temperature, the association of $[BMIM]^+$–Cl^- was stronger than $[BMIM]^+$–I^-. The energy analysis (Table 6.8) of cation-anion of ionic liquids also agree with this

observation, as shown in Figure 6.14 the interaction energy between $[BMIM]^+$ and Cl^- was significantly lower than the interaction energy between $[BMIM]^+$ and I^-. These results are consistent with the previous study of interactions between BMIM cation and halide anions (Cl^-, Br^- and I^-) by ab initio calculations[224]: smaller anions such as Cl^- had stronger electrostatic attraction to the BMIM cation and tended to bind more closely with BMIM cation than I^-.

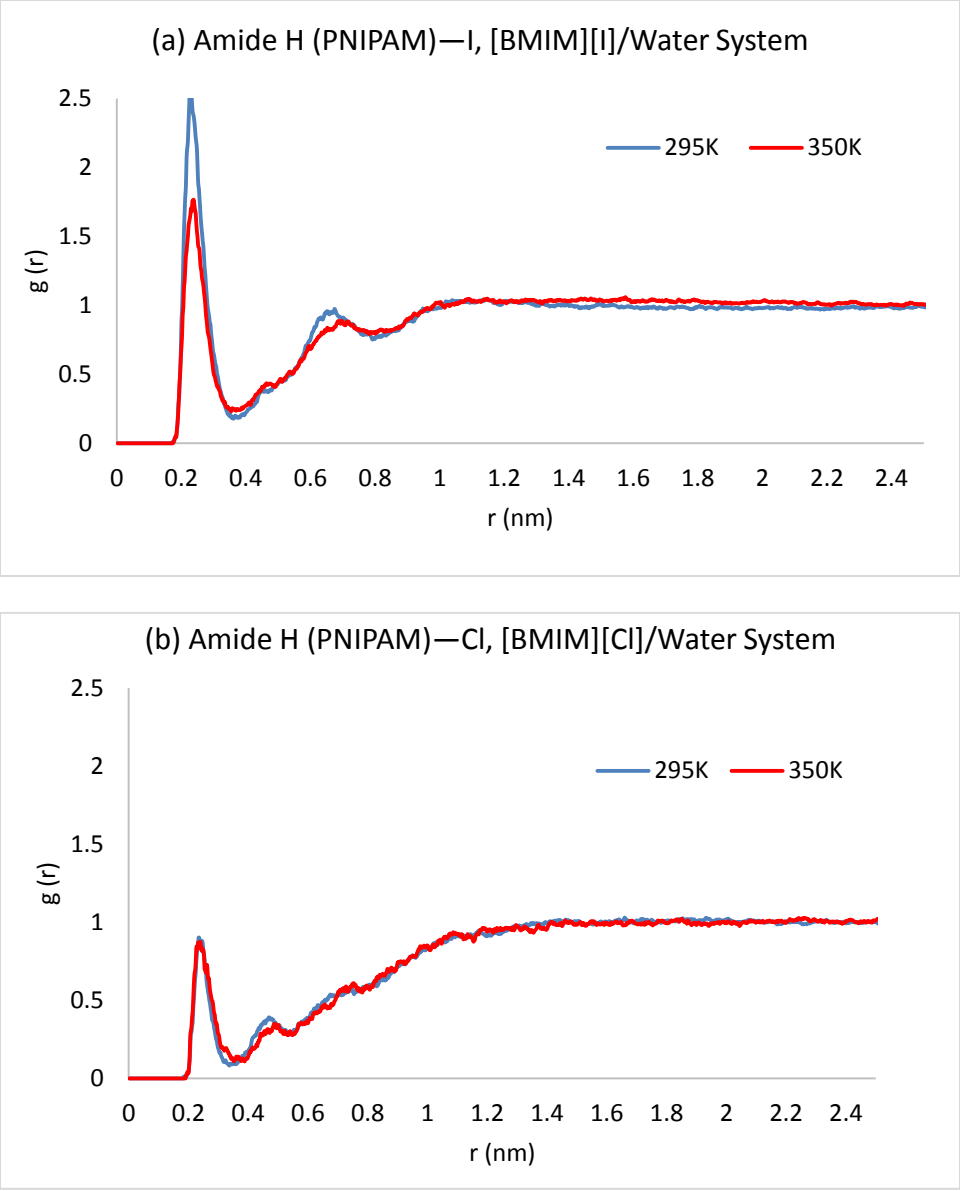

Figure 6-9 Radial Distribution Functions (RDF) of (a) the I^- anion around the amide hydrogen of PNIPAM in the [BMIM][I]/water system, (b) the Cl^- anion around the amide hydrogen of PNIPAM in the [BMIM][Cl]/water system.

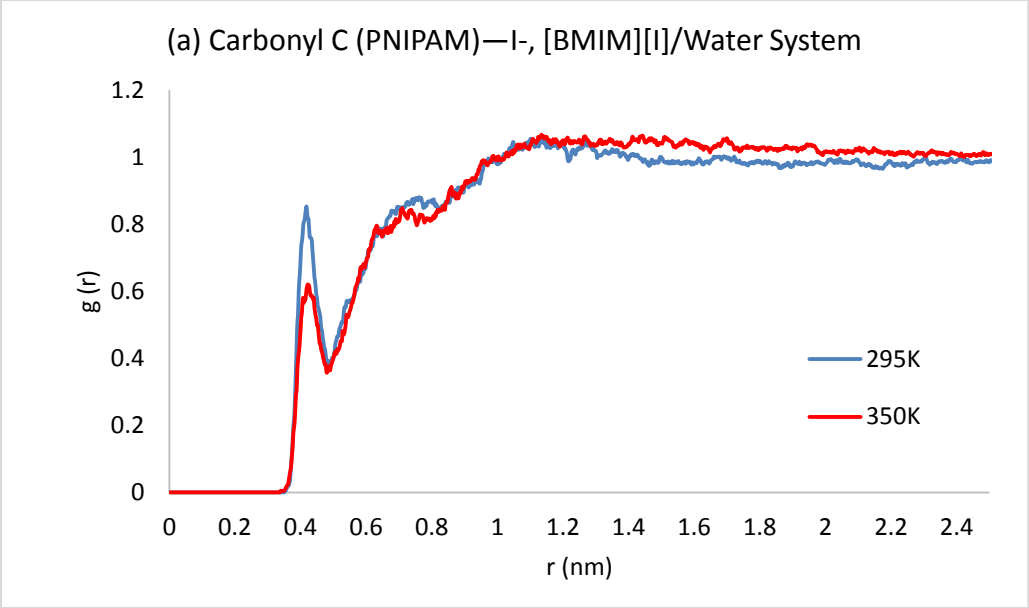

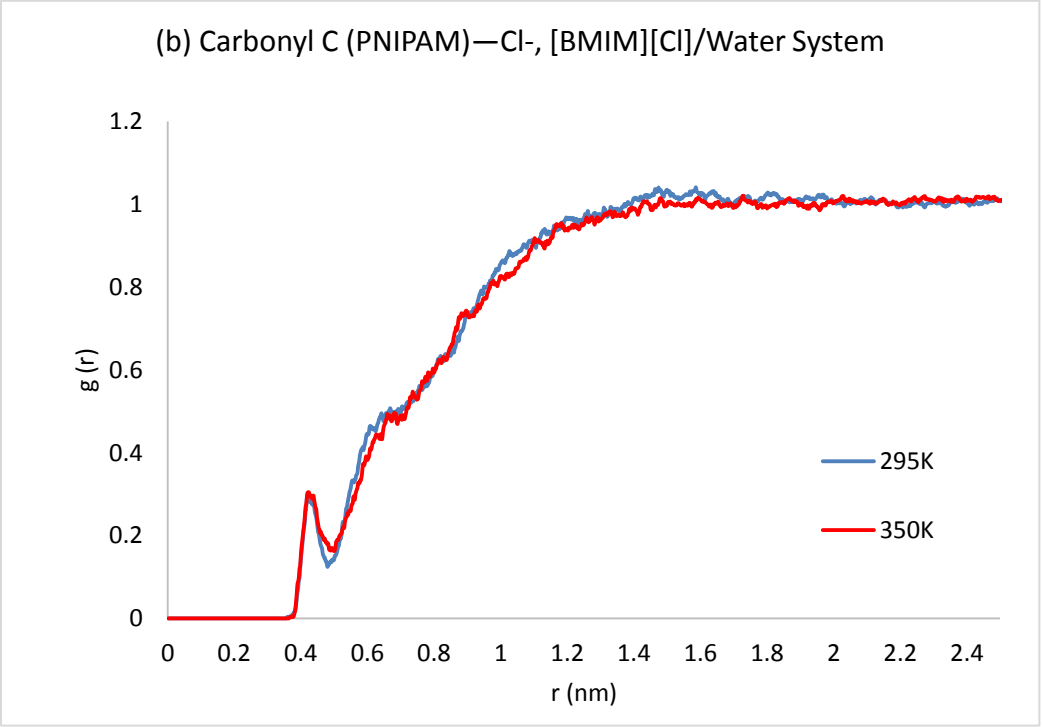

Figure 6-10 Radial Distribution Functions (RDF) of (a) the I^- anion around the carbonyl carbon of PNIPAM in the [BMIM][I]/water system, (b) the Cl^- anion around the carbonyl carbon of PNIPAM in the [BMIM][Cl]/water system.

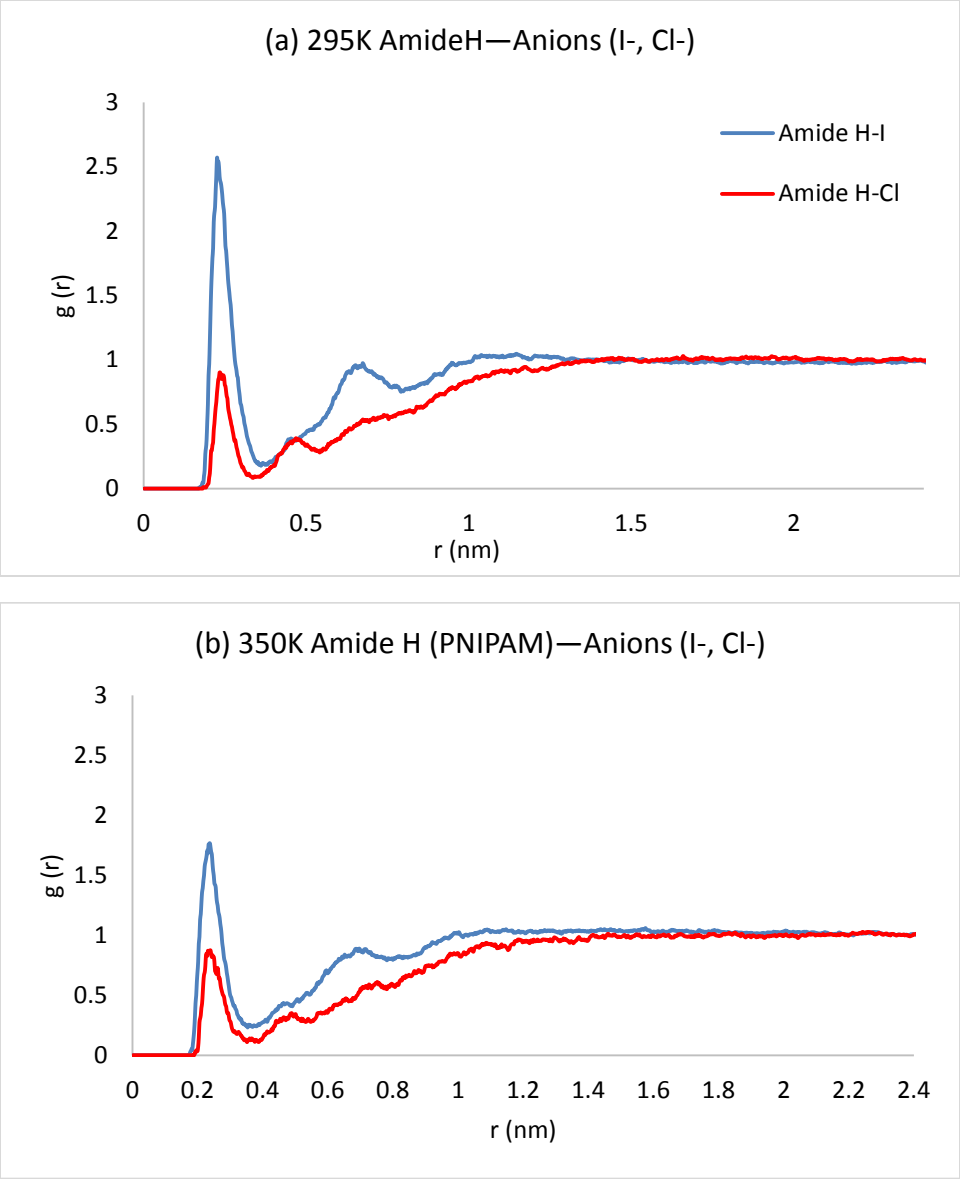

Figure 6-11 Comparison of RDF of anions (I^-, Cl^-) around amide hydrogen of PNIPAM at (a) 295K, (b) 350K.

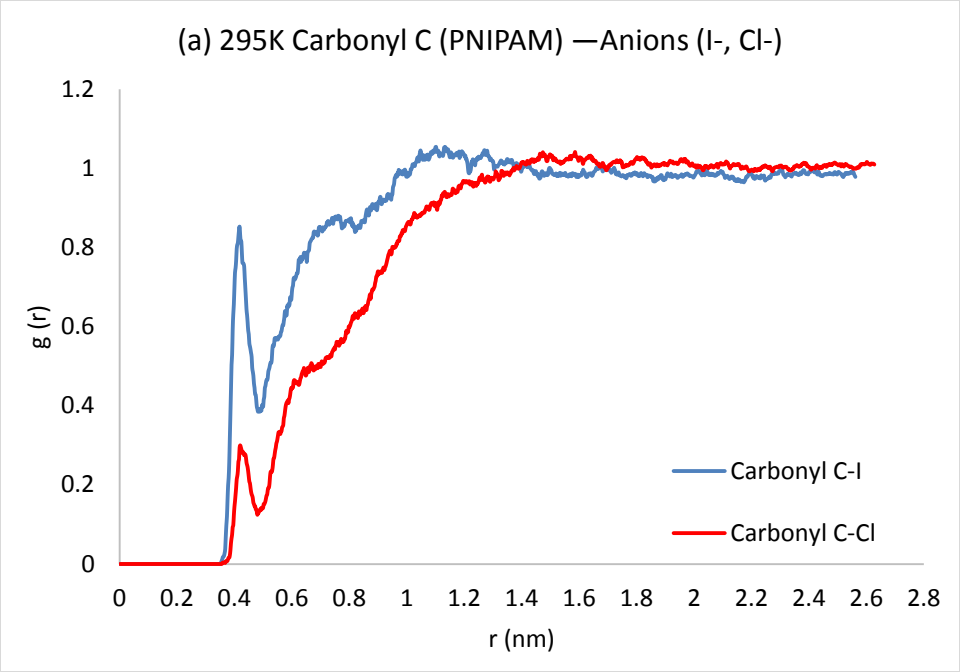

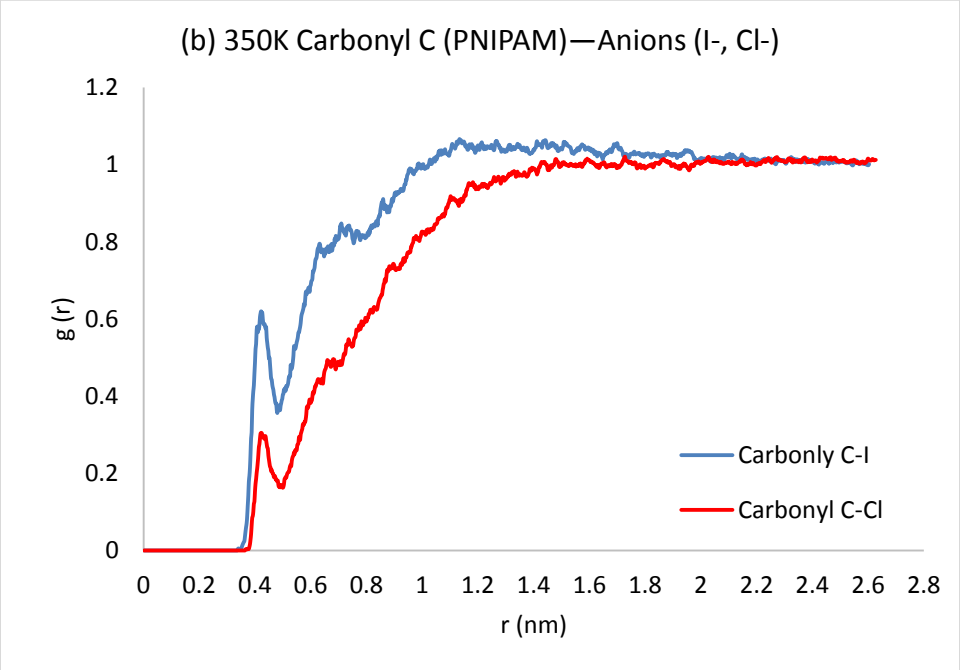

Figure 6-12 Comparison of RDF of anions (I^-, Cl^-) around carbonyl carbon of PNIPAM at (a) 295K, (b) 350K.

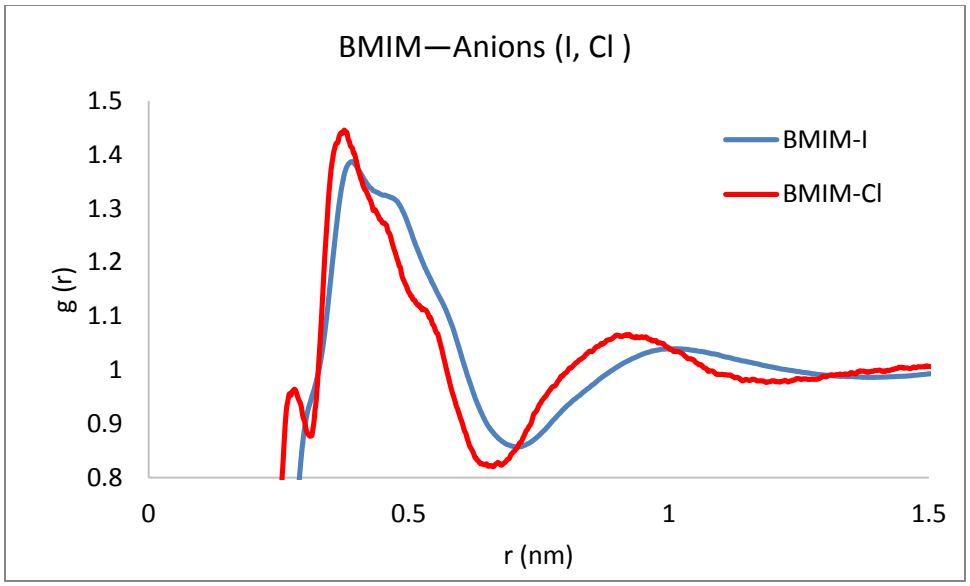

Figure 6-13 Comparison of RDF of anions (I^-, Cl^-) with respect to BMIM cations of PNIPAM at 300K.

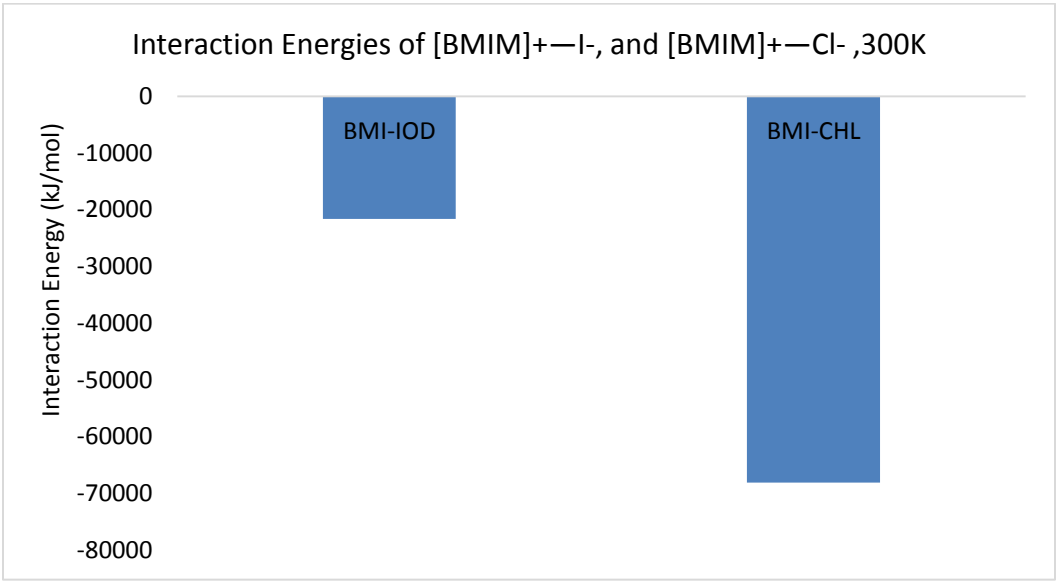

Figure 6-14 Interaction energies of $[BMIM]^+$-I^- (BMI-IOD) and $[BMIM]^+$-Cl^- (BMI-CHL) at 300K.

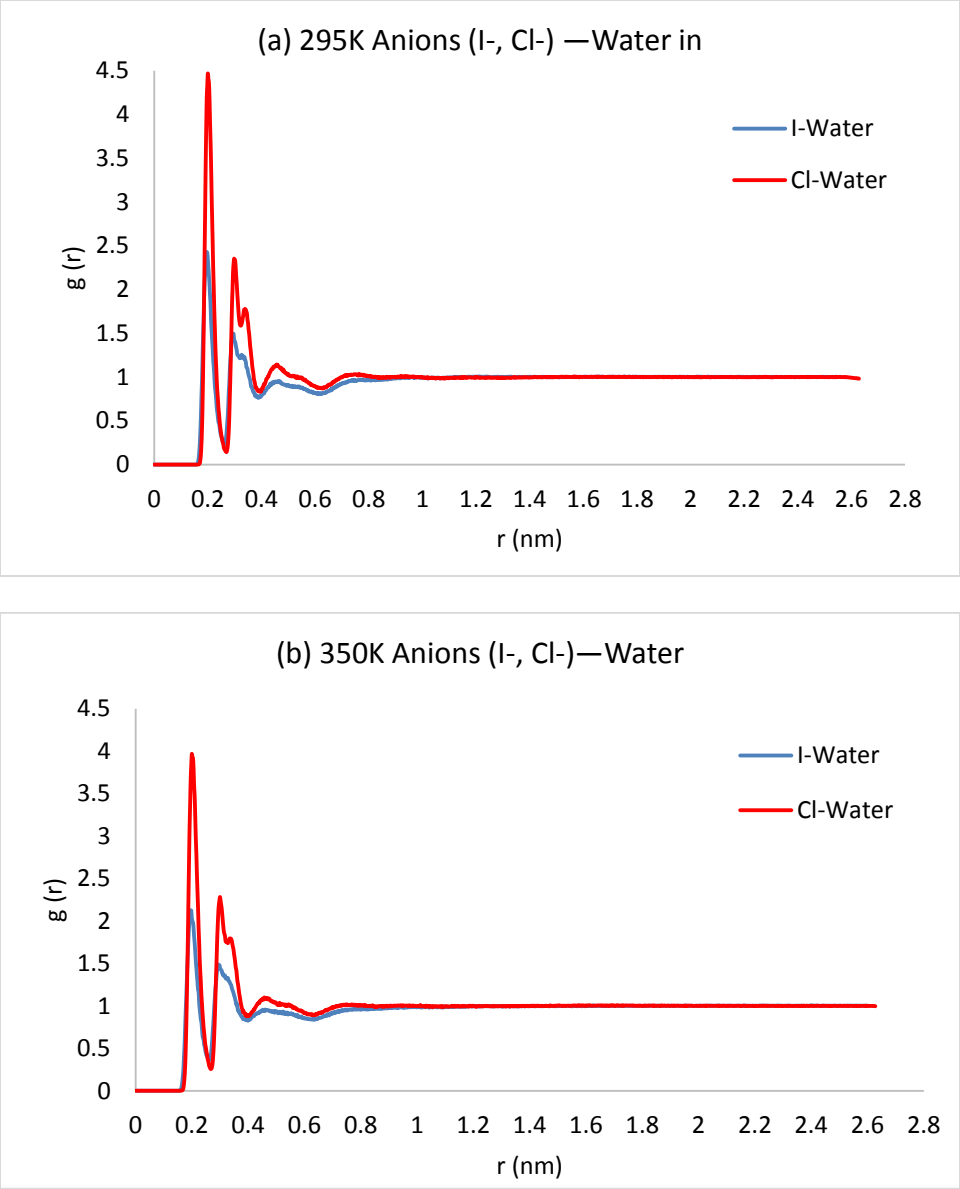

Figure 6-15 Radial Distribution Functions (RDF) of anions (I^-, Cl^-) around water molecules in [BMIM][I]/water and [BMIM][Cl]/water systems (a) at 295K, (b) at 350K.

The interactions between anions (I^-, Cl^-) and water were also investigated in our study. Figure 6.15 shows the RDF plots of I^- and Cl^- with respect to water molecules, which clearly indicates that Cl^- had stronger association with water molecule than I^-. The energy analysis between anions and water (Figure 6.16) were consistent with the RDF

calculation. Specifically, Cl^- had obviously lower interaction energy with water molecules than I^-, suggesting that Cl^- was better solvated than I^-. This result is not surprising since Cl^- is more hydrophilic than I^-. Combining the above RDF and energy analysis of BMIM-anions and water-anions allows us to provide a possible explanation why I^- had stronger interaction with PNIPAM than Cl^-. In particular, in our simulation systems PNIPAM, BMIM cations, and water molecules were competing for binding with the anions (I^- or Cl^-). Since Cl^- had stronger affinity with both BMIM cations and water molecules than I^-, its association with PNIPAM was relatively weaker.

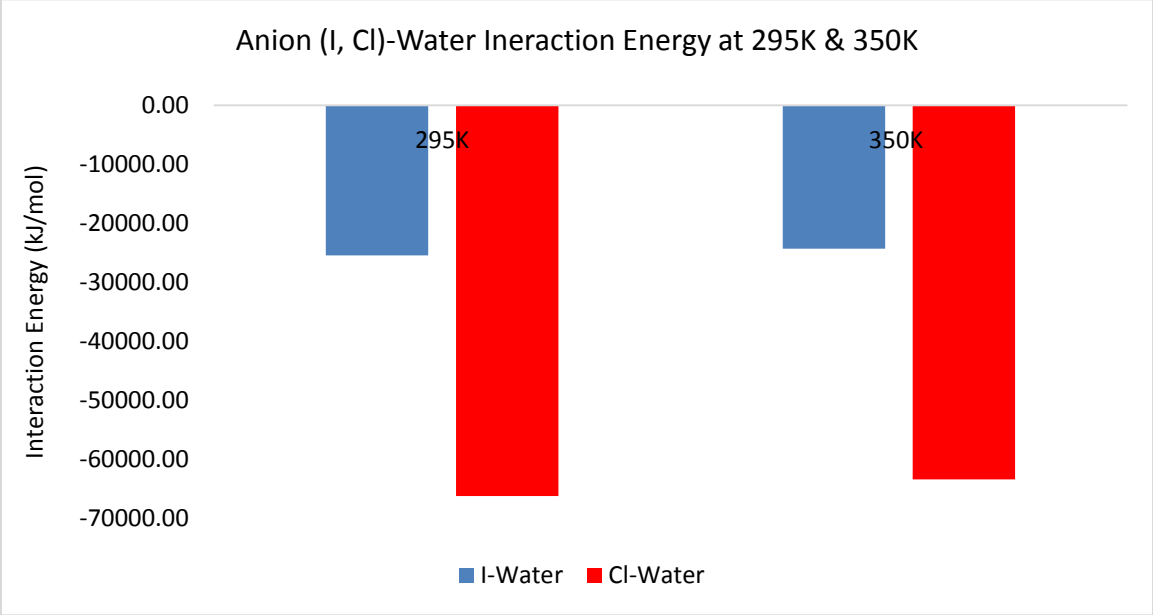

Figure 6-16 Interaction energies of water-I- vs. water-Cl- at 295K and 350K.

6.3.4. Comparison with Salt Solutions

The effects of salt ions on the LCST of macromolecules in aqueous solutions were more extensively studied than the impact of ions of ionic liquids on the LCST of PNIPAM in ionic liquids/water systems. And our hydrophilic ionic liquids [BMIM][I] and [BMIM][Cl] were in certain extent similar to salts such as NaI and NaCl. Thus, for the purpose of identifying the similarity/uniqueness of the ILs/water systems, we compared our simulation results with the previous studies of PNIPAM in the salt solutions (e.g. PNIPAM in NaI and NaCl solutions)[105,143,203,209,210,214,215] and have some interesting findings. First, in the MD simulation study of PNIPAM in salt solutions, [105,143,214,215] it appeared that the salt anions (e.g. I^-, Cl^-) exhibited very weak or no interactions with PNIPAM. Instead, the interactions mainly took place between PNIPAM and salt cations (e.g. Na^+, K^+). While the results were usually in conflict with the simulation studies in the experimental investigations,[203,209,216–218] it is suggested that the salt ions interacted with PNIPAM mostly by direct binding between anions of the salts (e.g. I^-, Cl^-) and the amide groups of PNIPAM. The interactions between PNIPAM and cations were negligible. In our simulation study of PNIPAM in the ionic liquid/water systems, we found PNIPAM actually had strong interaction with both cations and ions of the ionic liquids, but the interactions originated from different mechanism. The cation (BMIM)–PNIPAM interactions were mainly due to hydrophobic effect which took place between the nonpolar group of BMIM butyl and PNIPAM isopropyl side chain. For the anion (I^-, Cl^-)–PNIPAM interactions, the binding mostly took place between the charged group of PNIPAM (amide hydrogen, carbonyl carbon) and I^- or Cl^-, which originated from electrostatic force. In addition, the interactions between PNIPAM and I^- was

significantly stronger than the interaction between PNIPAM and Cl^-, which was in agreement with the order of anion-PNIPAM interaction strength in the experimental studies of PNIPAM in salt solutions.[203,209,216–218]

6.4.Conclusions

PNIPAM was simulated in water, [BMIM][I]/water and [BMIM][Cl]/water systems at 295K and 350K in our study. Extended-to-coiled phase transition was observed in all three simulation systems. The enthalpy change in the pure water system was significantly higher than the ionic liquid/water systems, which may explain why PNIPAM tended to have a LCST type transition at lower temperatures in the imidazolium based IL/water systems. In addition, it was found that the number of inter-molecular hydrogen bonds between PNIPAM and water were notably lower in the [BMIM][I]/water and [BMIM][Cl]/water systems than the pure water systems, suggesting fewer hydrogen bonds were required to break in the ionic liquid/water systems, which may also explain why PNIPAM could precipitated in the ionic liquid/water system at lower temperatures. The Radial Distribution Functions between PNIPAM and ions revealed that PNIPAM had strong interactions with both cations and anions of the ionic liquids. However, the PNIPAM-cation (BMIM) and PNIPAM-anions (I^-, Cl^-) interactions had different origins. The PNIPAM-BMIM cation interactions were mainly from the nonpolar groups, the isopropyl side chain of PNIPAM and the butyl group of BMIM cation, while the PNIPAM-anions (I^-, Cl^-) interactions mostly took place between the charged part of PNIPAM (amide hydrogen, carbonyl carbon) and the anions (I^-, Cl^-). In addition, we found the interactions between PNIPAM and I^- were significantly stronger than Cl^-. Based on a series of energy analysis and RDF calculations, it was found I^- had weaker

associations with other ‘competitors’ such as BMIM cation and water molecules in the simulation box than Cl^-. This may lead to I^- having relatively stronger interaction with PNIPAM than Cl^-.

7. SUMMARY

Colloidal systems including nanoparticles and macromolecules dispersed at a liquid interface have attracted lots of attention because they offer a simple, flexible, and highly reproducible template for the assembly of a large variety of nanoscale objects, which can find many potential applications in catalysis, emulsion, sensing, and drug delivery. However, the fundamentals of the diffusion and self-assembly of nanoscale objects at/across liquid-liquid interfaces have not been fully explored. Some big challenges are to understand multiphase interactions, self-assembly processes, and self-assembled structures of small objects, especially when the size of the object is comparable with the molecular dimension of the surrounding liquids. Molecular simulation, particularly molecular dynamics (MD) simulation has been proven to be a very powerful tool to probe the above-mentioned interactions and to elucidate the microscopic mechanism of macroscopic observations.

In this project, systematic MD simulations have been carried out to achieve the project goal. In our study of nanoparticle in oil/water system, the objective was to reveal the effects of nanoparticles' structural and chemical properties on their diffusive behaviors at/across the water-benzene interface. Single-walled carbon nanotube, buckyball, and hydrocarbon particles were used to investigate the effect of shape, size, and surface composition on the diffusion and self-assembly process of nanoparticles at a liquid-liquid interface. The results demonstrate that a highly symmetrical nanoparticle with uniform surface such as a buckyball may lead to a uniform interaction force filed with the solvent molecules, so that a better-defined solvation shell is formed, and this

solvation shell makes the "effective radius" of the nanoparticle larger than its own radius, which causes a decrease in the diffusion coefficient. In the study of macromolecule in immiscible ionic liquids/water systems, the objective was to study the interfacial behaviors of poly(N-isopropylacrylamide) (PNIPAM) in the biphasic water-ionic liquids (ILs) systems since our understanding of thermal-responsive macromolecule's interfacial behaviors at the water-ILs interface is far from clear. PNIPAM in water-ionic liquid system was studied to probe the behavior of macromolecules at a liquid-liquid interface. PNIPAM exhibited a clear phase preference for different configurations depending on the nature of examined ionic liquids, which shed a light on alternative mechanisms to explain the thermal-induced phase behavior of PNIPAM. In our study of PNIPAM in miscible ionic liquids-water systems, the objective was to study the effects of ions in ILs on the phase behaviors of PNIPAM. PNIPAM in a pure water phase, a miscible [BMIM][I]/water mixture, and a miscible [BMIM][Cl]/water mixture are studied, respectively to seek further understanding of how cations and anions of the ionic liquids interact with different moieties of PNIPAM at atomic level.

In summary, MD simulations have been performed in three different systems to demonstrate its capability of elucidating the microscopic mechanism of interfacial behavior of nanoparticles and macromolecules in liquid-liquid systems at molecular level. Physical properties including particle size and shape and chemical properties including hydrophobicity and hydrogen bonding ability are investigated in detail to understand the diffusion and self-assembly behavior of small objects in colloidal systems. The future work may involve the force field development dedicated to the water-ionic

liquid system and systematic experimental studies to validate the model and the force field.

REFERENCES

1. de Folter, J. W. J. *et al.* Particle Shape Anisotropy in Pickering Emulsions: Cubes and Peanuts. *Langmuir* **30,** 955–964 (2014).
2. Binks, B. P. & Lumsdon, S. O. Influence of Particle Wettability on the Type and Stability of Surfactant-Free Emulsions †. *Langmuir* **16,** 8622–8631 (2000).
3. Bresme, F. & Oettel, M. Nanoparticles at fluid interfaces. *J. Phys. Condens. Matter* **19,** 413101 (2007).
4. Edel, J. B., Kornyshev, A. A., Kucernak, A. R. & Urbakh, M. Fundamentals and applications of self-assembled plasmonic nanoparticles at interfaces. *Chem. Soc. Rev.* **45,** 1581–1596 (2016).
5. Rezvantalab, H., Drazer, G. & Shojaei-Zadeh, S. Molecular simulation of translational and rotational diffusion of Janus nanoparticles at liquid interfaces. *J. Chem. Phys.* **142,** 14701 (2015).
6. Giner-Casares, J. J. & Reguera, J. Directed self-assembly of inorganic nanoparticles at air/liquid interfaces. *Nanoscale* 16589–16595 (2016). doi:10.1039/C6NR05054A
7. Kohno, Y. & Ohno, H. Ionic liquid/water mixtures: from hostility to conciliation. *Chem. Commun. Chem. Commun* **104314,** 7119–7130 (2012).
8. Lin, Y. Nanoparticle Assembly and Transport at Liquid-Liquid Interfaces. *Science (80-.).* **299,** 226–229 (2003).
9. Binks, B. P. & Horozov, T. S. in *Colloidal Particles at Liquid Interfaces* (eds. Binks, B. P. & Horozov, T. S.) 1–74 (Cambridge University Press, 2006). doi:10.1017/CBO9780511536670.002
10. Böker, A., He, J., Emrick, T. & Russell, T. P. Self-assembly of nanoparticles at interfaces. *Soft Matter* **3,** 1231–1248 (2007).
11. Nakashima, T. & Kimizuka, N. Water/ionic liquid interfaces as fluid scaffolds for the two-dimensional self-assembly of charged nanospheres. *Langmuir* **27,** 1281–1285 (2011).
12. Xia, H. & Wang, D. Fabrication of macroscopic freestanding films of metallic nanoparticle monolayers by interfacial self-assembly. *Adv. Mater.* **20,** 4253–4256 (2008).
13. Lin, Y. *et al.* Ultrathin Cross-Linked Nanoparticle Membranes. *J. Am. Chem. Soc.* **125,** 12690–12691 (2003).
14. Russell, J. T. *et al.* Self-assembly and cross-linking of bionanoparticles at liquid-liquid interfaces. *Angew. Chemie - Int. Ed.* **44,** 2420–2426 (2005).
15. Glogowski, E., Tangirala, R., He, J., Russell, T. P. & Emrick, T. Microcapsules of PEGylated gold nanoparticles prepared by fluid-fluid interfacial assembly. *Nano Letters* **7,** 389–393 (2007).

16. Arumugam, P. *et al.* Self-assembly and cross-linking of FePt nanoparticles at planar and colloidal liquid-liquid interfaces. *Journal of the American Chemical Society* **130,** 10046–10047 (2008).

17. Dinsmore, A. D. *et al.* Colloidosomes: Selectively Permeable Capsules Composed of Colloidal Particles. *Science (80-.).* **298,** (2002).

18. Skaff, H. *et al.* Crosslinked capsules of quantum dots by interfacial assembly and ligand crosslinking. *Adv. Mater.* **17,** 2082–2086 (2005).

19. Duan, H. *et al.* Magnetic colloidosomes derived from nanoparticle interfacial self-assembly. *Nano Lett.* **5,** 949–952 (2005).

20. Clegg, P. S. Fluid-bicontinuous gels stabilized by interfacial colloids: low and high molecular weight fluids. *J. Phys. Condens. Matter* **20,** 113101 (2008).

21. Cauvin, S., Colver, P. J. & Bon, S. A. F. Pickering Stabilized Miniemulsion Polymerization: Preparation of Clay Armored Latexes. *Macromolecules* **38,** 7887–7889 (2005).

22. Binks, B. P. & Lumsdon, S. O. Pickering emulsions stabilized by monodisperse latex particles: Effects of particle size. *Langmuir* **17,** 4540–4547 (2001).

23. Pickering, S. U. CXCVI.—Emulsions. *J. Chem. Soc., Trans.* **91,** 2001–2021 (1907).

24. Pardhy, N. P. & Budhlall, B. M. Pickering Emulsion as a Template to Synthesize Janus Colloids with Anisotropy in the Surface Potential. *Langmuir* **26,** 13130–13141 (2010).

25. Tarimala, S. & Dai, L. L. L. Structure of microparticles in solid-stabilized emulsions. *Langmuir* **20,** 3492–3494 (2004).

26. Huan Ma & Lenore L. Dai. Particle-Laden Emulsions. *Taylor Fr. Online Part. Lad. Emuls. - Encycl. Surf. Colloid Sci. Second Ed.* 1–17 (2007). doi:10.1081/E-ESCS-120045945

27. Binks, B. P. & Horozov, T. S. in *Colloidal Particles at Liquid Interfaces* (eds. Binks, B. P. & Horozov, T. S.) 1–74 (Cambridge University Press, 2006). doi:10.1017/CBO9780511536670.002

28. Frost, D. Self-Assembly at Ionic Liquid-Based Interfaces: Fundamentals and Applications. (Arizona State University, 2013).

29. Binks, B. P. & Lumsdon, S. O. Influence of particle wettability on the type and stability of surfactant-free emulsions. *Langmuir* **16,** 8622–8631 (2000).

30. Binks, B. P. Particles as surfactants—similarities and differences. *Curr. Opin. Colloid Interface Sci.* **7,** 21–41 (2002).

31. Amirfazli, A. & Neumann, A. W. Status of the three-phase line tension: A review. *Adv. Colloid Interface Sci.* **110,** 121–141 (2004).

32. Yang, Z. *et al.* LSPR properties of metal nanoparticles adsorbed at a liquid-liquid interface. *Phys. Chem. Chem. PhysicsPhysical Chem. Chem. Phys. PCCP* **15,**

5374–8 (2013).

33. Wang, M., Zhang, Z. & He, J. A SERS Study on the Assembly Behavior of Gold Nanoparticles at the Oil/Water Interface. *Langmuir* **31,** 12911–12919 (2015).

34. Booth, S. G., Cowcher, D. P., Goodacre, R. & Dryfe, R. A. W. Electrochemical modulation of SERS at the liquid/liquid interface. *Chem. Commun.* **50,** 4482–4 (2014).

35. Guo, Y., Tang, D., Du, Y. & Liu, B. Controlled fabrication of hexagonally close-packed langmuir-blodgett silica particulate monolayers from binary surfactant and solvent systems. *Langmuir* **29,** 2849–2858 (2013).

36. Giner-Casares, J. J. & Reguera, J. Directed self-assembly of inorganic nanoparticles at air/liquid interfaces. *Nanoscale* 16589–16595 (2016). doi:10.1039/C6NR05054A

37. Edel, J. B., Kornyshev, A. A., Kucernak, A. R. & Urbakh, M. Fundamentals and applications of self-assembled plasmonic nanoparticles at interfaces. *Chem. Soc. Rev.* **45,** 1581–1596 (2016).

38. Chevalier, Y. & Bolzinger, M.-A. Emulsions stabilized with solid nanoparticles: Pickering emulsions. *Colloids Surfaces A Physicochem. Eng. Asp.* **439,** 23–34 (2013).

39. Pickering, S. U. CXCVI.—Emulsions. *J. Chem. Soc., Trans.* **91,** 2001–2021 (1907).

40. Ramsden, W. Separation of Solids in the Surface-Layers of Solutions and 'Suspensions'. *Proc. R. Soc. London* **72,** 156–164 (1903).

41. Chevalier, Y. & Bolzinger, M.-A. Emulsions stabilized with solid nanoparticles: Pickering emulsions. *Colloids Surfaces A Physicochem. Eng. Asp.* **439,** 23–34 (2013).

42. Stiller, S. *et al.* Investigation of the stability in emulsions stabilized with different surface modified titanium dioxides. *Colloids Surfaces A Physicochem. Eng. Asp.* **232,** 261–267 (2004).

43. Timgren, A., Rayner, M., Sjöö, M. & Dejmek, P. Starch particles for food based Pickering emulsions. *Procedia Food Sci.* **1,** 95–103 (2011).

44. Nallamilli, T., Mani, E. & Basavaraj, M. G. A Model for the Prediction of Droplet Size in Pickering Emulsions Stabilized by Oppositely Charged Particles. *Langmuir* **30,** 9336–9345 (2014).

45. Booth, S. G. & Dryfe, R. A. W. Assembly of Nanoscale Objects at the Liquid/Liquid Interface. *J. Phys. Chem. C* **119,** 23295–23309 (2015).

46. Chaikof, E. L. Engineering and Material Considerations in Islet Cell Transplantation. *Annu. Rev. Biomed. Eng.* **1,** 103–127 (1999).

47. Lattuada, M. & Hatton, T. A. Synthesis, properties and applications of Janus nanoparticles. *Nano Today* **6,** 286–308 (2011).

48. Hong, L., Jiang, S. & Granick, S. Simple method to produce janus colloidal particles in large quantity. *Langmuir* **22,** 9495–9499 (2006).

49. Pardhy, N. P. & Budhlall, B. M. Pickering emulsion as a template to synthesize Janus colloids with anisotropy in the surface potential. *Langmuir* **26,** 13130–41 (2010).

50. Frost, D. S. & Dai, L. L. Molecular dynamics simulations of charged nanoparticle self-assembly at ionic liquid-water and ionic liquid-oil interfaces. *J. Chem. Phys.* **136,** 84706 (2012).

51. Moreira, N. H. & Skaf, M. S. in *Surface and Colloid Science* 81–85 (Springer Berlin Heidelberg, 2004). doi:10.1007/b97086

52. Zhang, Y., Feller, S. E., Brooks, B. E. & Pastor, R. W. Computer simulation of liquid/liquid interfaces. I. Theory and application to octane/water. *J. Chem. Phys.* **103,** 10252–10266 (1995).

53. Frost, D. S. & Dai, L. L. Molecular dynamics simulations of nanoparticle self-assembly at ionic liquid-water and ionic liquid-oil interfaces. *Langmuir* **27,** 11339–46 (2011).

54. Frost, D. S. & Dai, L. L. Molecular dynamics simulations of charged nanoparticle self-assembly at ionic liquid-water and ionic liquid-oil interfaces. *J. Chem. Phys.* **136,** 84706 (2012).

55. Wilkes, J. S. A short history of ionic liquids—from molten salts to neoteric solvents. *Green Chem.* **4,** 73–80 (2002).

56. Plechkova, N. V. & Seddon, K. R. Applications of ionic liquids in the chemical industry. *Chem. Soc. Rev.* **37,** 123–150 (2008).

57. Plechkova, N. V. & Seddon, K. R. Applications of ionic liquids in the chemical industry. *Chem. Soc. Rev.* **37,** 123–150 (2008).

58. Rogers, R. D. & Seddon, K. R. Ionic Liquids--Solvents of the Future? *Science (80-.).* **302,** (2003).

59. Brennecke, J. F. & Maginn, E. J. Ionic liquids: Innovative fluids for chemical processing. *AIChE J.* **47,** 2384–2389 (2001).

60. Freemantle, M. An Introduction to Ionic Liquids. *The Royal Society of Chemistry* 281 (2010). doi:10.1016/S1351-4180(10)70136-7

61. Wilkes, J. S. Properties of ionic liquid solvents for catalysis. *J. Mol. Catal. A Chem.* **214,** 11–17 (2004).

62. Ngo, H. L., LeCompte, K., Hargens, L. & McEwen, A. B. Thermal properties of imidazolium ionic liquids. in *Thermochimica Acta* **357–358,** 97–102 (2000).

63. Freemantle, M. An Introduction to Ionic Liquids. *The Royal Society of Chemistry* 281 (2010). doi:10.1016/S1351-4180(10)70136-7

64. Lide, D. R. & Chemical Rubber Kew ; Southampton ; Trinity College Dublin ; University of London - ULRLS, C. C. N.-B. ; B. L. ; C. ; E. ; G. ; K. C. L. ; M. ; R.

B. G. *CRC handbook of chemistry and physics : a ready-reference book of chemical and physical data*. (2000).

65. Seddon, K. R. Ionic Liquids for Clean Technology. *J. Chem. Technol. Biotechnol.* **68,** 351–356 (1997).

66. Rani, M. A. A. *et al.* Understanding the polarity of ionic liquids. *Phys. Chem. Chem. Phys. Phys. Chem. Chem. Phys* **13,** 16831–16840 (2011).

67. Canongia Lopes, J. N., Costa Gomes, M. F. & Pádua, A. A. H. Nonpolar, Polar, and Associating Solutes in Ionic Liquids. *J. Phys. Chem. B* **110,** 16816–16818 (2006).

68. Reichardt, C. *et al.* Polarity of ionic liquids determined empirically by means of solvatochromic pyridinium N-phenolate betaine dyes. *Green Chem.* **7,** 339 (2005).

69. Anderson, J. L., Ding, J., Welton, T. & Armstrong, D. W. Characterizing Ionic Liquids On the Basis of Multiple\nSolvation Interactions. *J. Am. Chem. Soc.* **124,** 14247–14254 (2002).

70. Armand, M., Endres, F., MacFarlane, D. R., Ohno, H. & Scrosati, B. Ionic-liquid materials for the electrochemical challenges of the future. *Nat. Mater.* **8,** 621–629 (2009).

71. Zhu, S. *et al.* Dissolution of cellulose with ionic liquids and its application: a mini-review. *Green Chem.* **8,** 325 (2006).

72. Swatloski, R. P., Spear, S. K., Holbrey, J. D. & Rogers, R. D. Dissolution of Cellose with Ionic Liquids. *J. Am. Chem. Soc.* **124,** 4974–4975 (2002).

73. Wu, J. *et al.* Homogeneous Acetylation of Cellulose in a New Ionic Liquid. *Biomacromolecules* **5,** 266–268 (2004).

74. Dobler, D., Schmidts, T., Klingenhöfer, I. & Runkel, F. Ionic liquids as ingredients in topical drug delivery systems. *Int. J. Pharm.* **441,** 620–627 (2013).

75. Jaitely, V., Karatas, A. & Florence, A. T. Water-immiscible room temperature ionic liquids (RTILs) as drug reservoirs for controlled release. *Int. J. Pharm.* **354,** 168–173 (2008).

76. Moniruzzaman, M., Tamura, M., Tahara, Y., Kamiya, N. & Goto, M. Ionic liquid-in-oil microemulsion as a potential carrier of sparingly soluble drug: Characterization and cytotoxicity evaluation. *Int. J. Pharm.* **400,** 243–250 (2010).

77. Ward, M. A. & Georgiou, T. K. Thermoresponsive polymers for biomedical applications. *Polymers (Basel).* **3,** 1215–1242 (2011).

78. Roy, I. & Gupta, M. N. Smart Polymeric Materials: Emerging Biochemical Applications. *Chem. Biol.* **10,** 1161–1171 (2003).

79. Lahann, J. *et al.* Smart Materials with Dynamically Controllable Surfaces. *MRS Bull.* **30,** 185–188 (2005).

80. Aguilar, M. R. & San Román, J. in *Smart Polymers and their Applications* **2,** 1–11 (Elsevier, 2014).

81. Ward, M. A. & Georgiou, T. K. Thermoresponsive Polymers for Biomedical Applications. *Polymers (Basel).* **3,** 1215–1242 (2011).

82. Shimizu, K., Fujita, H. & Nagamori, E. Oxygen plasma-treated thermoresponsive polymer surfaces for cell sheet engineering. *Biotechnol. Bioeng.* **106,** 303–10 (2010).

83. Guan, Y. *et al.* PNIPAM microgels for biomedical applications: from dispersed particles to 3D assemblies. *Soft Matter* **7,** 6375 (2011).

84. Schmaljohann, D. Thermo- and pH-responsive polymers in drug delivery. *Advanced Drug Delivery Reviews* **58,** 1655–1670 (2006).

85. Rösler, A., Vandermeulen, G. W. M. & Klok, H.-A. Advanced drug delivery devices via self-assembly of amphiphilic block copolymers. *Adv. Drug Deliv. Rev.* **64,** 270–279 (2012).

86. Pasparakis, G. & Vamvakaki, M. Multiresponsive polymers: nano-sized assemblies, stimuli-sensitive gels and smart surfaces. *Polym. Chem.* **2,** 1234 (2011).

87. Aguilar, M. R. & San Román, J. in *Smart Polymers and their Applications* **2,** 1–11 (Elsevier, 2014).

88. Costa, R. O. . & Freitas, R. F. . Phase behavior of poly(N-isopropylacrylamide) in binary aqueous solutions. *Polymer (Guildf).* **43,** 5879–5885 (2002).

89. Kokardekar, R. R., Shah, V. K., Mody, H. R. & Hiranandani, L. H. Internet Journal of Medical Update PNIPAM Poly (N-isopropylacrylamide): A Thermoresponsive " Smart " Polymer in Novel Drug Delivery Systems. *Internet J. Med. Updat.* **7,** 60–63 (2012).

90. Dhandayuthapani, B. *et al.* Polymeric Scaffolds in Tissue Engineering Application: A Review. *Int. J. Polym. Sci.* **2011,** 1–19 (2011).

91. Lutz, J.-F. Polymerization of oligo(ethylene glycol) (meth)acrylates: Toward new generations of smart biocompatible materials. *J. Polym. Sci. Part A Polym. Chem.* **46,** 3459–3470 (2008).

92. Gandhi, A., Paul, A., Sen, S. O. & Sen, K. K. Studies on thermoresponsive polymers: Phase behaviour, drug delivery and biomedical applications. *Asian J. Pharm. Sci.* **10,** 99–107 (2015).

93. Weber, C., Hoogenboom, R. & Schubert, U. S. Temperature responsive bio-compatible polymers based on poly(ethylene oxide) and poly(2-oxazoline)s. *Prog. Polym. Sci.* **37,** 686–714 (2012).

94. Heskins, M. & Guillet, J. E. Solution Properties of Poly(N-isopropylacrylamide). *J. Macromol. Sci. Part A - Chem.* **2,** 1441–1455 (1968).

95. Du, H. The effects of salt on the lower critical solution temperatures of poly(N-isopropylacrylamide) and its copolymer studied from molecular dynamics simulations. (2011).

96. Kita, R., Kircher, G. & Wiegand, S. Thermally induced sign change of Soret coefficient for dilute and semidilute solutions of poly(N-isopropylacrylamide) in ethanol. *J. Chem. Phys.* **121,** 9140–6 (2004).

97. Smartisan's CEO wants to be the next 'Steve Jobs of China'.

98. Xia, L.-W. *et al.* Nano-structured smart hydrogels with rapid response and high elasticity. *Nat. Commun.* **4,** 588–590 (2013).

99. JagadeeshBabu, P. E., Suresh Kumar, R. & Maheswari, B. Synthesis and characterization of temperature sensitive P-NIPAM macro/micro hydrogels. *Colloids Surfaces A Physicochem. Eng. Asp.* **384,** 466–472 (2011).

100. Mohsen, R., Vine, G. J., Majcen, N., Alexander, B. D. & Snowden, M. J. Characterization of thermo and pH responsive NIPAM based microgels and their membrane blocking potential. *Colloids Surfaces A Physicochem. Eng. Asp.* **428,** 53–59 (2013).

101. Kono, K. Thermosensitive polymer-modified liposomes. *Adv. Drug Deliv. Rev.* **53,** 307–319 (2001).

102. Kim, B. S. & Lee, T. R. in *Nanoparticles Technology* (InTech, 2015). doi:10.5772/61262

103. Shen, B. B., Gao, X. C., Yu, S. Y., Ma, Y. & Ji, C. H. Fabrication and potential application of a di-functional magnetic system: magnetic hyperthermia therapy and drug delivery. *CrystEngComm* **18,** 1133–1138 (2016).

104. Pang, J., Yang, H., Ma, J. & Cheng, R. Solvation Behaviors of *N* -Isopropylacrylamide in Water/Methanol Mixtures Revealed by Molecular Dynamics Simulations. *J. Phys. Chem. B* **114,** 8652–8658 (2010).

105. Du, H. & Qian, X. Molecular dynamics simulations of PNIPAM-co-PEGMA copolymer hydrophilic to hydrophobic transition in NaCl solution. *J. Polym. Sci. Part B Polym. Phys.* **49,** 1112–1122 (2011).

106. Du, H., Wickramasinghe, R. & Qian, X. Effects of Salt on the Lower Critical Solution Temperature of Poly (N -Isopropylacrylamide). *J. Phys. Chem. B* **114,** 16594–16604 (2010).

107. Kojima, H., Tanaka, F., Scherzinger, C. & Richtering, W. Temperature dependent phase behavior of PNIPAM microgels in mixed water/methanol solvents. *J. Polym. Sci. Part B Polym. Phys.* **51,** 1100–1111 (2013).

108. Deshmukh, S. A. *et al.* Atomistic insights into solvation dynamics and conformational transformation in thermo-sensitive and non-thermo-sensitive oligomers. *Polymer (Guildf).* **54,** 210–222 (2013).

109. Deshmukh, S. A., Sankaranarayanan, S. K. R. S., Suthar, K. & Mancini, D. C. Role of Solvation Dynamics and Local Ordering of Water in Inducing Conformational Transitions in Poly(*N* -isopropylacrylamide) Oligomers through the LCST. *J. Phys. Chem. B* **116,** 2651–2663 (2012).

110. Keerl, M., Smirnovas, V., Winter, R. & Richtering, W. Copolymer Microgels from Mono- and Disubstituted Acrylamides: Phase Behavior and Hydrogen Bonds. *Macromolecules* **41,** 6830–6836 (2008).

111. Longhi, G., Lebon, F., Abbate, S. & Fornili, S. L. Molecular dynamics simulation of a model oligomer for poly(N-isopropylamide) in water. *Chem. Phys. Lett.* **386,** 123–127 (2004).

112. Reddy, P. M. & Venkatesu, P. Ionic liquid modifies the lower critical solution temperature (LCST) of poly(N-isopropylacrylamide) in aqueous solution. *J. Phys. Chem. B* **115,** 4752–4757 (2011).

113. Bai, Z. & Lodge, T. P. Pluronic micelle shuttle between water and an ionic liquid. *Langmuir* **26,** 8887–8892 (2010).

114. Bai, Z. F., He, Y. Y., Young, N. P. & Lodge, T. P. A Thermoreversible Micellization− Transfer− Demicellization Shuttle between Water and an Ionic Liquid. *Macromolecules* **41,** 6615–6617 (2008).

115. Ueki, T. & Watanabe, M. Lower critical solution temperature behavior of linear polymers in ionic liquids and the corresponding volume phase transition of polymer gels. *Langmuir* **23,** 988–990 (2007).

116. Mukae, K. *et al.* Swelling of poly(N-isopropylacrylamide) gels in water-alcohol (C1-C4) mixed solvents. *J. Phys. Chem.* **97,** 737–741 (1993).

117. Winnik, F. M., Ringsdorf, H. & Venzmer, J. Methanol-water as a co-nonsolvent system for poly(N-isopropylacrylamide). *Macromolecules* **23,** 2415–2416 (1990).

118. Walter, J., Sehrt, J., Vrabec, J. & Hasse, H. Molecular Dynamics and Experimental Study of Conformation Change of Poly(*N* -isopropylacrylamide) Hydrogels in Mixtures of Water and Methanol. *J. Phys. Chem. B* **116,** 5251–5259 (2012).

119. Destribats, M. *et al.* Soft microgels as Pickering emulsion stabilisers: role of particle deformability. *Soft Matter* **7,** 7689 (2011).

120. Suzuki, D., Tsuji, S. & Kawaguchi, H. Janus Microgels Prepared by Surfactant-Free Pickering Emulsion-Based Modification and Their Self-Assembly. *J. Am. Chem. Soc.* **129,** 8088–8089 (2007).

121. Ngai, T., Behrens, S. H. & Auweter, H. Novel emulsions stabilized by pH and temperature sensitive microgels. *Chem. Commun.* 331 (2005). doi:10.1039/b412330a

122. Destribats, M. *et al.* Pickering Emulsions Stabilized by Soft Microgels: Influence of the Emulsification Process on Particle Interfacial Organization and Emulsion Properties. *Langmuir* **29,** 12367–12374 (2013).

123. Wang, P. editor. *Smart Materials for Advanced Environmental Applications*. (Royal Society of Chemistry, 2016). doi:10.1039/9781782622192

124. Van Der Spoel, D. *et al.* GROMACS: Fast, flexible, and free. *Journal of Computational Chemistry* **26,** 1701–1718 (2005).

125. Abraham, M. J. *et al.* GROMACS: High performance molecular simulations through multi-level parallelism from laptops to supercomputers. *SoftwareX* **1,** 19–25 (2015).

126. Fu, C.-F. & Tian, S. X. A Comparative Study for Molecular Dynamics Simulations of Liquid Benzene. *J. Chem. Theory Comput.* **7,** 2240–2252 (2011).

127. Oostenbrink, C., Villa, A., Mark, A. E. & van Gunsteren, W. F. A biomolecular force field based on the free enthalpy of hydration and solvation: the GROMOS force-field parameter sets 53A5 and 53A6. *J. Comput. Chem.* **25,** 1656–76 (2004).

128. van der Spoel, D., van Maaren, P. J. & Caleman, C. GROMACS molecule & liquid database. *Bioinformatics* **28,** 752–753 (2012).

129. Schmid, N. *et al.* Definition and testing of the GROMOS force-field versions 54A7 and 54B7. *Eur. Biophys. J.* **40,** 843–856 (2011).

130. Garate, J. A., Perez-Acle, T. & Oostenbrink, C. On the thermodynamics of carbon nanotube single-file water loading: free energy, energy and entropy calculations. *Phys. Chem. Chem. Phys.* **16,** 5119–28 (2014).

131. Larin, S. V. *et al.* Influence of the carbon nanotube surface modification on the microstructure of thermoplastic binders. *RSC Adv.* **5,** 51621–51630 (2015).

132. Lai, B. & Oostenbrink, C. Binding free energy, energy and entropy calculations using simple model systems. *Theor. Chem. Acc.* **131,** 1–13 (2012).

133. Wong-Ekkabut, J. & Karttunen, M. Assessment of common simulation protocols for simulations of nanopores, membrane proteins, and channels. *J. Chem. Theory Comput.* **8,** 2905–2911 (2012).

134. Luo, M. *et al.* Molecular Dynamics Simulation of Nanoparticle Self-Assembly at a Liquid - Liquid Interface. **22,** 6385–6390 (2006).

135. Mazyar, O. A. & Hase, W. L. Dynamics and kinetics of heat transfer at the interface of model diamond [111] nanosurfaces. *J. Phys. Chem. A* **110,** 526–36 (2006).

136. Luo, M. *et al.* Molecular dynamics simulation of nanoparticle self-assembly at a liquid-liquid interface. *Langmuir* **22,** 6385–90 (2006).

137. Song, Y., Luo, M. & Dai, L. L. Understanding nanoparticle diffusion and exploring interfacial nanorheology using molecular dynamics simulations. *Langmuir* **26,** 5–9 (2010).

138. Luo, M. *et al.* Molecular Dynamics Simulation of Nanoparticle Self-Assembly at a Liquid−Liquid Interface. *Langmuir* **22,** 6385–6390 (2006).

139. Luo, M. *et al.* Molecular Dynamics Simulation of Nanoparticle Self-Assembly at a Liquid−Liquid Interface. *Langmuir* **22,** 6385–6390 (2006).

140. Jorgensen, W. L., Madura, J. D. & Swenson, C. J. Optimized intermolecular potential functions for liquid hydrocarbons. *J. Am. Chem. Soc.* **106,** 6638–6646 (1984).

141. Jorgensen, W. L., Maxwell, D. S. & Tirado-Rives, J. Development and testing of the OPLS all-atom force field on conformational energetics and properties of organic liquids. *J. Am. Chem. Soc.* **118,** 11225–11236 (1996).

142. Kaminski, G. A., Friesner, R. A., Tirado-Rives, J. & Jorgensen, W. L. Evaluation and reparametrization of the OPLS-AA force field for proteins via comparison with accurate quantum chemical calculations on peptides. *J. Phys. Chem. B* **105,** 6474–6487 (2001).

143. Algaer, E. A. & van der Vegt, N. F. A. Hofmeister Ion Interactions with Model Amide Compounds. *J. Phys. Chem. B* **115,** 13781–13787 (2011).

144. Boţan, V., Ustach, V., Faller, R. & Leonhard, K. Direct Phase Equilibrium Simulations of NIPAM Oligomers in Water. *J. Phys. Chem. B* **120,** 3434–3440 (2016).

145. Jorgensen, W. L., Maxwell, D. S. & Tirado-Rives, J. Development and Testing of the OPLS All-Atom Force Field on Conformational Energetics and Properties of Organic Liquids. *J. Am. Chem. Soc.* **118,** 11225–11236 (1996).

146. Jorgensen, W. L. & Tiradorives, J. The Opls Potential Functions for Proteins - Energy Minimizations for Crystals of Cyclic-Peptides and Crambin. *J. Am. Chem. Soc.* **110,** 1657–1666 (1988).

147. Kamath, G., Deshmukh, S. A., Baker, G. A., Mancini, D. C. & Sankaranarayanan, S. K. R. S. Thermodynamic considerations for solubility and conformational transitions of poly-N-isopropyl-acrylamide. *Phys. Chem. Chem. Phys.* **15,** 12667 (2013).

148. Walter, J., Ermatchkov, V., Vrabec, J. & Hasse, H. Molecular dynamics and experimental study of conformation change of poly(N-isopropylacrylamide) hydrogels in water. *Fluid Phase Equilib.* **296,** 164–172 (2010).

149. Bhargava, B. L. & Balasubramanian, S. Refined potential model for atomistic simulations of ionic liquid [bmim][PF[sub 6]]. *J. Chem. Phys.* **127,** 114510 (2007).

150. Lopes, J. N. C. & Pádua, A. A. H. Molecular force field for ionic liquids composed of triflate or bistriflylimide anions. *J. Phys. Chem. B* **108,** 16893–16898 (2004).

151. Frost, D. S., Machas, M. & Dai, L. L. Molecular dynamics studies on the adaptability of an ionic liquid in the extraction of solid nanoparticles. *Langmuir* **28,** 13924–32 (2012).

152. Nickerson, S. D. *et al.* A Combined Experimental and Molecular Dynamics Study of Iodide-Based Ionic Liquid and Water Mixtures. *J. Phys. Chem. B* **119,** 8764–8772 (2015).

153. Canongia Lopes, J. N., Deschamps, J. & Pádua, A. A. H. Modeling Ionic Liquids Using a Systematic All-Atom Force Field. *J. Phys. Chem. B* **108,** 2038–2047 (2004).

154. Bhargava, B. L. & Balasubramanian, S. Insights into the structure and dynamics of a room-temperature ionic liquid: Ab initio molecular dynamics simulation studies

of 1-n-butyl-3- methylimidazolium hexafluorophosphate ([bmim][PF6]) and the [bmim][PF6]-CO2 mixture. *J. Phys. Chem. B* **111,** 4477–4487 (2007).

155. Canongia Lopes, J. N., Deschamps, J. & Pádua, A. A. H. Modeling Ionic Liquids Using a Systematic All-Atom Force Field. *J. Phys. Chem. B* **108,** 2038–2047 (2004).

156. Steinhauser, M. O. & Hiermaier, S. A review of computational methods in materials science: examples from shock-wave and polymer physics. *Int. J. Mol. Sci.* **10,** 5135–216 (2009).

157. van der Spoel, D. *et al.* Gromacs User Manual version 4.0. *Optimization* 308 (2005).

158. Berendsen, H. J. C. H. J. C., Postma, J. P. M. J. P. M., Van Gunsteren, W. F. W. F., DiNola, A. & Haak, J. R. J. R. Molecular dynamics with coupling to an external bath. **81,** 3684 (1984).

159. de Folter, J. W. J. *et al.* Particle shape anisotropy in pickering emulsions: cubes and peanuts. *Langmuir* **30,** 955–64 (2014).

160. Moreira, N. H. & Skaf, M. S. in *Surface and Colloid Science* 81–85 (Springer Berlin Heidelberg, 2004). doi:10.1007/b97086

161. Frost, D. S. & Dai, L. L. Molecular Dynamics Simulations of Nanoparticle Self-Assembly at Ionic Liquid–Water and Ionic Liquid–Oil Interfaces. *Langmuir* **27,** 11339–11346 (2011).

162. Berendsen, H. J. C., Vanderspoel, D. & Vandrunen, R. GROMACS - A Message-Passing Parallel Molecular-Dynamics Implemenation. *Comput. Phys. Commun.* **91,** 43–56 (1995).

163. Frost, D. S. & Dai, L. L. Molecular Dynamics Simulations of Nanoparticle Self-Assembly at Ionic Liquid–Water and Ionic Liquid–Oil Interfaces. *Langmuir* **27,** 11339–11346 (2011).

164. Humphrey, W., Dalke, A. & Schulten, K. VMD: Visual molecular dynamics. *J. Mol. Graph.* **14,** 33–38 (1996).

165. Malde, A. K. *et al.* An Automated Force Field Topology Builder (ATB) and Repository: Version 1.0. *J. Chem. Theory Comput.* **7,** 4026–4037 (2011).

166. Chandler, D. Statistical mechanics of isomerization dynamics in liquids and the transition state approximation. *J. Chem. Phys.* **68,** 2959 (1978).

167. Kirkwood, J. G. Statistical Mechanics of Fluid Mixtures. *J. Chem. Phys.* **3,** 300 (1935).

168. Roux, B. The calculation of the potential of mean force using computer simulations. *Comput. Phys. Commun.* **91,** 275–282 (1995).

169. Hub, J. S., De Groot, B. L. & Van Der Spoel, D. G-whams-a free Weighted Histogram Analysis implementation including robust error and autocorrelation estimates. *J. Chem. Theory Comput.* **6,** 3713–3720 (2010).

170. Kumar, S., Rosenberg, J. M., Bouzida, D., Swendsen, R. H. & Kollman, P. A. THE weighted histogram analysis method for free-energy calculations on biomolecules. I. The method. *J. Comput. Chem.* **13,** 1011–1021 (1992).

171. Luo, M., Song, Y. & Dai, L. L. Heterogeneous or competitive self-assembly of surfactants and nanoparticles at liquid–liquid interfaces. *Mol. Simul.* **35,** 773–784 (2009).

172. Goodwin, R. D. Benzene Thermophysical Properties from 279 to 900 K at Pressures to 1000 Bar. *J. Phys. Chem. Ref. Data* **17,** 1541 (1988).

173. Cupples, H. L. Interfacial Tension by the Ring Method: The Benzene-Water Interface. *J. Phys. Colloid Chem.* **51,** 1341–1345 (1947).

174. Einstein, A. Über die von der molekularkinetischen Theorie der Wärme geforderte Bewegung von in ruhenden Flüssigkeiten suspendierten Teilchen. *Ann. Phys.* **322,** 549–560 (1905).

175. Tuteja, A., Mackay, M. E., Narayanan, S., Asokan, S. & Wong, M. S. Breakdown of the continuum Stokes-Einstein relation for nanoparticle diffusion. *Nano Lett.* **7,** 1276–1281 (2007).

176. Chen, S.-H. Tracer diffusion in polyatomic liquids. III. *J. Chem. Phys.* **77,** 2540 (1982).

177. Cussler, E. *Diffusion: Mass transfer in fluid systems*. *Engineering* (Cambridge University Press, 1997).

178. Cussler, E. *Diffusion: Mass transfer in fluid systems*. *Engineering* (Cambridge University Press, 1997).

179. Binks, B. P. & Lumsdon, S. O. Influence of Particle Wettability on the Type and Stability of Surfactant-Free Emulsions †. *Langmuir* **16,** 8622–8631 (2000).

180. Chandler, D. Interfaces and the driving force of hydrophobic assembly. *Nature* **437,** 640–7 (2005).

181. Russo, D., Hura, G. & Head-Gordon, T. Hydration dynamics near a model protein surface. *Biophys. J.* **86,** 1852–62 (2004).

182. Zhang, L. *et al.* Mapping hydration dynamics around a protein surface. *Proc. Natl. Acad. Sci. U. S. A.* **104,** 18461–18466 (2007).

183. Andrievsky, G. V., Klochkov, V. K., Bordyuh, A. B. & Dovbeshko, G. I. Comparative analysis of two aqueous-colloidal solutions of C60 fullerene with help of FTIR reflectance and UV–Vis spectroscopy. *Chem. Phys. Lett.* **364,** 8–17 (2002).

184. Storm, D. & Sheu, E. Characterization of colloidal asphaltenic particles in heavy oil. *Fuel* (1995).

185. Southall, N. T., Dill, K. A. & Haymet, A. D. J. A view of the hydrophobic effect. *Journal of Physical Chemistry B* **106,** 521–533 (2002).

186. Ngai, T., Auweter, H. & Behrens, S. H. Environmental responsiveness of microgel

particles and particle-stabilized emulsions. *Macromolecules* **39,** 8171–8177 (2006).

187. Li, Z. & Ngai, T. Microgel particles at the fluid–fluid interfaces. *Nanoscale* **5,** 1399 (2013).

188. Brugger, B. & Richtering, W. Magnetic, Thermosensitive Microgels as Stimuli-Responsive Emulsifiers Allowing for Remote Control of Separability and Stability of Oil in Water-Emulsions. *Adv. Mater.* **19,** 2973–2978 (2007).

189. Richtering, W. Responsive Emulsions Stabilized by Stimuli-Sensitive Microgels: Emulsions with Special Non-Pickering Properties. *Langmuir* **28,** 17218–17229 (2012).

190. Chen, H., Kelley, M., Guo, C., Yarger, J. L. & Dai, L. L. Adsorption and release of surfactant into and from multifunctional zwitterionic poly(NIPAm-co-DMAPMA-co-AAc) microgel particles. *J. Colloid Interface Sci.* **449,** 332–340 (2015).

191. Chatterjee, P., Dai, A., Yu, H., Jiang, H. & Dai, L. L. Thermal and mechanical properties of poly(*N* -isopropylacrylamide)-based hydrogels as a function of porosity and medium change. *J. Appl. Polym. Sci.* **132,** n/a-n/a (2015).

192. Ngai, T., Behrens, S. H. & Auweter, H. Novel emulsions stabilized by pH and temperature sensitive microgels. *Chem. Commun.* 331 (2005). doi:10.1039/b412330a

193. Chatterjee, P. *et al.* Controlled morphology of thin film silicon integrated with environmentally responsive hydrogels. *Langmuir* **29,** 6495–6501 (2013).

194. Yu, C. *et al.* Thermoresponsiveness of Integrated Ultra-Thin Silicon with Poly(N-isopropylacrylamide) Hydrogels. *Macromol. Rapid Commun.* **32,** 820–824 (2011).

195. Kikuchi, A. & Okano, T. Nanostructured designs of biomedical materials: applications of cell sheet engineering to functional regenerative tissues and organs. *J. Control. Release* **101,** 69–84 (2005).

196. Bai, Z., He, Y., Young, N. P. & Lodge, T. P. A Thermoreversible Micellization−Transfer−Demicellization Shuttle between Water and an Ionic Liquid. *Macromolecules* **41,** 6615–6617 (2008).

197. Du, H., Wickramasinghe, R. & Qian, X. Effects of Salt on the Lower Critical Solution Temperature of Poly (*N* -Isopropylacrylamide). *J. Phys. Chem. B* **114,** 16594–16604 (2010).

198. Jorgensen, W. L., Maxwell, D. S. & Tirado-Rives, J. Development and Testing of the OPLS All-Atom Force Field on Conformational Energetics and Properties of Organic Liquids. *J. Am. Chem. Soc.* **118,** 11225–11236 (1996).

199. Heggen, B., Zhao, W., Leroy, F., Dammers, A. J. & Müller-Plathe, F. Interfacial Properties of an Ionic Liquid by Molecular Dynamics. *J. Phys. Chem. B* **114,** 6954–6961 (2010).

200. Qiao, Y., Yan, F., Xia, S., Yin, S. & Ma, P. Densities and Viscosities of

[Bmim][PF $_6$] and Binary Systems [Bmim][PF $_6$] + Ethanol, [Bmim][PF $_6$] + Benzene at Several Temperatures and Pressures: Determined by the Falling-Ball Method. *J. Chem. Eng. Data* **56,** 2379–2385 (2011).

201. Lee, S. H. & Lee, S. B. The Hildebrand solubility parameters, cohesive energy densities and internal energies of 1-alkyl-3-methylimidazolium-based room temperature ionic liquids. *Chem. Commun.* 3469 (2005). doi:10.1039/b503740a

202. Lee, S. H. & Lee, S. B. The Hildebrand solubility parameters, cohesive energy densities and internal energies of 1-alkyl-3-methylimidazolium-based room temperature ionic liquids. *Chem. Commun.* 3469 (2005). doi:10.1039/b503740a

203. Zhang, Y., Furyk, S., Bergbreiter, D. E. & Cremer, P. S. Specific Ion Effects on the Water Solubility of Macromolecules: PNIPAM and the Hofmeister Series. *J. Am. Chem. Soc.* **127,** 14505–14510 (2005).

204. Lee, L.-T. & Cabane, B. Effects of Surfactants on Thermally Collapsed Poly(*N* -isopropylacrylamide) Macromolecules. *Macromolecules* **30,** 6559–6566 (1997).

205. Mylonas, Y., Staikos, G. & Lianos, P. Investigation of the Poly(*N* -isopropylacrylamide)-Sodium Dodecyl Sulfate Complexation with Viscosity, Dialysis, and Time-resolved Fluorescence-Quenching Measurements. *Langmuir* **15,** 7172–7175 (1999).

206. Zhu, P. W. & Napper, D. H. Effects of Anionic Surfactant on the Coil-to-Globule Transition of Interfacial Poly(*N* -isopropylacrylamide). *Langmuir* **12,** 5992–5998 (1996).

207. Walter, R., Rička, J., Quellet, C., Nyffenegger, R. & Binkert, T. Coil−Globule Transition of Poly(*N* -isopropylacrylamide): A Study of Polymer−Surfactant Association. *Macromolecules* **29,** 4019–4028 (1996).

208. Tiktopulo, E. I. *et al.* 'Domain' Coil-Globule Transition in Homopolymers. *Macromolecules* **28,** 7519–7524 (1995).

209. Zhang, Y. *et al.* Effects of Hofmeister Anions on the LCST of PNIPAM as a Function of Molecular Weight †. *J. Phys. Chem. C* **111,** 8916–8924 (2007).

210. Freitag, R. & Garret-Flaudy, F. Salt Effects on the Thermoprecipitation of Poly-(*N* -isopropylacrylamide) Oligomers from Aqueous Solution. *Langmuir* **18,** 3434–3440 (2002).

211. Schild, H. G., Muthukumar, M. & Tirrell, D. A. Cononsolvency in mixed aqueous solutions of poly(N-isopropylacrylamide). *Macromolecules* **24,** 948–952 (1991).

212. Sagle, L. B. *et al.* Investigating the Hydrogen-Bonding Model of Urea Denaturation. *J. Am. Chem. Soc.* **131,** 9304–9310 (2009).

213. Eeckman, F., Moës, A. J. & Amighi, K. Evaluation of a new controlled-drug delivery concept based on the use of thermoresponsive polymers. *Int. J. Pharm.* **241,** 113–125 (2002).

214. Du, H., Wickramasinghe, R. & Qian, X. Effects of Salt on the Lower Critical

Solution Temperature of Poly (N -Isopropylacrylamide). *J. Phys. Chem. B* **114,** 16594–16604 (2010).

215. Du, H., Wickramasinghe, S. R. & Qian, X. Specificity in Cationic Interaction with Poly(N-isopropylacrylamide). *J. Phys. Chem. B* **117,** 5090–5101 (2013).

216. Zhang, Y. & Cremer, P. S. Interactions between macromolecules and ions: the Hofmeister series. *Curr. Opin. Chem. Biol.* **10,** 658–663 (2006).

217. Zhang, Y. & Cremer, P. S. Chemistry of Hofmeister Anions and Osmolytes. *Annu. Rev. Phys. Chem.* **61,** 63–83 (2010).

218. Zhang, Y. *et al.* Specific Ion Effects on the Water Solubility of Macromolecules: PNIPAM and the Hofmeister Series. *J. Am. Chem. Soc.* **127,** 14505–14510 (2005).

219. Youngs, T. G. A. & Hardacre, C. Application of Static Charge Transfer within an Ionic-Liquid Force Field and Its Effect on Structure and Dynamics. *ChemPhysChem* **9,** 1548–1558 (2008).

220. Liu, H. & Maginn, E. J. A molecular dynamics investigation of the structural and dynamic properties of the ionic liquid 1-n-butyl-3-methylimidazolium bis(trifluoromethanesulfonyl)imide. *J. Chem. Phys.* **135,** 124507 (2011).

221. Saba, H., Zhu, X., Chen, Y. & Zhang, Y. Determination of physical properties for the mixtures of [BMIM]Cl with different organic solvents. *Chinese J. Chem. Eng.* **23,** 804–811 (2015).

222. Chang, C.-J. *et al.* Influence of imidazolium based green solvents on volume phase transition temperature of crosslinked poly(N-isopropylacrylamide-co-acrylic acid) hydrogel. *Soft Matter* **11,** 785–792 (2015).

223. Nayak, P. Thermo-Responsive Poly(N-Isopropylacrylamide) and its Critical Solution Temperature Type Behavior in Presence of Hydrophilic Ionic Liquids. *Masters Theses May 2014 - Curr.* (2015).

224. Tsuzuki, S., Katoh, R. & Mikami, M. Analysis of interactions between 1-butyl-3-methylimidazolium cation and halide anions (Cl-, Br- and I-) by ab initio calculations: anion size effects on preferential locations of anions. *Mol. Phys.* **106,** 1621–1629 (2008).

225. Zhang, Y. *et al.* Effects of Hofmeister Anions on the LCST of PNIPAM as a Function of Molecular Weight †. *J. Phys. Chem. C* **111,** 8916–8924 (2007).

226. Zhang, Y., Furyk, S., Bergbreiter, D. E. & Cremer, P. S. Specific Ion Effects on the Water Solubility of Macromolecules: PNIPAM and the Hofmeister Series. *J. Am. Chem. Soc.* **127,** 14505–14510 (2005).

227. Ueki, T. & Watanabe, M. Upper Critical Solution Temperature Behavior of Poly(*N* -isopropylacrylamide) in an Ionic Liquid and Preparation of Thermo-sensitive Nonvolatile Gels. *Chem. Lett.* **35,** 964–965 (2006).